

Institut für Osteologie und Biomechanik
Zentrum für Experimentelle Medizin
Universitätsklinikum Hamburg-Eppendorf

Rsk2 and Lrp5 deficiency limit osteosarcoma growth in *cFos*-transgenic mice by different mechanisms

Dissertation

zur Erlangung der Würde des Doktorgrades (rer. nat.) an der Fakultät für
Mathematik, Informatik und Naturwissenschaften, Fachbereich Chemie an der
Universität Hamburg

Vorgelegt von

Armelle Marie Leila Carreau

2023

Datum der Disputation: 30.06.2023

Datum der Druckfreigabe: 30.06.2023


1. Supervisor: Prof. Dr. rer. nat. Thorsten Schinke
2. Co-supervisor: Prof. Dr. rer. nat. Sandra Pohl
3. Chair: Prof. Dr. med. Elke Oetjen

This dissertation was conducted between August 2019 and May 2023 at the Institute for Osteology and biomechanics at the University Hospital Hamburg-Eppendorf under the supervision of Prof. Dr. rer. nat. Thorsten Schinke.

Ich versichere, dass dieses gebundene Exemplar der Dissertation und das in elektronischer Form eingereichte Dissertationsexemplar (über den Docata-Upload) und das bei der Fakultät (zuständiges Studienbüro bzw. Promotionsbüro Chemie) zur Archivierung eingereichte gedruckte gebundene Exemplar der Dissertationsschrift identisch sind.

Hamburg, 02.05.23

Ort, Datum

Armelle Carreau 

Vorname und Nachname, Unterschrift

I. Oral Presentations and abstract publications

- 1) **European calcified Tissue Society (ECTS)** annual meeting 2022, Helsinki, Finland.

Presentation entitled: *“Lrp5- and Rsk2-deficiency limit osteosarcoma growth in cFos-transgenic mice by different mechanisms.”*

- 2) **MusculoSkeletal Interdisciplinary Translational Young Researchers (MuSkITYR)** Symposium 2022, Frankfurt, Germany.

Presentation entitled: *“The role of Wnt and Rsk2 pathways in controlling osteosarcoma development in a c-Fos transgenic mouse model.”*

II. Table of Contents

1. English abstract	1
2. German abstract.....	3
3. Introduction	5
3.1. Bone anatomy and function.....	5
3.2. Bone remodeling	6
3.3. Bone disorders and the LRP5 pathway	8
3.4. The Wnt pathway.....	9
3.5. Osteosarcoma	11
3.6. Osteosarcoma development in <i>c-Fos</i> -transgenic mice.....	12
3.7. Rsk2 and osteosarcoma formation	14
4. Objectives of the thesis.....	18
5. Results	19
5.1. Pharmacological targeting of the Rsk pathway in <i>FosTg</i> osteosarcoma cells.....	19
5.1.1. Pharmacological inhibition of Rsk in <i>FosTg</i> osteosarcoma cell lines.....	19
5.1.2. Influence of Aurora kinase B inhibition on <i>FosTg</i> osteosarcoma cells	21
5.1.3. Pharmacological growth inhibition of a human osteosarcoma cell line	24
5.2. Impact of <i>Lrp5</i> on osteosarcoma development in <i>FosTg</i> mice	26
5.2.1. Generation and analysis of <i>FosTg</i> mice with different <i>Lrp5</i> genotypes	26
5.2.2. Influence of <i>Lrp5</i> on osteosarcoma growth in <i>FosTg</i> mice.....	29
5.2.3. Histomorphometric analysis of osteosarcomas in <i>FosTg</i> mice with different <i>Lrp5</i> genotypes	32
5.2.4. Isolation and characterization of osteosarcoma cell lines derived from <i>FosTg</i> mice with <i>Lrp5</i> activation or inactivation	38
5.2.5. Transcriptomic comparison of <i>FosTg</i> cell lines	41
5.2.6. Differential gene expression in osteosarcomas <i>in vivo</i>	44
5.2.7. Increased concentration of Fgf21 in sera from <i>FosTg</i> mice.....	46
6. Discussion	48
6.1. Pharmacological inhibition of the Rsk2 pathway.....	48
6.2. Aurora kinase B, another putative target for osteosarcoma therapy	50
6.3. The <i>Lrp5</i> pathway and osteosarcoma progression	52
6.4. <i>Lrp5</i> and <i>FosTg</i> -dependent osteosarcoma growth	53
6.5. Transcriptomic comparison of <i>FosTg</i> osteosarcoma cells	55

6.6.	Fgf21, a potential new target to counteract tumor-induced lipodistrophy	60
7.	Materials.....	61
7.1.	Instruments and softwares	61
7.2.	Chemicals, substances and powders.....	63
7.3.	Buffers and solutions.....	65
7.4.	Consumables and commercial kit	66
8.	Methods.....	67
8.1.	Mouse models.....	67
8.2.	Genotyping.....	67
8.2.1.	Mice euthanasia and skeleton storage.....	68
8.2.2.	Serum glucose and serum collection	69
8.3.	Micro-computed tomography.....	69
8.4.	Histology.....	69
8.4.1.	Undecalcified acrylate histology	69
8.4.1.1.	Preparation of spine samples	69
8.4.1.2.	Staining.....	69
8.4.1.3.	Tumor area and bone mass calculation on spine	70
8.4.2.	Decalcified paraffin sections of spine and immunohistochemistry of Fbln3	70
8.4.3.	Histomorphometry measurements	71
8.5.	Protein analysis	71
8.5.1.	Antibody assay	71
8.5.2.	Enzyme-linked immunosorbent assay (ELISA).....	72
8.5.3.	Western Blot	72
8.6.	Cell culture	73
8.6.1.	Cell lines derived from tumors.....	73
8.6.2.	Commercial cell line.....	74
8.6.3.	Growth and mineralization analysis	74
8.6.4.	Cell treatments and dose effect curves	75
8.6.5.	Fluorescence microscopy.....	75
8.7.	Transcriptomic analysis	76
8.7.1.	RNA extraction <i>in vitro</i> and <i>in vivo</i>	76
8.7.2.	Affymetrix gene chip hybridization.....	76
8.7.3.	CDNA synthesis	77

8.7.4. QPCR gene expression	78
8.7.5. Statistical analysis	79
9. Bibliography	80
10. Appendix.....	94
10.1. List of hazardous substances used in the study according to GHS.	94
10.2. List of hazard statements	95
10.3. List of precautionary statements	96
11. Acknowledgements	97

III. Abbreviations

Abbreviations	Name
μCT	Micro computed tomography
Abca1	ATP-binding cassette transporter A1
ANOVA	Analysis of variance
AP-1	Activating protein-1
APC	Adenomatous polyposis coli
ATCC	American Type Culture Collection
ATP	Adenosine triphosphate
AurkB	Aurora kinase B
BAT	Brown adipose tissue
bp	Base pair
BV/TV	Bone volume per tissue volume
Car12	Carbonic anhydrase 12
Ccl2	C-C motif chemokine ligand 2
Ccnb1	Cyclin B1
Ccnd1	Cyclin D1
Ccnd2	Cyclin D2
Ccne1	Cyclin E1
Cdc25a	Cell division cycle 25A
Cdc25b	Cell division cycle 25B
Cdc25c	Cell division cycle 25C
Cdca5	Cell division cycle associated 5
Cdk1,2,4,6	Cyclin-dependent kinase 1-6
Cdkn1a (p21)	Cyclin-dependent kinase inhibitor 1A
Cdkn2a (p16)	Cyclin-dependent kinase inhibitor 2A
cDNA	Complementary DNA
Chek 1,2	Checkpoint kinase 1-2
Ct.Th	Cortical thickness
Ctrl	Control
CTX	Serum cross-linked C-telopeptide of type I collagen
Dkk1	Dickkopf 1
Dmp1	Dentin matrix acidic phosphoprotein 1
DMSO	Dimethylsulfoxid
DNA	Deoxyribonucleic acid
dNTP	Deoxyribose nucleoside triphosphate
Dynap	Dynactin-associated protein
Efemp1	EGF containing fibulin extracellular matrix protein 1
E2f2	E2F transcription factor 2
ELISA	Enzyme-linked immunosorbent assay
Erk(1-2)	Extracellular signal-regulated kinases
FACS	Fluorescence activated cell sorter

FBJ-MSV	FBJ murine osteosarcoma virus
Fbln3	Fibulin 3
Fgf21	Fibroblast growth factor 21
Fgf23	Fibroblast growth factor 23
Fos	Fos proto-oncogene, AP-1 transcription factor subunit
FosTg	Fos transgenic
Foxm1	Forkhead box M1
Fra (1-2)	Fos-related antigen 1-2
Fzd	Frizzled receptors
Gapdh	Glycerinaldehyde 3-phosphate dehydrogenase
GSK3 β	Glycogen synthase kinase-3 beta
HBM	High bone mass
HSC	Hematopoietic stem cell
HRP	Horseradish peroxidase
Ki67	Cell proliferation marker
Lrp5	LDL receptor related protein 5
M-CSF	Macrophage colony stimulating factor
MSC	Mesenchymal stem cell
N.Ob/B.Pm	Number of osteoblasts per bone perimeter
N.Oc/B.Pm	Number of osteoclasts per bone perimeter
N.Ot/B.Pm	Number of osteocytes per bone perimeter
OPG	Osteoprotegerin
OPPG	Osteoporosis pseudoglioma syndrome
OS	Osteosarcoma
OS/BS	Osteoid surface per bone surface
Osx	Osterix
PCR	Polymerase chain reaction
PINP	Procollagen type I N-propeptide
Prl2c2-3	Prolactin2 C2-3
Ptgs2	Prostaglandin-endoperoxide synthase 2
PTH(1-34)	Parathyroid hormone
PTH1R	Parathyroid hormone 1 receptor
Ptprz1	Protein tyrosine phosphatase receptor type Z1
qPCR	Quantitative real time PCR
Rabgap1	Rab GTPase-activating protein 1
Racgap1	Rac GTPase-activating protein 1
Rank	Receptor activator of NF- κ B
Rankl	Receptor activator of NF- κ B ligand
Rb	Retinoblastoma protein
RIPA	Radio-immunoprecipitation assay
RNA	Ribonucleic acid
Ror2	Receptor tyrosine kinase like orphan receptor 2
Rpm	Round per minute
RPS6KA3	Ribosomal protein S6 kinase A3

Rptpζ	Receptor protein tyrosine phosphatase zeta
Rsk1-4	Serine/threonine kinase p90 ribosomal S6 kinase 1-4
Runx2	Runt-related transcription factor 2
SEM	Standard error of the mean
Sfrp	Secreted frizzled-related protein
Slc13a5	Solute carrier family 13 member 5
Sost	Sclerostin
TCF/LEF	T-cell factor/lymphoid enhancer factor
TRAP	Triiodothyronine receptor auxiliary protein
Trp53	Transformation related protein 53
TUNEL	Terminal deoxynucleotidyl transferase dUTP nick end labeling
Ucp1	Uncoupling protein 1
WAT	White adipose tissue
Wee1	WEE1 G2 checkpoint kinase
Wif1	WNT inhibitory factor 1
WT	Wildtype

1. English abstract

The *c-Fos* transgenic mouse model, where the transgene is placed under the control of the H2Kb promoter, has been described to spontaneously develop osteosarcomas due to the transformation of the osteoblastic lineage. Moreover, the ribosomal S6 kinase 2 (Rsk2), which activates *c-Fos* by phosphorylation on serine 362, was found to be essential for *c-Fos*-induced osteosarcoma formation in mice. Using cell lines derived from *FosTg;Rsk2^{-/-}* tumors it was further observed that Rsk2 deficiency impaired the growth advantage of *FosTg* cells, which was explained by aberrant nuclei number due to impaired cytokinesis suggesting the induction of “mitotic catastrophe”. Thus, Rsk2 was defined as a potential target for the design of new osteosarcoma therapies.

In this thesis a pharmacological Rsk inhibitor (BI-D1870) was tested for its ability to inhibit proliferation of osteosarcoma cells. Here, the effects observed by the genetic inactivation of Rsk2 were mimicked. Moreover, since BI-D1870 administration to *FosTg* cell lines reduced expression of aurora kinase B, the influence of a pharmacological aurora kinase B inhibitor (Hesperadin) was also tested. Similar to BI-D1870, Hesperadin caused impaired cytokinesis, resulting in the accumulation of polynuclear cells, an effect that was not only observed in *FosTg* cell lines, but also in the human osteosarcoma cell line U2OS.

The second part of this thesis focused on targeting a more osteoblast-specific pathway involving the transmembrane protein Lrp5, which acts as a co-receptor of Wnt ligands. Importantly, *LRP5* mutations were found to be the cause of two major human bone diseases, associated with either high bone mass (*Lrp5* activation) or osteoporosis (*Lrp5* inactivation). To analyze the role of Lrp5 in osteosarcoma growth, *FosTg* mice were crossed with *Lrp5*-deficient mice or with mice carrying a high bone mass mutation of Lrp5 (*Lrp5^{A213V/+}*). It was found that Lrp5 deficiency drastically reduced the osteosarcoma volume in *FosTg* mice, which was explained by a decreased number of active osteoblasts at the tumor surfaces associated with the appearance of large unmineralized areas. Cell lines were established from the three *FosTg* mouse models with different *Lrp5* genotypes, however growth curve and mineralization analyses did not reveal significant differences, thereby suggesting a non-cell-autonomous mechanism.

Nevertheless, the investigation of potential downstream effectors by microarray analysis and their confirmation by qPCR permitted to identify specific genes with differential expression,

which will be further analyzed for their implication in bone remodeling and cancer development. Moreover, an antibody assay performed with serum from the different mice led to the identification of Fgf21 as a potential factor causing lipodystrophy in *FosTg* mice. In summary, by targeting the Rsk2 or the Lrp5 pathway, this project identified two different mechanisms to impair osteosarcoma growth in *c-Fos* transgenic mice.

2. German abstract

Für das c-Fos-transgene Mausmodell, in dem das Transgen unter der Kontrolle des H2Kb-Promotors steht, wurde eine Osteosarkom-Entwicklung beschrieben, die durch Transformation von Zellen der Osteoblasten-Linie bedingt ist. Zudem wurde gezeigt, dass die ribosomale S6 Kinase 2 (Rsk2), welche c-Fos durch Phosphorylierung an Serin 362 aktiviert, essentiell für die c-Fos-induzierte Osteosarkom-Entwicklung in Mäusen ist. Durch Untersuchung von Zelllinien aus *FosTg;Rsk2^{-/-}*-Tumoren konnte zudem gezeigt werden, dass die Rsk2-Defizienz den Wachstumsvorteil von *FosTg*-Zellen minimiert, was durch eine veränderte Zellkernzahl erklärt wurde, die durch gestörte Zytokinese entsteht, was als Hinweis auf eine „mitotische Katastrophe“ gedeutet wurde. Somit wurde Rsk2 als potentielles Zielmolekül für die Entwicklung neuer Osteosarkom-Therapien definiert.

In der vorliegenden Dissertation wurde ein pharmakologischer Rsk Inhibitor (BI-D1870) im Hinblick auf die Inhibierung der Proliferation von Osteosarkom-Zellen untersucht. Hier zeigten sich ähnliche Einflüsse wie zuvor für die genetische Rsk2-Inaktivierung gezeigt. Da die Behandlung mit BI-D1870 zudem zu einer reduzierten Expression von Aurora-Kinase B führte, wurde auch der Einfluss eines Inhibitors dieses Enzyms (Hesperadin) getestet. Ähnlich wie BI-D1870 führte auch Hesperadin zu einer gestörten Zytokinese und einer Akkumulation polynukleärer Zellen. Dieser Effekt wurde nicht nur in *FosTg*-Zelllinien beobachtet, sondern auch in der humanen Osteosarkom-Zelllinie U2OS.

Der zweite Teil der vorliegenden Dissertation fokussierte sich auf einen Osteoblasten-spezifischen Regulationsmechanismus vermittelt durch das Transmembranprotein Lrp5, welches als Co-Rezeptor für Wnt-Liganden fungiert. In der Tat sind *LRP5*-Mutationen ursächlich für zwei wichtige humane Knochenerkrankungen, die entweder mit hoher Knochendichte (*Lrp5*-Aktivierung) oder Osteoporose (*Lrp5*-Inaktivierung) assoziiert sind. Um die Rolle von *Lrp5* in der Osteosarkom-Entwicklung zu untersuchen, wurden *FosTg*-Mäuse mit *Lrp5*-defizienten Mäusen oder mit Mäusen, die eine aktivierende Mutation von *Lrp5* tragen (*Lrp5^{A213V/+}*), verpaart. Es zeigte sich, dass die *Lrp5*-Defizienz zu einer deutlichen Reduktion des Osteosarkomwachstums führte. Ursächlich dafür war eine verringerte Anzahl aktiver Osteoblasten an der Tumoroberfläche, die durch eine Anreicherung nicht-mineralisierter Areale begleitet wurde. Zelllinien, die aus den drei *FosTg*-Modellen mit unterschiedlichem *Lrp5*-Genotyp etabliert wurden, zeigten hingegen keine signifikanten Unterschiede im

Hinblick auf Wachstum und Mineralisation, was für einen nicht-zellautonomen Mechanismus spricht.

Trotzdem konnten durch Microarray-Analysen und anschließender qPCR spezifische Gene identifiziert werden, deren Einfluss auf Knochenumbau und Tumorstehung in zukünftigen Untersuchungen evaluiert werden kann. Zudem führte eine Antikörper-basierte Untersuchung von Seren der unterschiedlichen Mäuse zur Identifizierung von Fgf21 als potentielltem Faktor, der die Lipodystrophie der *FosTg*-Mäuse verursachen könnte.

Zusammenfassend konnte dieses Projekt mit *Rsk2* und *Lrp5* zwei unterschiedliche Ansatzpunkte definieren, um die Osteosarkom-Entwicklung in *FosTg*-Mäusen zu minimieren.

3. Introduction

3.1. Bone anatomy and function

The human adult skeleton comprises 206 bones, which can be differentiated into long, short, irregular, and flat bones. Femur, tibia and humerus belong to the long bones and have a common structure: two epiphyses, two metaphyses and one diaphysis. The epiphyses and metaphyses are composed of trabecular and cortical bone while the diaphysis is composed only of cortical bone (Figure 1). The cortical compartment is the densest part of the bone, where an orientated mineralized collagen network forms cylinders termed osteons. The trabecular bone is found in long bones, but also in vertebral bodies. It has a porous structure made of trabeculae with bone marrow cells located in between.

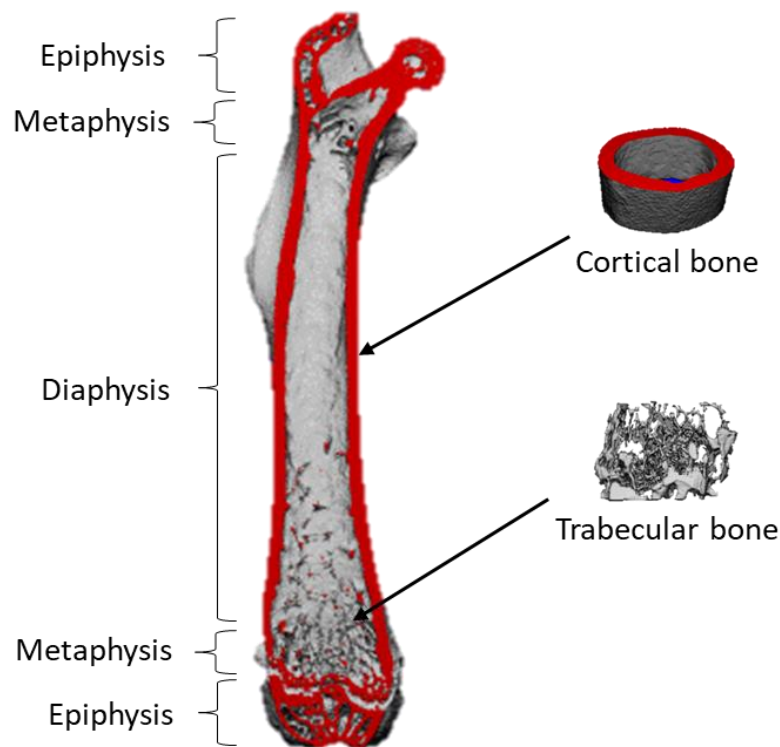


Figure 1: Bone structure

Representative μ CT image of a femur from a 16-week-old female C57BL/6 mouse indicating the different anatomical compartments.

The bone matrix consists of an organic phase and a mineral phase. The organic phase of bone is mostly composed of type I collagen fibers. These fibers bring flexibility and elasticity to the

bone, thereby permitting movement and body weight resistance. The mineral phase is mainly constituted of hydroxyapatite crystals and calcium carbonate inserted between collagen fibers. These minerals represent 70% of the total bone weight and provide strength and rigidity. There are also additional bone matrix proteins specifically produced by osteoblasts, such as bone sialoprotein (BSP), osteocalcin or dentin matrix protein 1 (Dmp1) (Holm et al., 2015; Kalajzic et al., 2004). Several functions are attributed to the skeleton, such as movement, stability and flexibility. Moreover, the bone marrow hosts the site of hematopoiesis, i.e. the production of immune cells and the maturation of different cell types. Finally, the bone matrix is also used as a mineral reservoir (Arnold et al., 2021).

Although bone was considered as a specialized tissue functionally separated from other organs, it is long established that bone turnover is influenced by hormones released from other organs, such as estrogen or parathyroid hormone (PTH). Moreover, due to its bone-anabolic effect, intermitted PTH injection is one therapeutic approach to counteract bone loss in osteoporotic patients (Hock et al., 1992; Neer et al., 2001). More recently, it was also found that bone cells are also releasing factors impacting the metabolism or functions of other organs. The most established bone-derived hormone is fibroblast growth factor 23 (FGF23), and its identification can be regarded as a major breakthrough in the osteology field, as it demonstrated an endocrine function of the bone (Fukamoto & Martin, 2009). Indeed, several bone diseases have been associated with FGF23 activation, such as different forms of hypophosphatemia rickets (ADHR consortium, 2000) or tumor-induced osteomalacia (Shimada et al., 2001; Florenzano et al., 2017). Altogether, these collective findings have defined FGF23 as the major hormone regulating serum phosphate homeostasis, produced by bone cells to regulate phosphate reabsorption by the kidney (Fukamoto & Martin, 2009).

3.2. Bone remodeling

Throughout adult life, the bone matrix is continuously remodeled by two main cell types, osteoblasts and osteoclasts. Osteoblasts are bone-forming cells derived from mesenchymal stem cells, which can also differentiate into adipocytes and chondrocytes. Differentiation into these different cell types is regulated by specific molecules. For instance, Runx2 (a transcription factor), Bmps (bone morphogenetic proteins) and components of the Wnt

pathway are mandatory for osteoblast lineage differentiation (Ponzetti & Rucci., 2021). Osteoblasts produce the bone matrix (osteoid), mostly consisting of type I collagen fibers that provide the scaffold for incorporating minerals to form mature mineralized bone. Osteocytes are terminally differentiated osteoblasts, embedded into the mineralized bone matrix (Figure 2). Functionally, they can be considered as sensors of bone integrity. Osteocytes constantly interact with each other and form a network of cells connected physically by their dendritic processes (Bonewald, 2011). They are also in direct contact with other cell types at the bone surface and regulate them via the release of different molecules. For instance, together with osteoblasts, osteocytes release the receptor activator of NF- κ B ligand (Rankl), a ligand of the Rank receptor present at the surface of osteoclast progenitor cells permitting their differentiation, maturation and recruitment for bone resorption. Osteoblasts and osteocytes are also regulating bone resorption by the release of osteoprotegerin (OPG), an inhibitor of osteoclastogenesis (Boyce & Xing, 2008). Finally, osteocytes release two specific inhibitors of bone formation, Dickkopf-1 (Dkk1) and Sclerostin (SOST) (Florencio-Silva et al., 2015).

Osteoclasts are multinuclear cells, originating from hematopoietic stem cells and responsible for bone matrix resorption (Teitelbaum, 2000). Osteoclast-mediated bone resorption involves the secretion of numerous hydrolases (cathepsin K, metalloproteinases and phosphatases) for the degradation of bone matrix proteins, whereas proteins implicated in the acidification of the resorption lacuna (carbonic anhydrase II, the chloride channel CLCN-7, or the vacuolar H⁺-ATPase), are required to dissolve hydroxyapatite crystals (Lehenkari et al., 1998; Bellido et al., 2019). Osteopetrosis, also called “marble bone disease”, is characterized by an impairment of osteoclast function leading to increased bone density, higher fracture risk and, in the most severe and life-threatening cases, to bone marrow displacement (Sobacchi et al., 2013). Importantly, long-term survival in the majority of the latter patients can be ensured by hematopoietic stem cell transplantation. Whereas the phenotypic severity of the rare inherited disorder osteopetrosis essentially demonstrates the importance of osteoclasts and intact bone remodeling for long-term skeletal integrity, it is also essential to state that a relative increase of osteoclastogenesis and bone resorption is the cause of a highly prevalent disorder, i.e. osteoporosis.

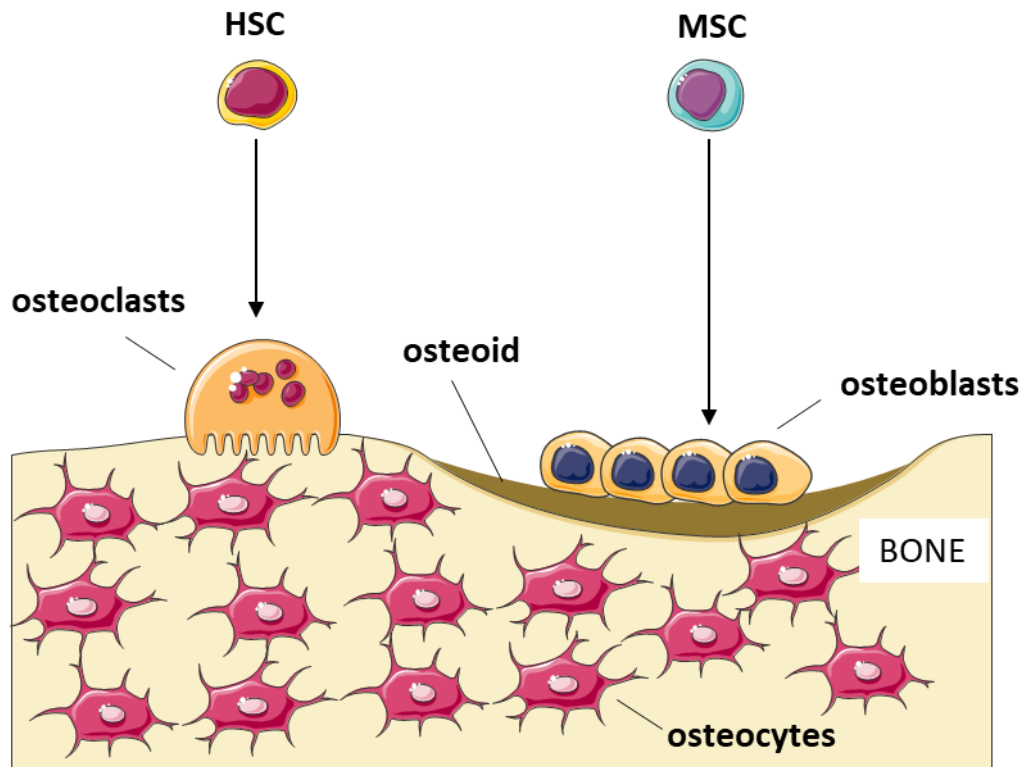


Figure 2: Bone remodeling. Schematic presentation showing the three major bone cell types. Whereas bone-resorbing osteoclasts develop by fusion of hematopoietic stem cells (HSC), bone-forming osteoblasts are derived from mesenchymal stem cells (MSC). Osteoblasts secrete an extracellular matrix (osteoid), which is initially unmineralized, but then incorporates minerals to form bone. Osteocytes, representing the most abundant bone cell type, are terminally differentiated osteoblasts forming a cellular network within the mineralized bone matrix. (The Figure was partly generated using Servier Medical Art, provided by Servier, licensed under a Creative Commons Attribution 3.0 unported license)

3.3. Bone disorders and the LRP5 pathway

Osteoporosis is the most common bone disorder with a high prevalence (1 of 3 women and 1 of 5 men) over the age of 50 years (Sözen et al., 2017; Kanis et al., 2019). The aging of the population is responsible for a continuously increasing prevalence of this disease, which also causes high costs for the healthcare system. The patients suffer from systemic bone loss, resulting in a high risk for non-traumatic bone fractures. While women are predominantly affected after menopause as they undergo a drop in estrogen levels (Black & Rosen, 2016), many cases of early-onset osteoporosis have recently been reported to be caused by pathogenic variants of specific genes. One particular form of inherited osteoporosis with early onset is the *Osteoporosis pseudoglioma syndrome* (OPGG). The affected patients suffer from

severe bone loss, sensitivity to multiple fractures and a characteristic phenotype of eye vascularization leading, in the most dramatic cases, to blindness in children. In 2001, a genetic analysis of twenty-eight families affected by OPGG identified frameshift or missense mutations in the gene *LRP5* (Gong Y. et al., 2001). The authors also found that osteoblastic lineage cells, but not osteoclasts, were specifically expressing *LRP5* through developmental phases. An osteoporotic phenotype was also confirmed in mice lacking *Lrp5* (Kato et al., 2002). Nearly at the same time, activating mutations of *LRP5* were found to be responsible for the high bone mass phenotype in individuals with osteosclerosis (Little et al., 2001; Boyden et al., 2002). One of these mutations is *LRP5*^{A213V}, which was subsequently shown to increase osteoblast-mediated bone formation when genetically introduced into mice (Cui et al., 2011). Since *LRP5* is presumably acting as a co-receptor for ligands of the Wnt family (Cong et al., 2004), the discovery of *LRP5* mutations causing either low or high bone mass strongly suggested that the Wnt signaling pathway is of major importance in bone formation.

3.4. The Wnt pathway

LRP5 is a single-pass transmembrane protein that acts as a co-receptor for ligands of the Wnt family, which consists of 19 different proteins. The binding of Wnt ligands can affect different cellular responses, and at least two different signaling pathways can be distinguished. The Wnt canonical pathway involves the binding of Wnt ligands to receptors of the Frizzled (FZD) family and its co-receptor *LRP5*. This leads to the stabilization of β -catenin, which subsequently translocates to the nucleus to activate different target genes (Figure 3). In the absence of a canonical Wnt ligand, or in the presence of specific inhibitors, such as *Wif1* or *Sfrps*, a complex composed of Axin, APC, Gsk3- β leads to phosphorylation of β -catenin, which induces its ubiquitination and proteasomal degradation (Aberle et al., 1997; Baron & Kneissel, 2013). Importantly, two negative regulators of bone formation, i.e. Sclerostin (*SOST*) and *DKK1*, function as inhibitors of the Wnt pathway directly binding to *LRP5* (Semënov et al., 2001; Semënov et al., 2005). Moreover, an antibody neutralizing sclerostin (Romosozumab) has recently been developed as an osteoanabolic treatment option for patients suffering from osteoporosis (Cosman et al., 2016; Prather et al., 2020).

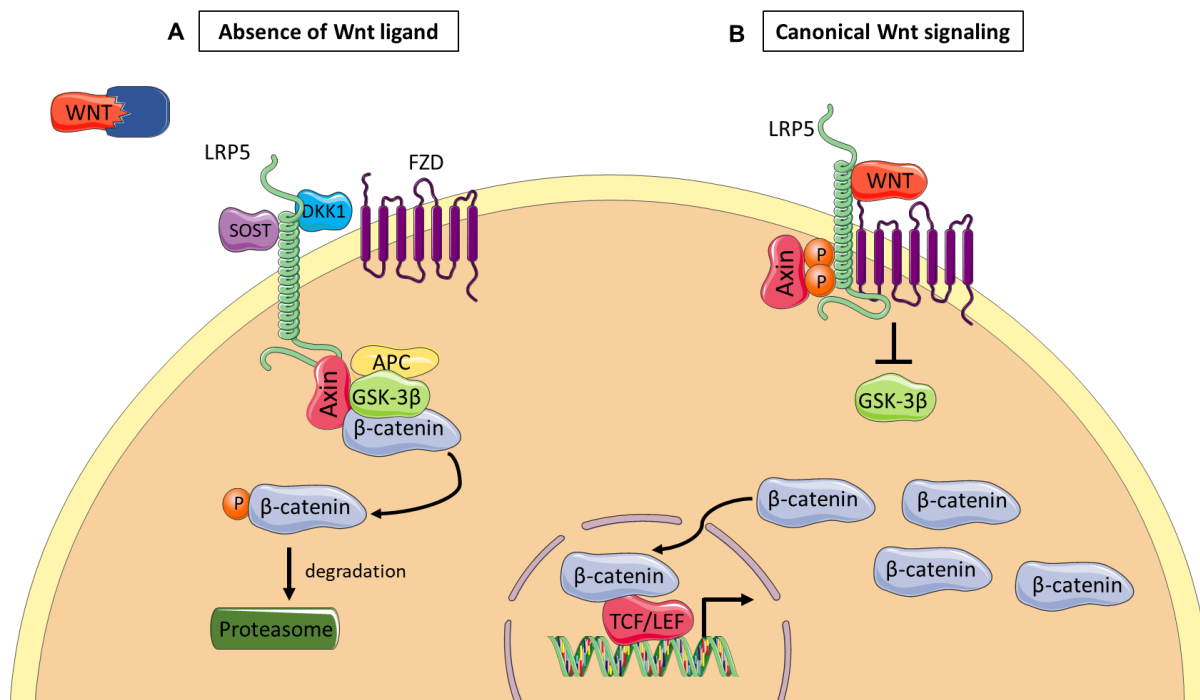


Figure 3: The canonical Wnt pathway.

A) In the absence of a Wnt ligand or in the presence of Wnt signaling inhibitors, β -catenin is degraded and there is no activation of canonical Wnt pathway target gene transcription. **B)** When a Wnt ligand binds to a Frizzled receptor and the co-receptor LRP5, β -catenin is not degraded and is able to translocate to the nucleus to activate the transcription of Wnt canonical target genes. (The Figure was partly generated using Servier Medical Art, provided by Servier, licensed under a Creative Commons Attribution 3.0 unported license)

The non-canonical Wnt pathway is independent of β -catenin and involves binding of Wnt ligands to other receptors, such as Ror2 or PTH1R. Initially considered as two independent pathways, there is recent evidence for a crosstalk between canonical and non-canonical Wnt signaling with functions that remain to be defined (Bryja et al., 2009). Importantly, β -catenin stabilization in mature osteoblasts of transgenic mice was reported to impact bone resorption rather than bone formation by inducing the secretion of OPG (Glass DA II et al., 2005). Later, Kramer et al. demonstrated an opposite influence on bone resorption, i.e. increased osteoclastogenesis, causing low bone mass in mice with osteocyte-specific β -catenin deficiency (Kramer et al., 2010). Since LRP5 activation and inactivation specifically affects osteoblast differentiation and bone formation, it is debatable whether β -catenin acts downstream of LRP5 in osteoblast lineage cells.

3.5. Osteosarcoma

Whereas genetic research in the last decades has substantially increased the molecular knowledge about bone remodeling disorders, which also established new treatment options for osteoporosis, there is still limited knowledge about specific causes and treatment options for another detrimental bone pathology, i.e. osteosarcoma. More specifically, osteosarcomas are the most common primary bone tumors with an incidence of 4.4 cases per million worldwide (Bleyer et al., 2006). Aggressive forms can lead to metastasis in lung, brain or other tissues. Notably, osteosarcoma formation primarily impacts children and adolescents (5-20 years of age) during bone growth. A second peak of incidence appears after the age of 60 years following bone trauma or Paget's disease (a bone pathology characterized by locally activated osteoclastogenesis). The overall relapse-free survival rate of osteosarcoma patients is 70% after 5 years, but it decreases drastically with the appearance of metastases (Kansara et al., 2014; Meltzer & Helman, 2021). Current treatments are composed of adjuvant chemotherapy and surgery. Unfortunately, however, in many cases patients must undergo amputation, which is a massive trauma especially in young patients.

Osteosarcomas are currently treated by high-dose of cytotoxic chemotherapy, but no specific molecular therapies are available yet. The transformation of osteoblast lineage cells mainly results from sporadic mutations in tumor suppressors and/or oncogenes, such as *TRP53*, *RB*, *c-MYC*, *NOCTH1*, *FOS*, *NF2*, *WIF1* or *APC* (Weinberg, 1991; Rickel et al., 2017). In some cases, inherited heterozygous gene variants in *TRP53* or *RB* were identified, which explains a higher risk of developing osteosarcomas (Miller et al., 1996; Berman et al., 2008; Fuchs & Winkler, 1993). It was also reported that acquired *TRP53* mutations are present in most osteosarcomas. This gene encodes the P53 protein, a major regulator of cell cycle progression. P53 is activated when cellular DNA is damaged, leading to an arrest of the cell cycle and the induction of either senescence or programmed cell death by apoptosis. The lack or inactivation of P53 in cancer cells often leads to anarchic cell proliferation, which causes accumulation of several anomalies (Rivlin et al., 2011). In mice, heterozygous deficiency of *Trp53* was described as a potential osteosarcoma model. However, respective studies in our laboratory showed that heterozygous *Trp53*-deficient mice failed to develop osteosarcomas after 1 year, unless they were additionally lacking *Ptprz1*, which encodes the protein tyrosine

phosphatase Rptp ζ , a potential tumor suppressor highly expressed in osteoblasts (Baldauf et al., 2015; Schinke et al., 2008). Moreover, our laboratory additionally developed a mouse model with osteoblast-specific *Trp53* deficiency (*Trp53*^{fl/fl}; Runx2-Cre), which also did not develop osteosarcomas, but displayed thymic lymphomas at 6 months of age, which prevented to study older animals (Liao et al., 2021).

It is likely that not all mutations causing osteosarcoma have been identified yet, which is also explained by the high genetic heterogeneity that is even observed within individual tumors. Therefore, research regarding a deeper genetic characterization is one crucial step for the development of targeted therapies limiting osteosarcoma growth. In this regard, it is relevant that osteosarcoma growth was suggested to be the result of highjacking bone-anabolic pathways, such as Wnt signaling, although several studies about different modulators of this pathway led to controversial results. Importantly however, LRP5 was described as a marker of aggressiveness and metastasis by its expression in human high-grade osteosarcoma (Hoang et al., 2004).

3.6. Osteosarcoma development in *c-Fos*-transgenic mice

The transcription factor AP-1 is composed of a member of the Fos family (*c-Fos*, *Fra1*, *Fra2* or *FosB*), which heterodimerizes with a member of the Jun family (*c-Jun*, *JunB* or *JunD*). AP-1 transcription factors are known to be implicated in fundamental cellular processes implicating proliferation and cell death. Of note, different bone pathologies have been associated with the activation and/or inactivation of most Fos family members (Eferl & Wagner, 2003). More specifically, *Fra1Tg*, *Fra2Tg* and Δ *FosBTg* mice, which ubiquitously overexpress the respective genes, have been reported to display osteosclerosis, i.e. high bone mass due to increased bone formation (Jochum et al., 2000; Bozec et al., 2010; Sabatakos et al., 2000). In contrast, deficiency of *Fra1* and *Fra2* in mice causes a low bone mass phenotype (Eferl et al., 2004), whereas *Fos*-deficient mice display osteopetrosis. Most importantly, overexpression of *c-Fos*, but not of the other AP-1 family members, was reported to cause osteosarcoma development (Grigoriadis et al., 1993).

Indeed, v-Fos, the viral homologue of c-Fos, was first identified as the transformed gene in the Finkel Biskis Jinkis murine sarcoma virus (FBJ-MSV), named after its discovering researchers in 1966 (Finkel et al., 1966). In 1982, v-Fos was found to be the result of the fusion of c-Fos with the FBJ virus (Curran et al., 1982). The injection of v-Fos in mice led to osteosarcoma formation showing that bone is a specific target of Fos. It was the first proof of the transforming ability of Fos *in vivo*. Moreover, increased expression of Fos was observed in most human and murine osteosarcomas, and its expression level correlates with aggressiveness.

With the aim to develop an osteosarcoma mouse model the group of Erwin Wagner designed a transgenic mouse model, where they placed the Fos oncogene under the control of a H2kB class I promoter permitting its ubiquitous overexpression (Rüther et al., 1989). The transgene expression, first detected 3 weeks after birth, specifically provoked transformation of the osteoblast lineage cells, thereby causing osteosarcoma formation throughout the skeleton (Figure 4A). First lesions could be observed at 8 weeks, but visible tumors appeared after 10 weeks with further growth of tumors in the following months. The tumors found in FosTg mice were reported to be highly mineralized with the presence of osteoblasts, but also chondrocytes. Interestingly, even so chondrocytes were present inside the tumors, cartilage tissue did not seem to be affected by Fos overexpression (Grigoriadis et al., 1993). It was further found that c-Jun overexpression in mice exacerbated osteosarcoma development in FosTg mice, although no tumors were observed in mice only overexpressing c-Jun (Wang et al., 1995). Unpublished studies from our group further revealed that FosTg mice develop lipodystrophy in addition to osteosarcomas (Figure 4B-D). Although the cause of this pathology is still not fully clarified, it is noteworthy to state that it is accompanied by an induction of *Ucp1* in subcutaneous fat, which indicates a browning of white adipose tissue (Figure 4E).

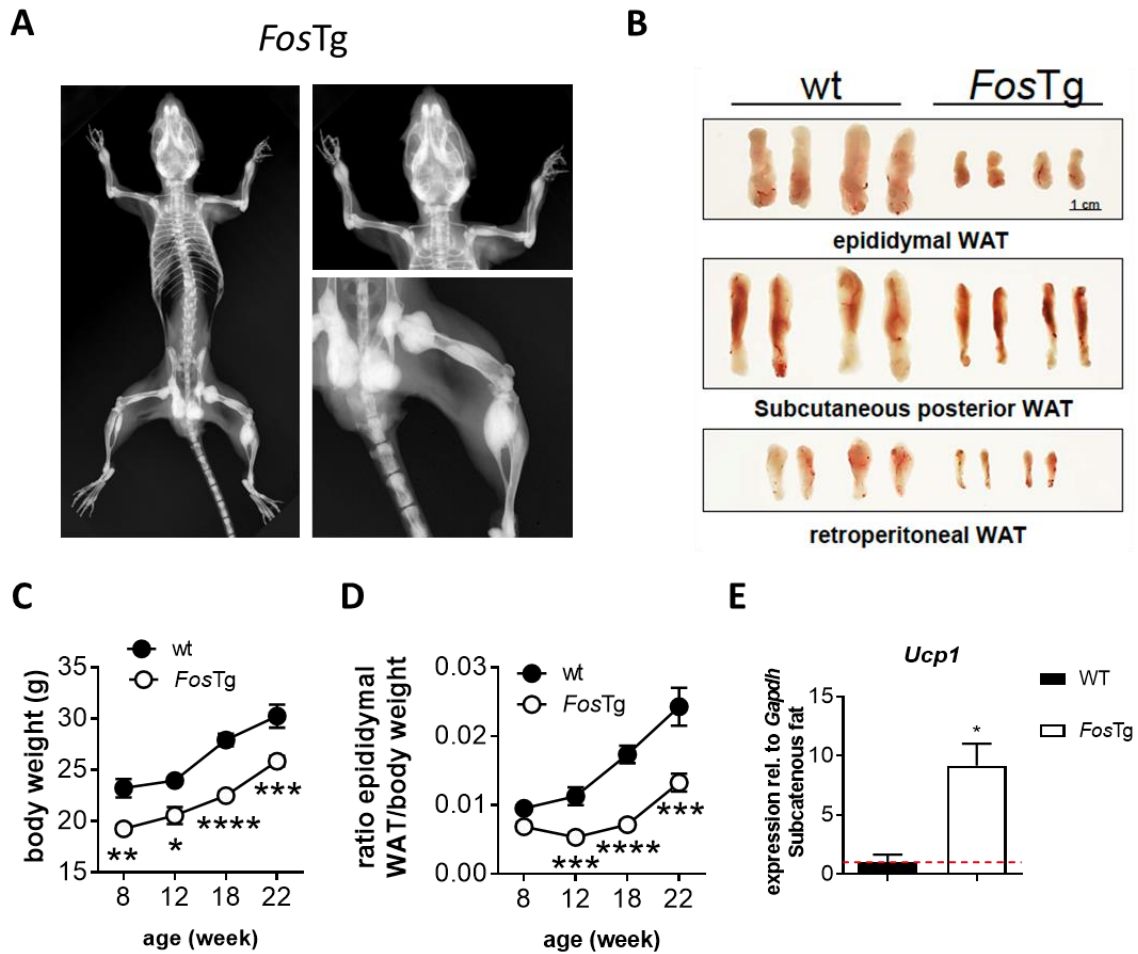


Figure 4: *FosTg* mice develop osteosarcomas and lipodystrophy.

A) Xray image of a 16-week-old mouse expressing *c-Fos* under the control of a H2kb promoter (*FosTg*). These mice develop bone tumors visualized in different skeletal locations. **B)** Images of different fat pads in wildtype and *FosTg* mice at the age of 18 weeks. **C)** Body weight curves of *FosTg* mice compared to wildtype littermates from 8 weeks to 22 weeks of age. **D)** Epididymal white adipose tissue (WAT) weight compared to total body weight in the same mice. **E)** qPCR indicates increased *Ucp1* expression in subcutaneous fat of *FosTg* mice (unpublished data).

3.7. Rsk2 and osteosarcoma formation

Rsk2 is a protein kinase that is required for the development of osteosarcomas in *FosTg* mice (David et al., 2005). It belongs to the Rsk (90 kDa ribosomal S6 kinase) protein family that is composed of four homologous serine/threonine protein kinases (Rsk1, Rsk2, Rsk3 and Rsk4), which are implicated in the cascade of kinases promoted by Ras and lead to the phosphorylation and activation of multiple transcription factors responsible for the regulation of proliferation, survival and differentiation (Anjum & Blenis, 2008). Importantly, Rsk2 is

responsible for the stabilizing phosphorylation of Fos on serine 362, which appears secondary to the activating phosphorylation of Fos by Erk on serine 374 (Chen et al., 1993; Chen et al., 1996). The role of Rsk2 in the skeleton was underscored by genetic evidence in patients with Coffin-Lowry syndrome, an X-linked disease caused by loss-of-function mutations in *RPS6KA3*, the gene encoding for RSK2. Besides mental retardation, the affected patients also display skeletal abnormalities, growth impairment and cranio-facial dystrophies (Coffin et al., 1966; Lowry et al., 1971).

Following these results, David et al. could demonstrate that deficiency of Rsk2 in mice resulted in low bone mass caused by reduced osteoblast activity with no change in osteoclast-mediated bone resorption (David et al., 2005). Based on these collective arguments, Rsk2 was a candidate molecule involved in osteosarcoma progression of *FosTg* mice. For that purpose, *FosTg* mice were crossed with *Rsk2*-deficient mice, and litters were studied until the age of 7 months (Figure 5A). Even so the incidence of tumors counted on Xrays was unchanged between *FosTg* mice and *FosTg;Rsk2^{-/-}* mice, the tumor volume was dramatically reduced in *FosTg;Rsk2^{-/-}* mice (Figure 5B). Furthermore, the mineralization of the tumors was reduced in *FosTg;Rsk2^{-/-}* mice compared to *FosTg* mice, as there was a strong enrichment of non-mineralized osteoid in the majority of tumors found in *FosTg;Rsk2^{-/-}* mice (Figure 5C). Moreover, immunofluorescent staining of the proliferation marker Ki67 and quantification of TUNEL-positive cells indicated decreased proliferation and enhanced apoptosis of tumor cells in *FosTg;Rsk2^{-/-}* osteosarcomas (Figure 5D-E).

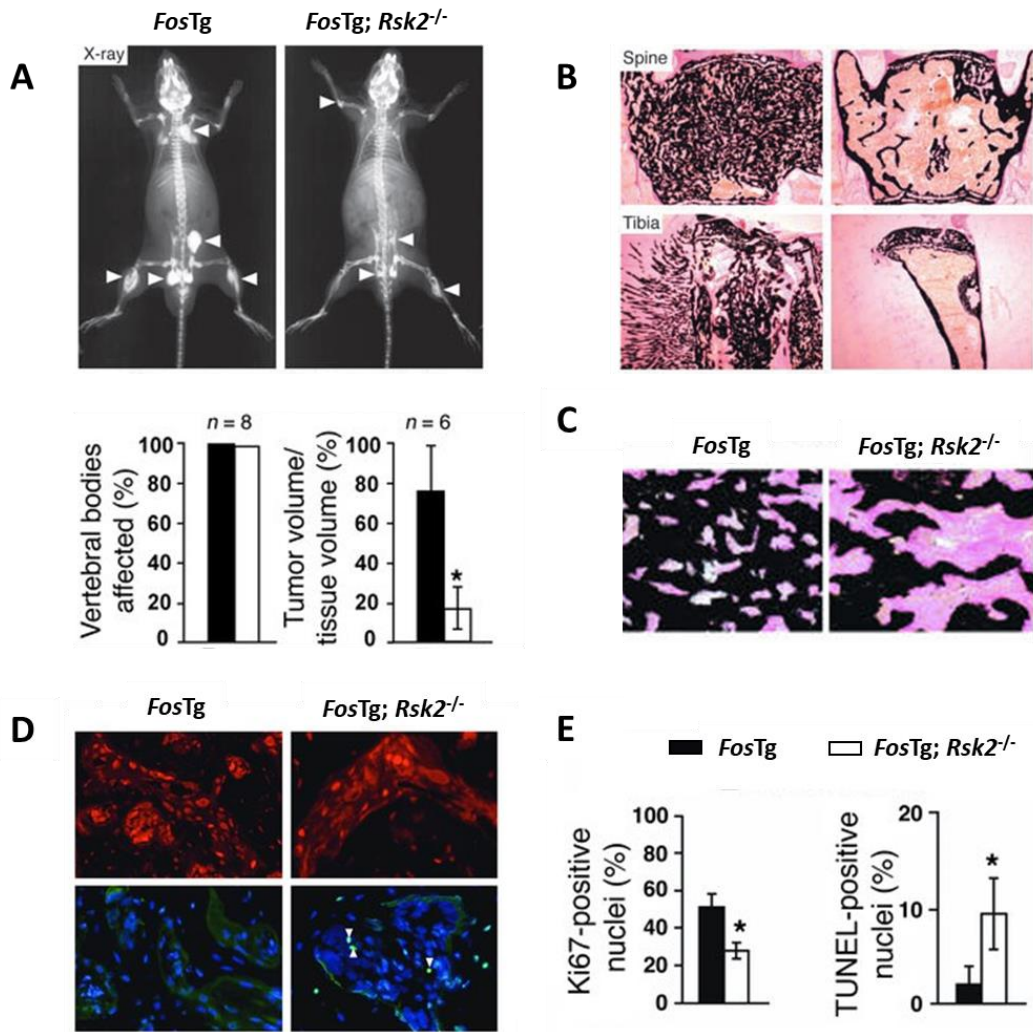


Figure 5: Rsk2 deficiency impairs osteosarcoma growth and promote apoptosis in *FosTg* mice. **A)** Representative Xrays of *FosTg* and *FosTg;Rsk2^{-/-}* mice at 7 months of age. White arrows highlight the presence of osteosarcomas. **B)** Von Kossa/van Gieson staining of undecalcified spine and tibia sections. Quantification of the affected vertebral bodies and the tumor volume per tissue volume is shown below the Xray images. **C)** Undecalcified tumor sections, where black staining indicates mineralized bone and pink areas represent unmineralized bone matrix (osteoid). **D)** Immunofluorescent staining of Ki67 (red) and TUNEL assay (green) in osteosarcomas sections of *FosTg* and *FosTg;Rsk2^{-/-}* mice. **E)** Quantification of the percentage of Ki67-positive cells reflecting proliferation and TUNEL-positive cells reflecting apoptosis. (David et al., 2005; adapted with permission)

When cell lines derived from osteosarcomas of *FosTg* and *FosTg;Rsk2^{-/-}* mice were isolated and compared *ex vivo*, it was found that *FosTg;Rsk2^{-/-}* cells displayed a severe growth impairment compared to *FosTg* cells (Figure 6A-B). Furthermore, the appearance of polynuclear cells in *FosTg;Rsk2^{-/-}* lines suggested impaired cell division (Figure 6C). Indeed, as indicated by immunofluorescence microscopy, Rsk2 was co-localizing with the mitotic spindle assembly complex (data not shown). Moreover, a cell cycle phase analysis by FACS could demonstrate an arrest of *FosTg;Rsk2^{-/-}* cells in the G2/M phase (Figure 6D).

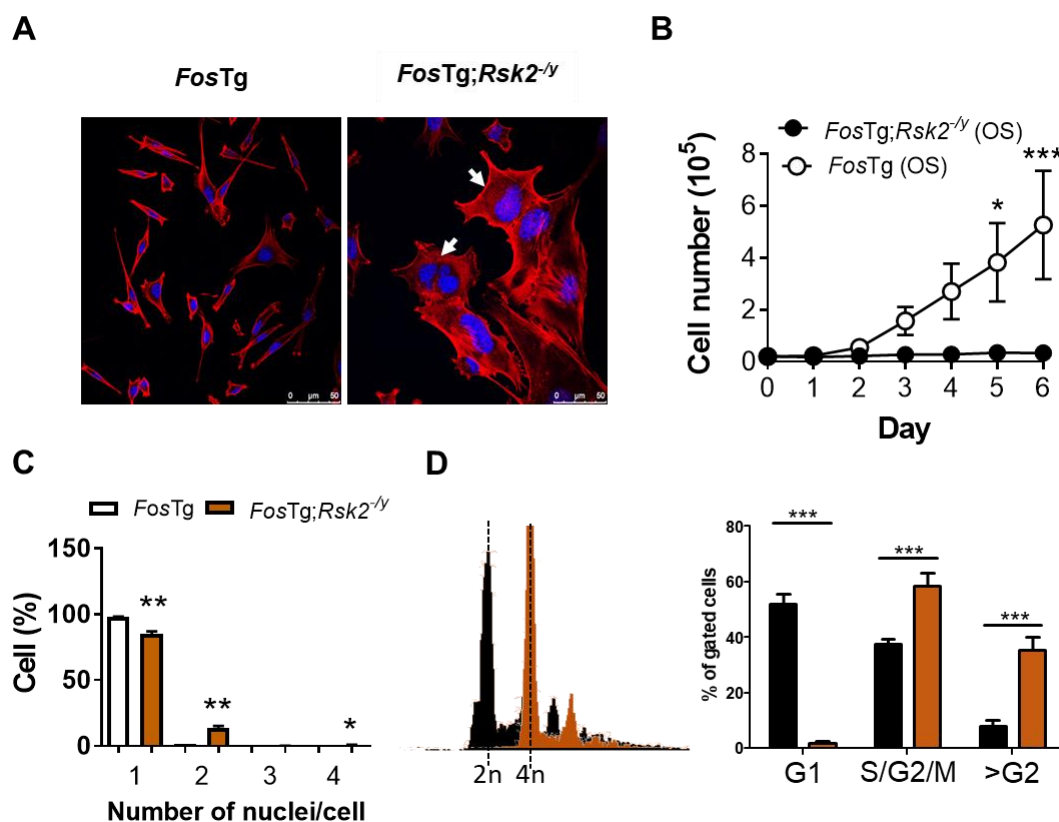


Figure 6: Genetic inactivation of Rsk2 in *FosTg* cell lines causes growth impairment, polyploidy and G2/M arrest of the cell cycle.

A) Actin staining by phalloidin red and DNA staining by DAPI of representative cell lines from the indicated genotype. White arrows indicate the presence of cells with more than one nucleus. **B)** Growth curves of established cell lines isolated from osteosarcomas developing in the long bones of *Fos* transgenic mice and *Fos* transgenic mice lacking Rsk2 (*FosTg;Rsk2^{-/-}*) (n=6 independent cell lines) **C)** Quantification of the proportion of cells with 1, 2, 3 or 4 nuclei (n=3 independent cell lines). **D)** Representative FACS profiles of DNA content in cell lines of the indicated genotypes and quantification of the proportion of cells in G1, S/G2/M of the cell cycle as well and polyploid cells (>G2), n=3 independent cell lines (unpublished data).

4. Objectives of the thesis

The first aim of this project was to define if pharmacological inhibition of Rsk2 or its downstream targets could reproduce the effect observed in *FosTg* osteosarcoma cell lines by genetic inactivation of Rsk2. Since pharmacological Rsk inhibitors, such as BI-D1870, an ATP competitive inhibitor of Rsk kinase activity, are available and some of them are currently tested in clinical studies, this project aimed at using such inhibitors to mimic the genetic deficiency of Rsk2 and study its downstream effectors for its therapeutic use.

The second aim of the thesis was to study if *FosTg* osteosarcoma cells are highjacking the Lrp5 pathway for their growth benefit. In order to confirm or falsify this hypothesis, genetically modified mice with either gain- or loss-of-function of Lrp5 were crossed with *FosTg* mice to determine if and how constitutive activation or inactivation of Lrp5 would affect osteosarcoma formation. As an LRP5 antagonist (BI-905677) is currently tested for its ability to reduce the growth of different solid tumors, there was also a direct clinical relevance of these studies.

5. Results

5.1. Pharmacological targeting of the Rsk pathway in *FosTg* osteosarcoma cells

5.1.1. Pharmacological inhibition of Rsk in *FosTg* osteosarcoma cell lines

Based on previous results obtained in cell lines isolated from osteosarcomas of *FosTg;Rsk2^{-/-}* mice, the first question was if pharmacological blockage of Rsk2 would affect cell division of *FosTg* osteosarcoma cells. For that purpose, the respective cell lines were treated with an inhibitor of Rsk (BI-D1870) at a dose of 10 μ M, as defined in the literature (Sapkota et al., 2007). It was found that treatment with BI-D1870 for 24 or 48 hours led to an accumulation of polynuclear cells, similar to what was previously observed for *FosTg;Rsk2^{-/-}* cell lines (Figure 7A). Quantitative analysis revealed that 20% of the cells were polynuclear after 24 hours of treatment with BI-D1870. After 48 hours of treatment this effect was even more pronounced with almost 50% of the cells treated with BI-D1870 carrying multiple nuclei (Figure 7B). Western blot analysis revealed that treatment with BI-D1870 for 24 hours strongly reduced the Rsk2 activating phosphorylation on serine 227 in *FosTg* cells (Figure 7C). Finally, whereas three independent *FosTg* cell lines continuously proliferated over an observation period of 6 days, BI-D1870 treatment resulted in a severe growth impairment of these cells (Figure 7D).

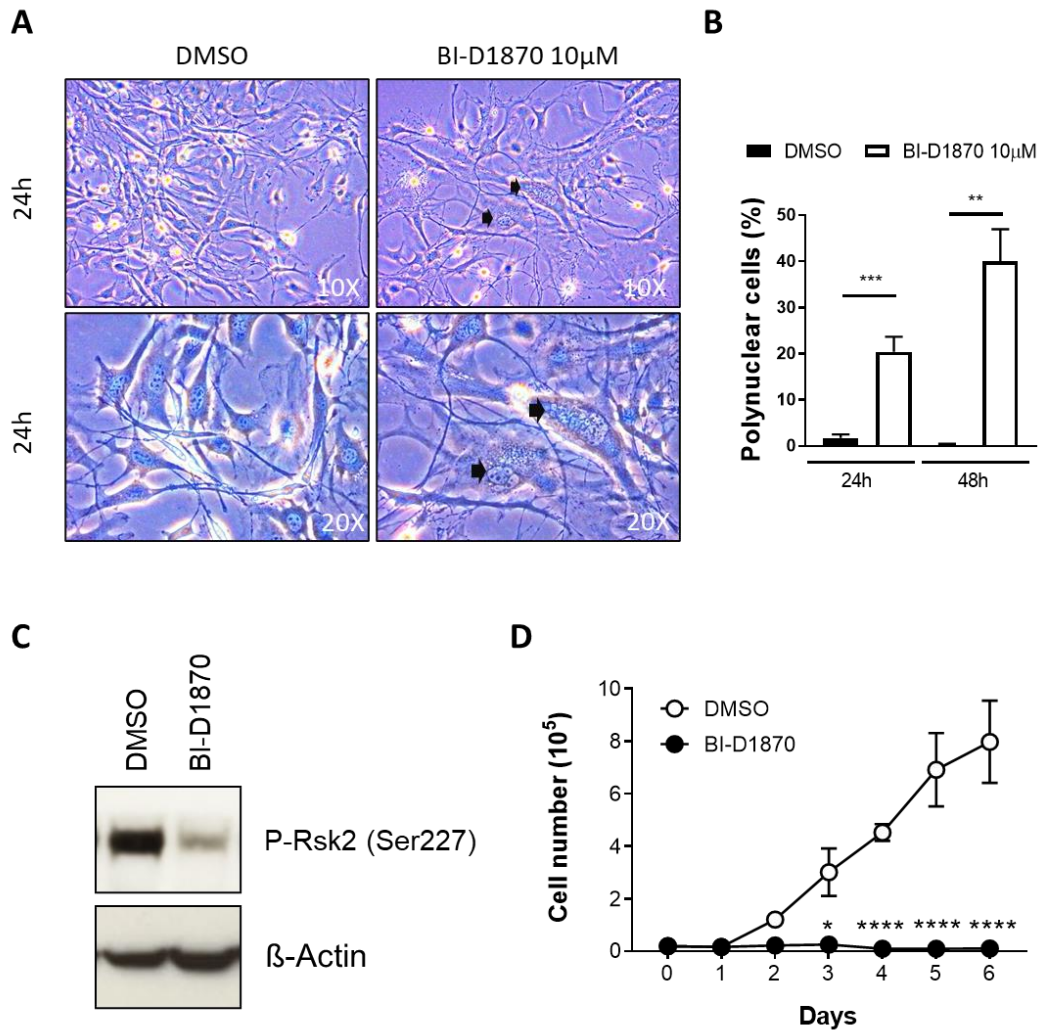


Figure 7: The Rsk inhibitor BI-D1870 impairs cell division of *FosTg* osteosarcoma cells.

A) Representative images of *FosTg* osteosarcoma cells treated for 24 hours with the Rsk inhibitor BI-D1870 (10 μM). Black arrows indicate the presence of polynuclear cells. **B)** Quantification of the percentage of polynuclear cells after treatment with vehicle (DMSO) or BI-D1870 (10 μM) for 24 and 48 hours. Data are expressed as mean ± SEM and analyzed by two-tailed Student's t test ** $p < 0.01$, *** $p < 0.001$ ($n = 4$ independent cell lines). **C)** Western blot analysis with antibodies detecting phosphorylated Rsk2 (serine 227) in protein extracts of *FosTg* cells treated with DMSO or BI-D1870 (10 μM). β-actin detection was used as a loading control. **D)** Growth curve analysis of *FosTg* cell lines treated with DMSO or BI-D1870 (10 μM). Data are expressed as mean ± SEM and analyzed by multiple comparison two-way ANOVA * $p < 0.05$, **** $p < 0.0001$.

In an attempt to define the cellular mechanism driving growth impairment and failure of undergoing complete mitosis, the expression of cell cycle genes was analyzed by quantitative real-time PCR (qPCR) of cells treated or not with BI-D1870 for 24 hours (Figure 8). It was found that treatment with BI-D1870 resulted in a lower expression of most relevant cell cycle genes,

like cyclins and their kinases (*Ccnd1*, *Cdk4*, *Cdk6*, *Cdk2*) or genes encoding proteins controlling the proper progression of the cell cycle (*Cdkn1a*, *Trp53*, *E2f2*). One of these genes was *AurkB*, coding for an aurora kinase which is known to have a critical function in mitosis and cytokinesis (Roy et al., 2022; Lens et al., 2010).

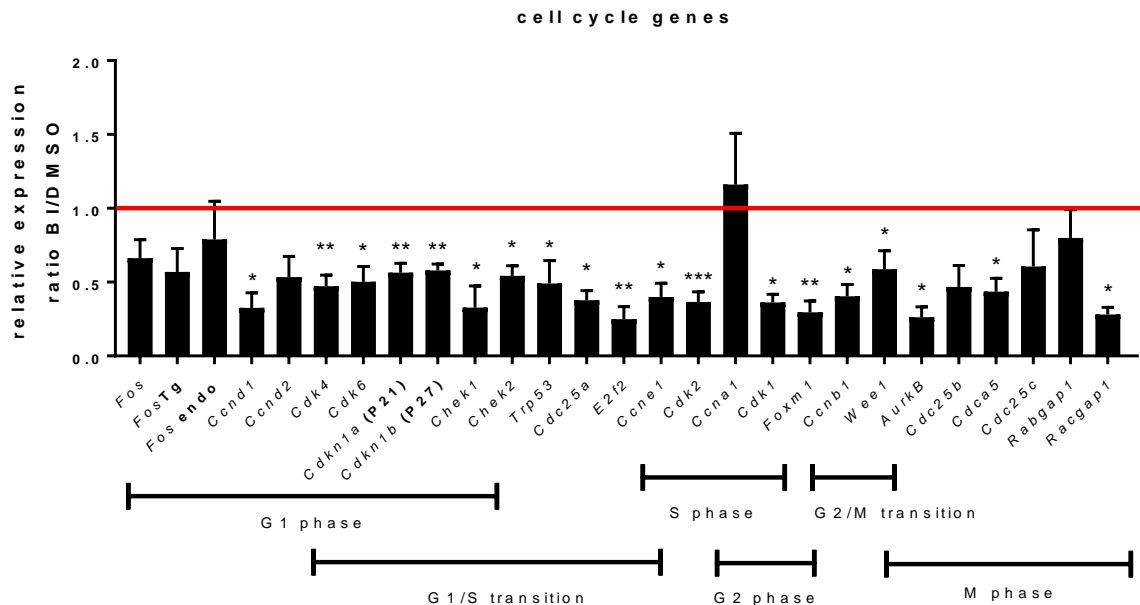


Figure 8: Reduced expression of specific cell cycle genes in *FosTg* osteosarcoma cells treated with BI-D1870.

qPCR expression analysis for the indicated genes in *FosTg* cells that were treated for 24 hours with BI-D1870 at the dose of 10 μ M. The graph shows the relative expression compared to *FosTg* cells treated with DMSO. The relevance of the selected genes for different phases of cell cycle progression is indicated below. Data are expressed as mean \pm SEM and analyzed by two-tailed paired Student's t test, vs DMSO * $p < 0.05$, ** $p < 0.01$, *** $p < 0.001$ (n=7 independent cell lines).

5.1.2. Influence of Aurora kinase B inhibition on *FosTg* osteosarcoma cells

Since several inhibitors of aurora kinases have been tested in clinical trials as anti-cancer agents (Dennis et al., 2012; Boss et al., 2011), Hesperadin and AZD1152, two selective inhibitors of Aurora kinase B, were chosen to treat the *FosTg* osteosarcoma cells. Here it was first assessed if treatment with these inhibitors for 24 hours would induce an accumulation of polynuclear cells. For visualization, the cytoskeleton was stained with phalloidin and the nuclei with DAPI (Figure 9A). Unlike it was the case in *FosTg* cells treated with BI-D1870, treatment with 200 nM AZD1152 did not lead to mitosis abnormalities. In contrast, the

treatment of *FosTg* cells with 100 nM Hesperadin resulted in the presence of multinucleated cells (up to 4 nuclei per cell), indicating a defect of cytokinesis similar to what was observed with BI-D1870 treatment (Figure 9B). Moreover, daily growth curve analysis demonstrated the growth defect of *FosTg* cells treated with Hesperadin compared to non-treated or AZD1152-treated cells (Figure 9C).

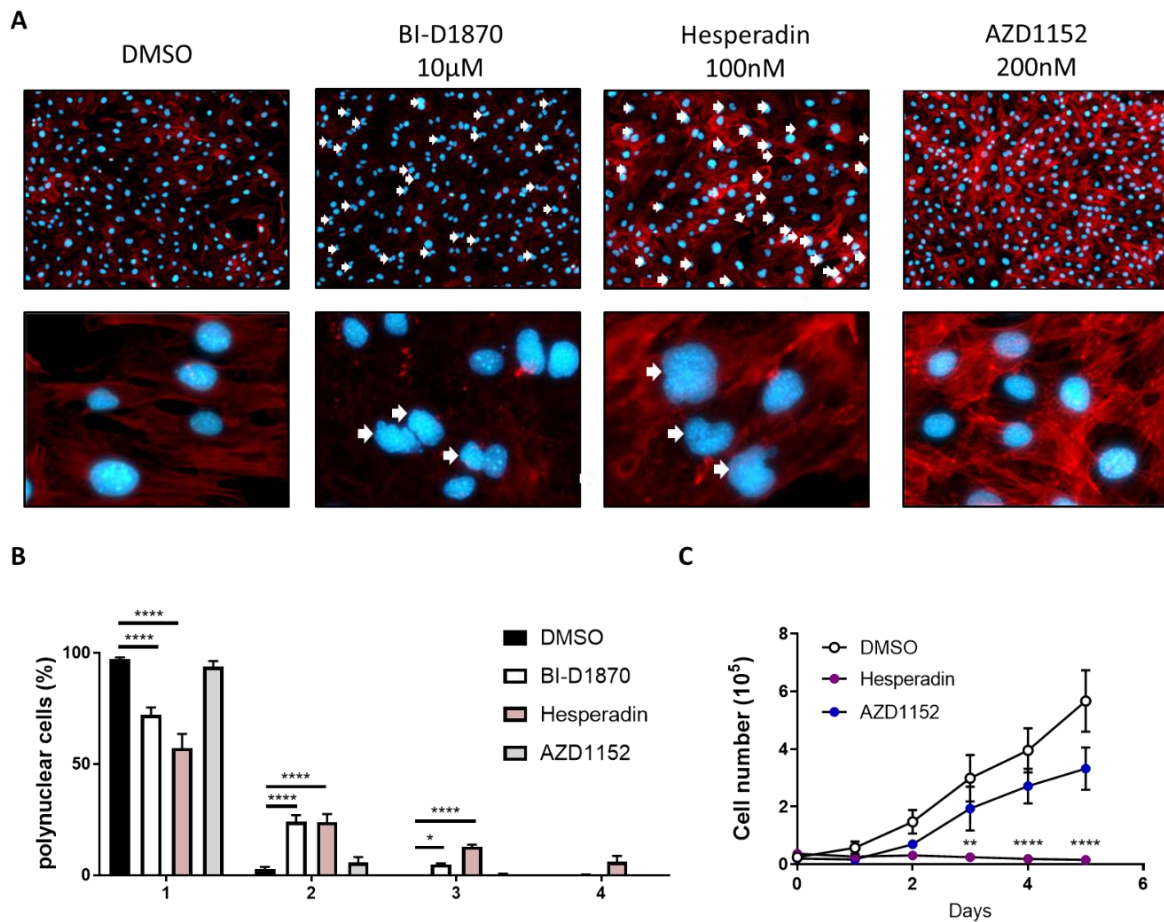


Figure 9: Hesperadin treatment induces polyploidy and impaired growth of *FosTg* cells.

A) Representative images of *FosTg* cell lines treated for 24 hours with DMSO, BI-D1870 (10 μM), Hesperadin (100 nM) or AZD1152 (200 nM) respectively. Nuclei were stained with DAPI and the cytoskeleton with phalloidin (40X). **B)** Quantification of the proportion of cells with 1, 2, 3 or 4 nuclei (n=3 independent cell lines) after 24 hours of respective treatments done using Image J cell counter. Data are expressed as mean ± SEM and analyzed by multiple comparisons two-way ANOVA *p<0.05, ****p<0.0001. **C)** Daily growth curve quantification during 5 consecutive days of *FosTg* cells treated at day 0 with either DMSO (control), Hesperadin (100 nM) or AZD1152 (200 nM). Data were analyzed by two-way ANOVA, vs DMSO *p< 0.05, ***p< 0.001 (n=3 independent cell lines quantified in triplicates).

Finally, the expression of cell cycle genes after treatment with Hesperadin for 24 hours was monitored by qPCR in order to analyze if genes regulated by inhibition of Rsk were also repressed after treatment with an Aurora kinase B inhibitor. Indeed, similar to what was observed for BI-D1870, Hesperadin caused an overall reduction in the expression of different genes, especially the ones expressed in the critical G2/M transition phase (Figure 10).

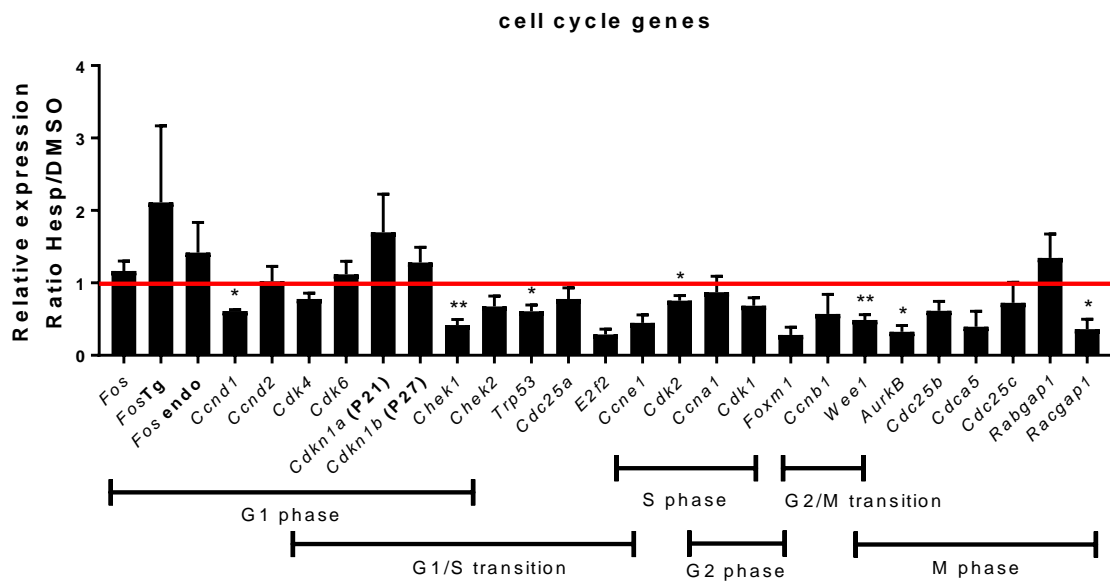


Figure 10: Hesperadin treatment reduces expression of specific cell cycle genes in *FosTg* osteosarcoma cells.

FosTg cells were treated for 24 hours with Hesperadin at the dose of 100 nM and gene expression was analyzed by qPCR. The graph represents the ratio of all genes expression under Hesperadin treatment relative to the expression of cells treated with DMSO. Data are expressed as mean \pm SEM and analyzed by two-tailed paired Student's t test, vs DMSO *p < 0.05, **p < 0.01 (n=4 independent cell lines).

Although these data were not fully unexpected, as Aurora kinase B is known to act as a regulator of G2/M cell cycle checkpoint genes (Terada et al., 1998), they were quite promising in terms of a potential therapeutic option to limit osteosarcoma growth. Therefore, it was also important to assess the efficacy of lower Hesperadin doses with respect to the inhibition of *FosTg* osteosarcoma cell growth. Here it was found that Hesperadin at a concentration of 25 nM was already sufficient to mediate an inhibitory influence on the growth of 3 different *FosTg* cell lines (Figure 11A). Likewise, this dose of Hesperadin resulted in the presence of polynuclear cells after 24 hours of treatment (Figure 11B-C).

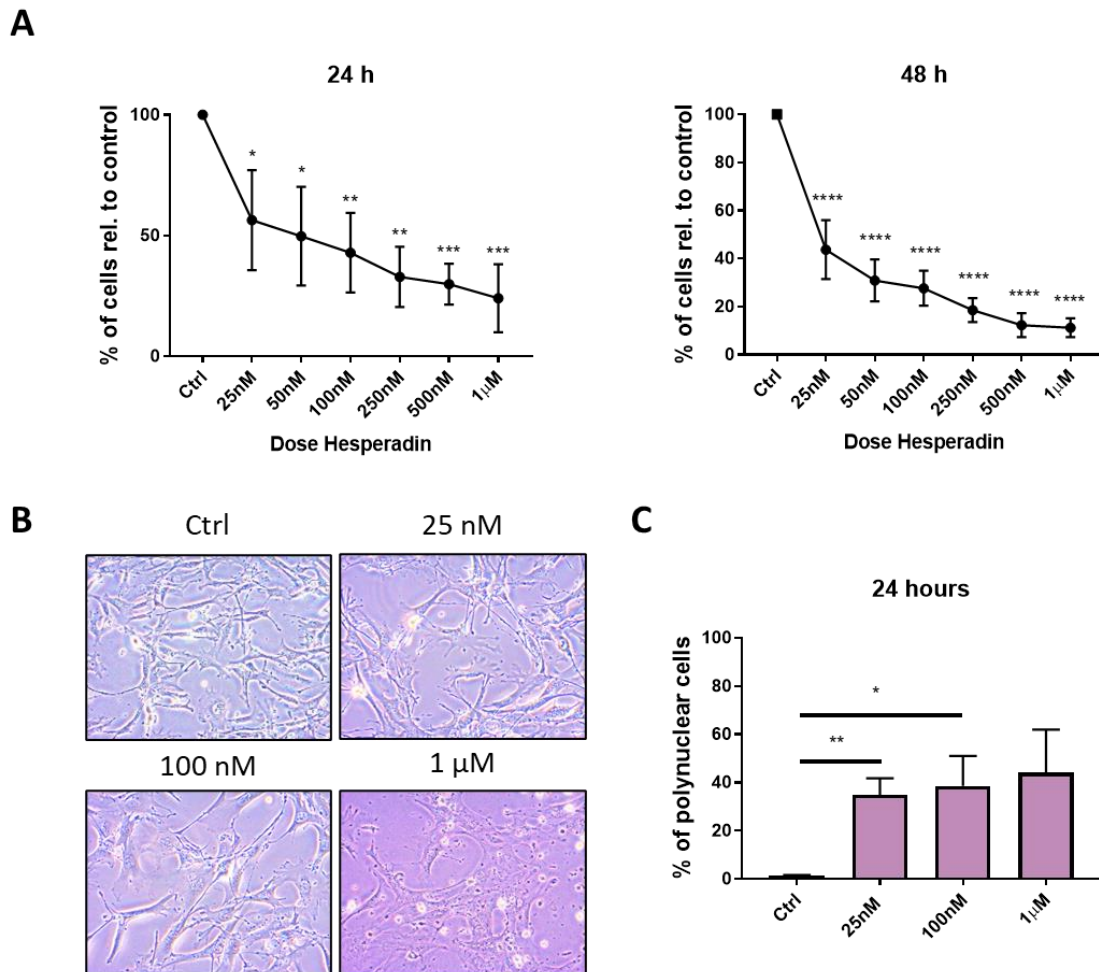


Figure 11: A dose of 25 nM Hesperadin is sufficient to induce polyploidy of *FosTg* osteosarcoma cells.

A) Dose effect curves of Hesperadin on *FosTg* cell lines treated for 24 or 48 hours. (n=3 independent cell lines) **B)** Representative images of *FosTg* cells treated with 0 nM, 25 nM, 100 nM or 1 µM of Hesperadin. **C)** Quantification of polynuclear cells after 24 hours with the respective treatment doses. Data are expressed as mean ± SEM and analyzed by two-tailed Student's t test *p<0.05, **p< 0.01, ****p<0.0001 (n=5 independent cell lines).

5.1.3. Pharmacological growth inhibition of a human osteosarcoma cell line

To determine if BI-D1870 or Hesperadin also cause a growth arrest not only in osteosarcoma cell lines from *FosTg* mice, their influence on an established human osteosarcoma cell line (U2OS) was analyzed (Figure 12A). BI-D1870 and Hesperadin treatment induced the polynucleation of these cells after 24 hours, as visualized by immunofluorescence microscopy (Figure 12B). Moreover, counting of these cells during 6 consecutive days revealed a cell growth impairment of U2OS treated with the two inhibitors compared to DMSO (Figure 12C).

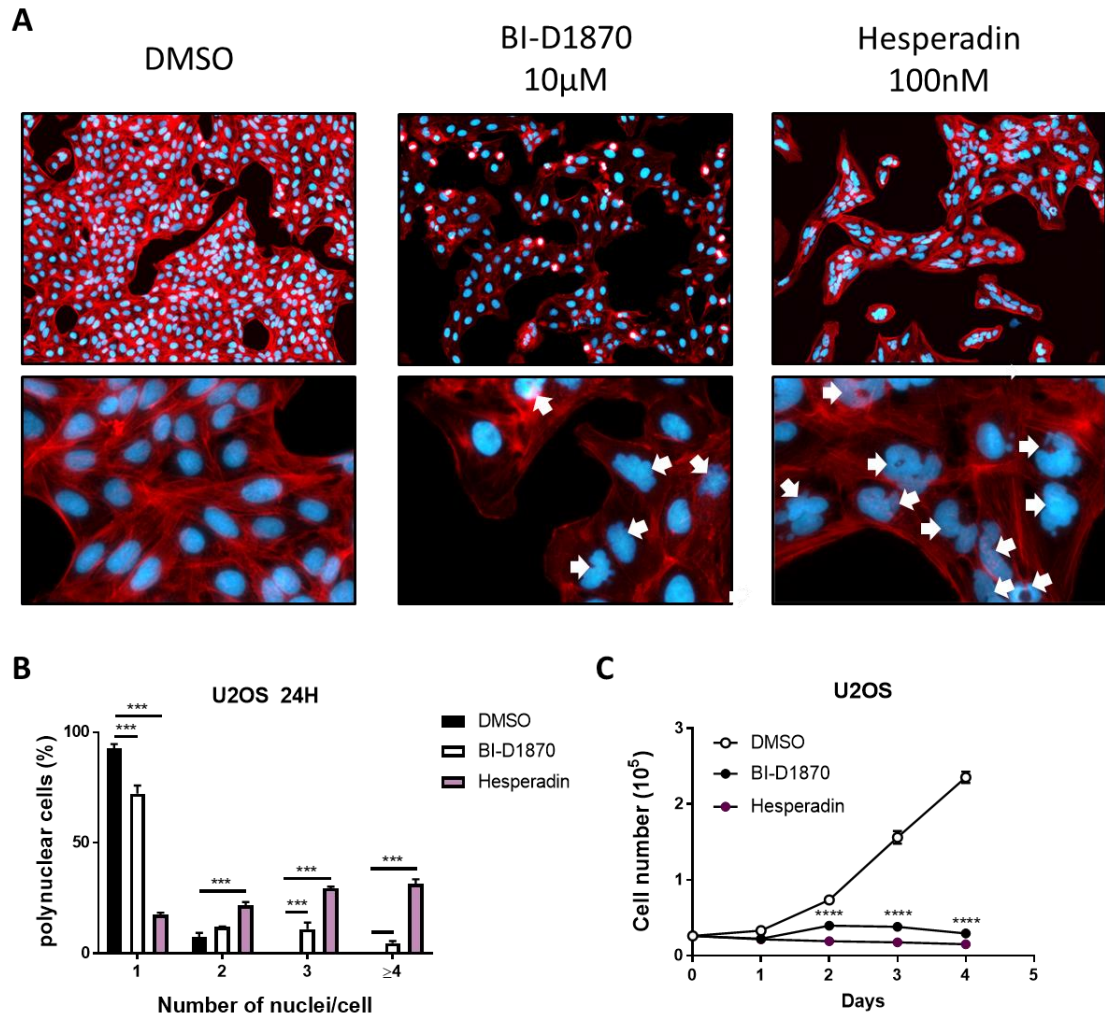


Figure 12: U2OS are sensitive to BI-D1870 and Hesperadin treatment.

A) Representative images of U2OS cells (human osteosarcoma cell line) treated for 24 hours with DMSO, BI-D1870 (10 μ M) or Hesperadin (100 nM) respectively (40X). **B)** Quantification of U2OS polynuclear cells after 24 hours of respective treatments. **C)** Daily growth curve quantification during 5 consecutive days of U2OS cells treated at day 0 with either DMSO (control) or Hesperadin (100 nM). Data were analyzed by two-way ANOVA, vs DMSO ***p < 0.001 (n=3).

In conclusion, this first part of the thesis, demonstrated that pharmacological Rsk inhibition induces a cell cycle arrest of *Rsk2*-deficient *FosTg* osteosarcoma cells by impairing proper cell division. Similar results were obtained with an established inhibitor of aurora kinase B, which was found to be effective at a much lower concentration. Whether Hesperadin treatment can be considered as a potential drug to reduce osteosarcoma growth remains to be further elucidated. Importantly however, since Rsk proteins and aurora kinases are also relevant for non-skeletal cell types, the second part of this thesis aimed at analyzing the impact of Lrp5 on

osteosarcoma growth, as mutations in the respective gene specifically affect osteoblast differentiation.

5.2. Impact of *Lrp5* on osteosarcoma development in *FosTg* mice

5.2.1. Generation and analysis of *FosTg* mice with different *Lrp5* genotypes

To address the question if either *Lrp5* activation or inactivation would impact osteosarcoma growth in *FosTg* mice, two mouse models were utilized. The first model (*Lrp5*^{A213V/+}) carries an activating mutation of *Lrp5*, which causes increased osteoblastogenesis and bone formation, thus resulting in a high bone mass phenotype (Cui et al., 2011). The second model (*Lrp5*^{-/-}) is deficient for *Lrp5*, which impairs osteoblastogenesis and bone formation, thereby causing osteoporosis (Clément-Lacroix et al., 2005; Kato et al., 2002). Cross-breedings of *FosTg* with *Lrp5*^{-/-} or *Lrp5*^{A213V/+} mice were set up to eventually generate wildtype, *Lrp5*^{-/-} and *Lrp5*^{A213V/+} littermates, either without or with the *Fos* transgene. These mice were first analyzed at 16 weeks of age by μ CT analysis of the femora (Figure 13A). Quantification of the trabecular number (Figure 13B) and the cortical thickness (Figure 13C) confirmed that *Lrp5*^{-/-} mice displayed low bone mass, whereas *Lrp5*^{A213V/+} animals showed significantly increased parameters compared to wildtype littermates. In principle, the same results were obtained in mice additionally carrying the *Fos* transgene. However, in these animals the quantification of the cortical thickness was hampered by the presence of tumors in the measurement area.

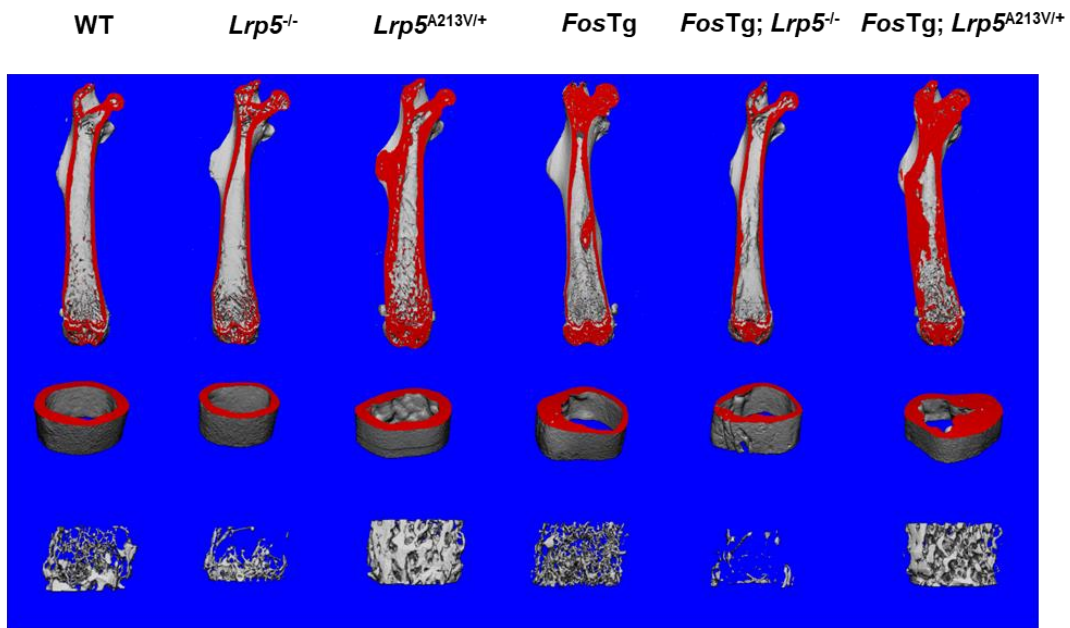
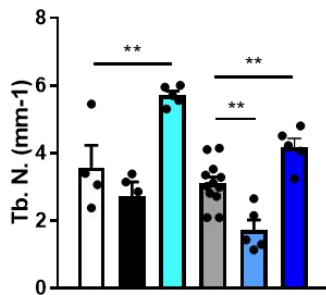
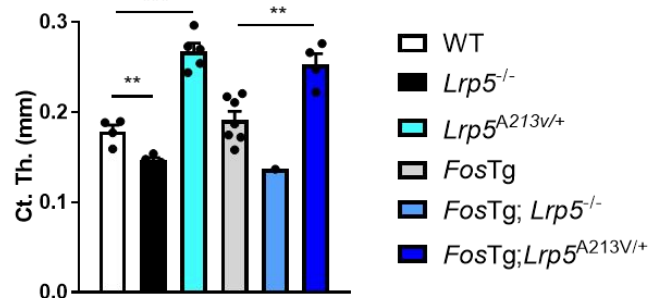
A**B****C**

Figure 13: μ CT of femora from wildtype and *FosTg* mice with different *Lrp5* genotypes.

A) Representative μ CT images of femora from 16 week-old mice with the indicated genotypes. **B)** Quantification of the trabecular number (Tb.N.) **C)** Quantification of cortical thickness (Ct.Th.) Data are expressed as mean \pm SEM and analyzed by two-tailed Student's t test ** $p < 0.01$, *** $p < 0.001$.

As *FosTg* mice were previously found to develop severe lipodystrophy with increasing age, the body weight of all mice was also monitored. Here it was found that female and male *FosTg* mice, regardless of the *Lrp5* genotype, displayed a moderately reduced body weight compared to wildtype controls (Figure 14A-B).

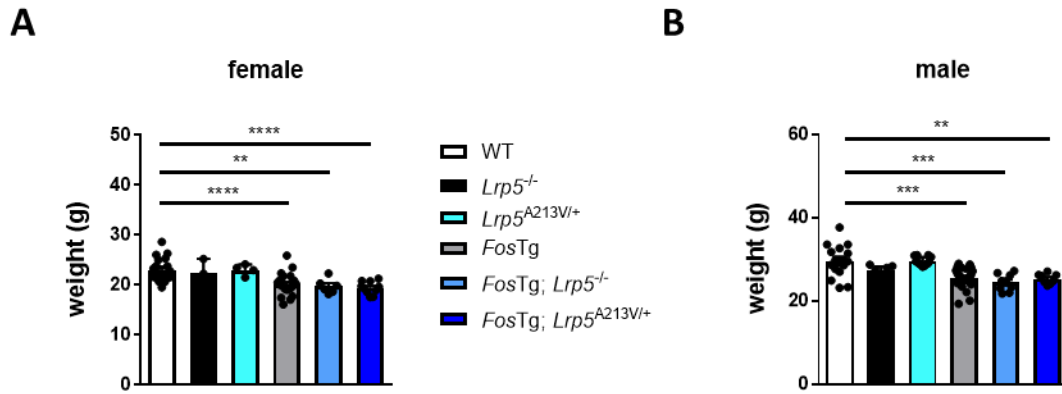


Figure 14: Body weight of 16 week-old wildtype or *FosTg* mice with different *Lrp5* genotypes.

A-B) Body weight of 16 week-old female (**A**) and male (**B**) mice with the indicated genotypes. (n= 4-13 mice per genotype) Data are expressed as mean \pm SEM and analyzed by two-tailed Student's t test vs WT **p< 0.01, ***p<0.001, ****p<0.0001.

Furthermore, the weight of different organs was quantified in the different groups of mice (Figure 15). Whereas no significant differences were observed for the weight of most organs, the weight of white fat was reduced in *FosTg* mice independent of the *Lrp5* genotype. On the other hand, these data showed that at the age of 16 weeks dramatic side-effects, such as severe lipodystrophy, caused by osteosarcoma formation were not fully pronounced yet.

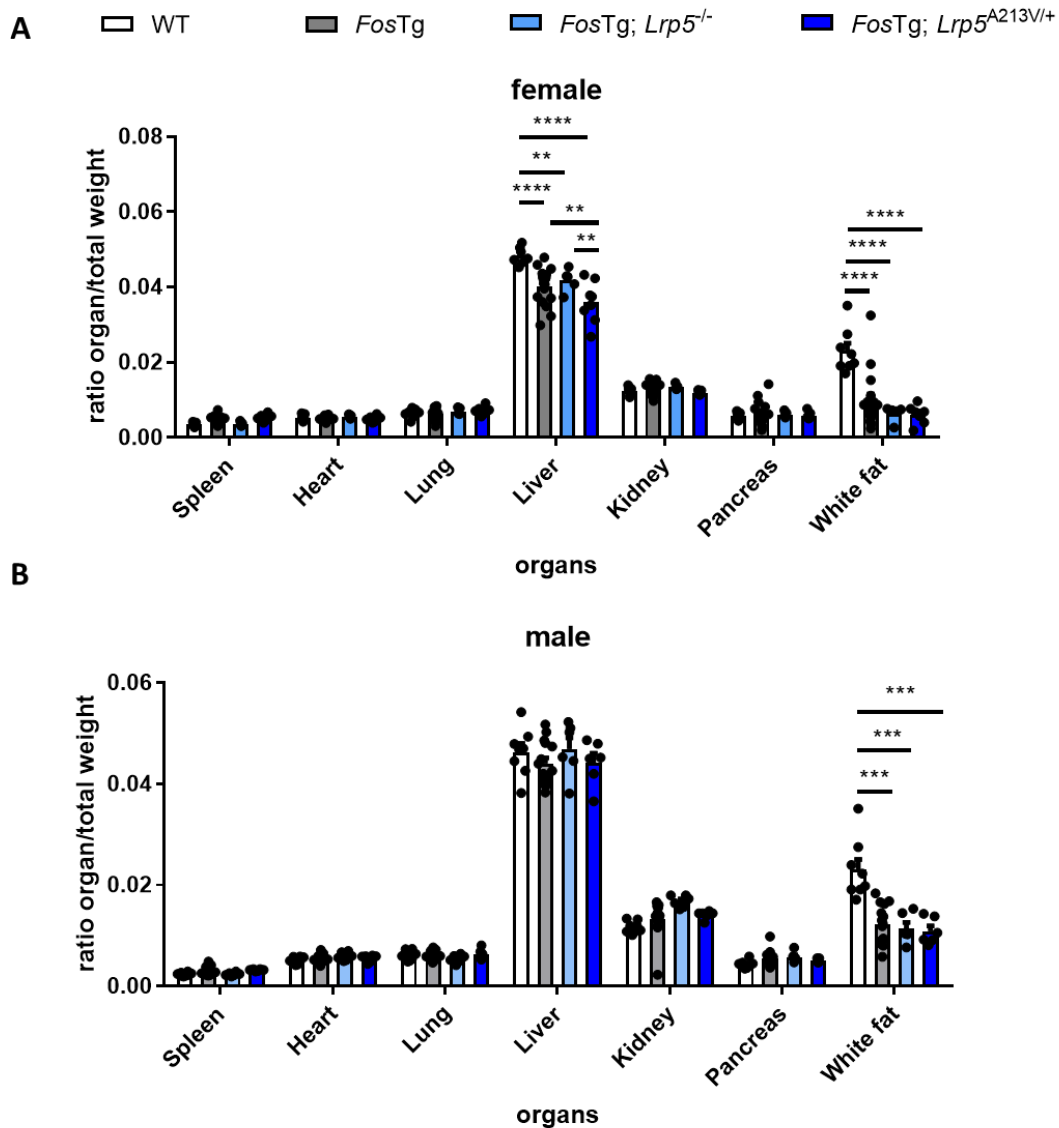


Figure 15: Organ weights of 16 week-old wildtype or *FosTg* mice with different *Lrp5* genotypes.

Organ weights (relative to body weight) in 16 week-old female (**A**) and male (**B**) mice of the indicated genotypes. (n=6-13 mice per genotype) Data are expressed as mean \pm SEM and analyzed by ANOVA: **p<0.01, ***p<0.001, ****p<0.0001.

5.2.2. Influence of *Lrp5* on osteosarcoma growth in *FosTg* mice

Since the central focus of this project was related to the impact of *Lrp5* on osteosarcoma growth, the number of visible tumors was first evaluated by analyzing contact Xrays of the whole skeleton. Although there was a high variability of the *FosTg* osteosarcoma phenotype, a significant reduction of the visible tumor number was observed in head, arms and spine in *Lrp5*-deficient *FosTg* mice (Figure 16). The number of tumors in *FosTg* mice carrying the

activating *Lrp5* allele (*FosTg;Lrp5^{A213V/+}*) was hard to evaluate, especially in the spine, as their bones appeared overexposed on Xrays due to their high bone mass phenotype. Despite this fact, however, no significant differences in the number of visible tumors were identified on Xrays between *FosTg* and *FosTg;Lrp5^{A213V/+}* mice.

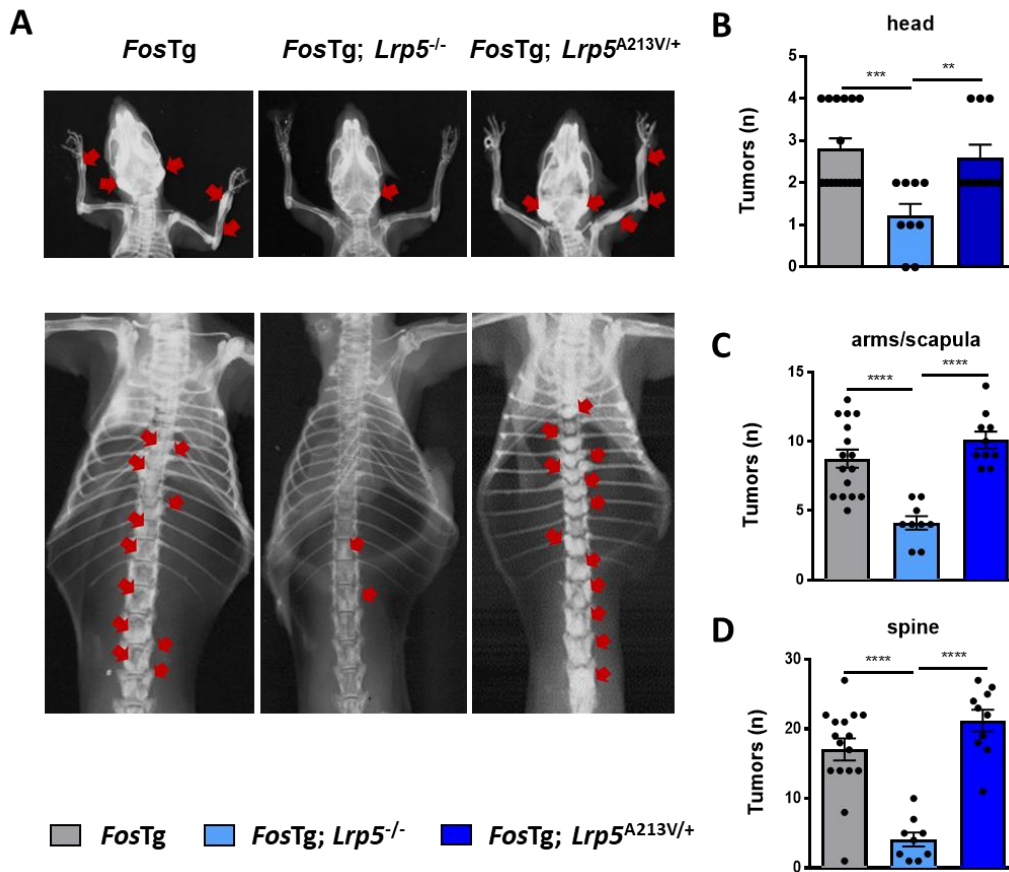


Figure 16: Reduction of osteosarcoma number in *FosTg/Lrp5*-deficient mice (upper body).

A) Xray images of 16 week-old mice with the indicated genotypes. Red arrows indicate the presence of osteosarcomas. Quantification of the number of visible tumors on Xrays in the head (**B**) arms and scapula (**C**) or spine (**D**) in mice. Data are expressed as mean \pm SEM and analyzed by one-way ANOVA: ** $p < 0.01$, *** $p < 0.001$, **** $p < 0.0001$ ($n = 9-16$ mice per genotype).

Osteosarcomas of varying sizes were also visible in the hips and legs of *FosTg* mice. Here the number of visible tumors was also significantly reduced in *Lrp5*-deficient *FosTg* mice (Figure 17). It is further essential to state that there was no difference between male and female mice regarding osteosarcoma development, which explains why the respective data were combined.

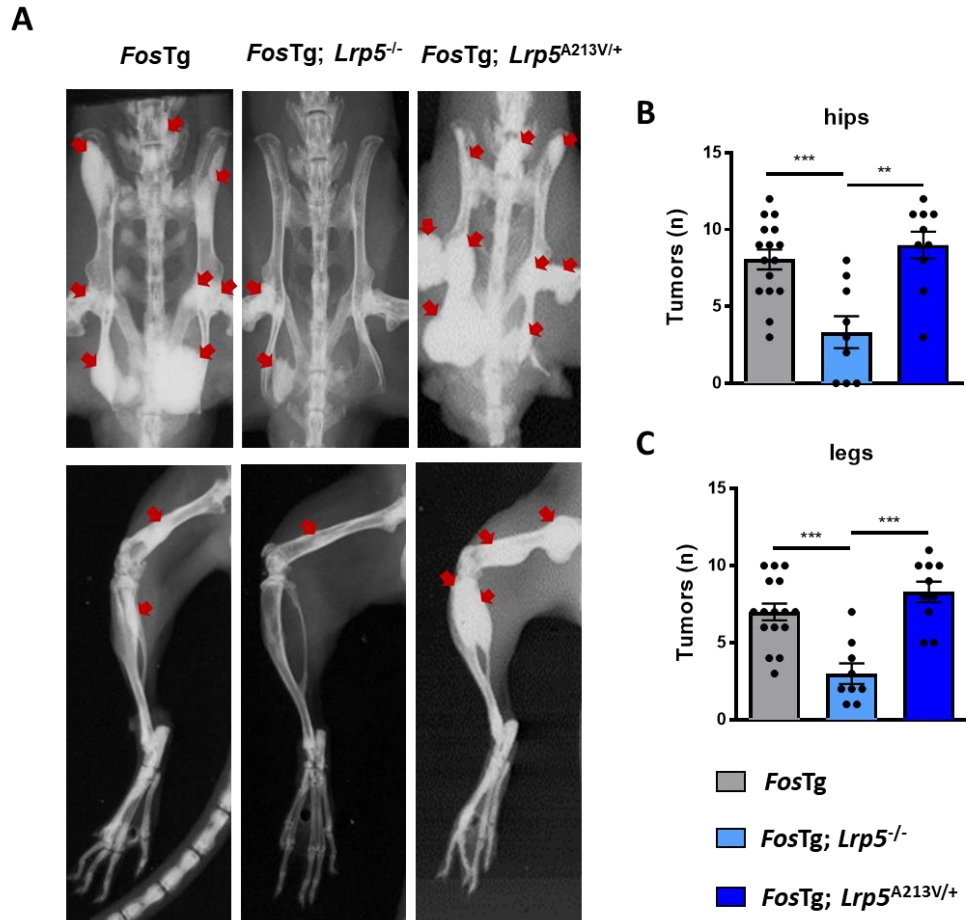


Figure 17: Reduction of osteosarcoma number in *FosTg/Lrp5*-deficient mice (lower body).

A) Xray images of 16 week-old mice with the indicated genotypes. Red arrows indicate the presence of osteosarcomas. Quantification of visible tumors in hips (**B**) or legs (**C**) in mice with the respective genotypes. Data are expressed as mean \pm SEM and analyzed by one-way ANOVA: ** $p < 0.01$, *** $p < 0.001$ (n=9-16 mice per genotype).

Given the striking differences between *FosTg* mice with different *Lrp5* genotypes, serum analysis was performed by ELISA to monitor bone formation and resorption markers. It was found that procollagen-type 1 N-terminal peptide (PINP), a marker of bone formation, was significantly increased in the serum of *FosTg* and *FosTg;Lrp5^{A213V/+}* mice compared to wildtype controls and *FosTg;Lrp5^{-/-}* mice (Figure 18A). Moreover, levels of C-terminal collagen crosslinks (CTX), serving as a biomarker of bone resorption, were also changed to the similar extent between the mice of the different genotypes (Figure 18B). Collectively, these findings do not only indicate that the osteosarcomas, due to excessive formation and remodelling, cause a striking increase of bone turnover markers in the serum, but also confirm that *Lrp5* deficiency strongly reduces this pathology. Since previous evidence suggested that an

increased bone remodelling also affects glucose homeostasis (Ferron et al., 2012), glucose levels were also determined in the serum, but here no differences were observed (Figure 18C).

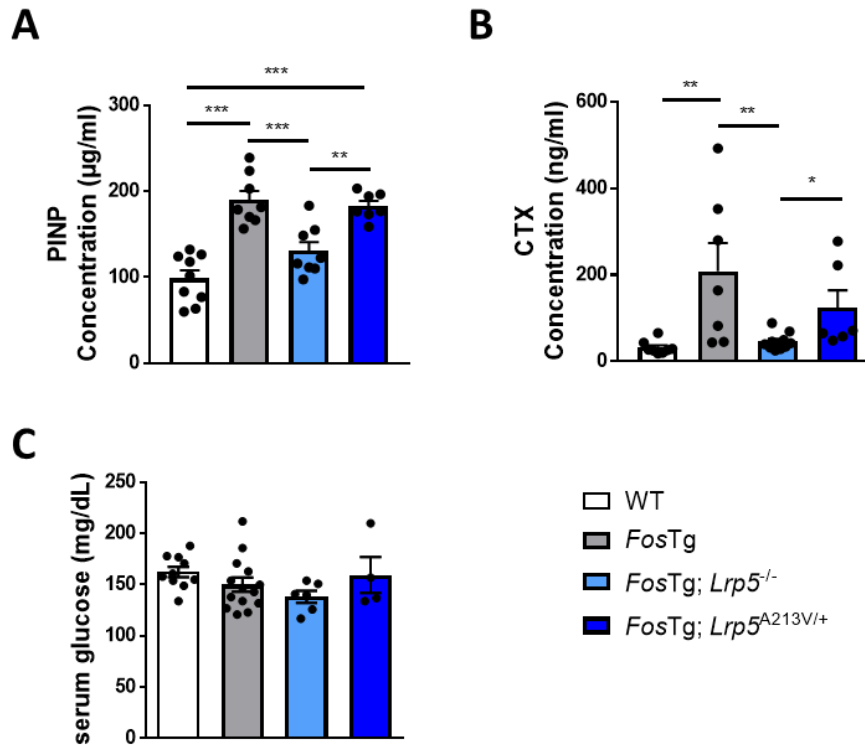


Figure 18: Increased levels of bone turnover biomarkers in the serum of *FosTg* mice.

A) Serum concentrations of procollagen type 1 N-terminal propeptide (PINP), a biomarker of bone formation in mice with the indicated genotypes. **B)** Serum concentrations of carboxyterminal collagen crosslinks (CTX), a biomarker of bone resorption in the same mice. Data are expressed as mean \pm SEM and analyzed by one-way ANOVA: * $p < 0.05$, ** $p < 0.01$, *** $p < 0.001$. **C)** Serum glucose concentrations in 16-week-old male mice of the indicated genotypes. Data are expressed as mean \pm SEM.

5.2.3 Histomorphometric analysis of osteosarcomas in *FosTg* mice with different *Lrp5* genotypes

To allow a robust statistical analysis regarding the volume of the osteosarcomas, undecalcified histology of the spine from *FosTg* mice with different *Lrp5* genotypes was applied. Here sections from 8 vertebral bodies per mouse were stained and analyzed for the presence of tumors. In the absence of the *Fos* transgene, the expected low bone mass phenotype of *Lrp5^{-/-}* mice was observed, whereas *Lrp5^{A213V/+}* mice displayed high bone mass (Figure 19A). In the presence of the *Fos* transgene, osteosarcomas were visible in mice of all

Lrp5 genotypes, but their size was remarkably different (Figure 19B). The precise quantification of tumors on these sections revealed that in *FosTg;Lrp5^{A213V/+}* mice the number and size of tumors were significantly increased (Figure 19C-D). Most importantly however, although the number of osteosarcomas was moderately significantly decreased in vertebral sections from *FosTg;Lrp5^{-/-}* mice, there was a drastic reduction of the tumor volume in the absence of *Lrp5*.

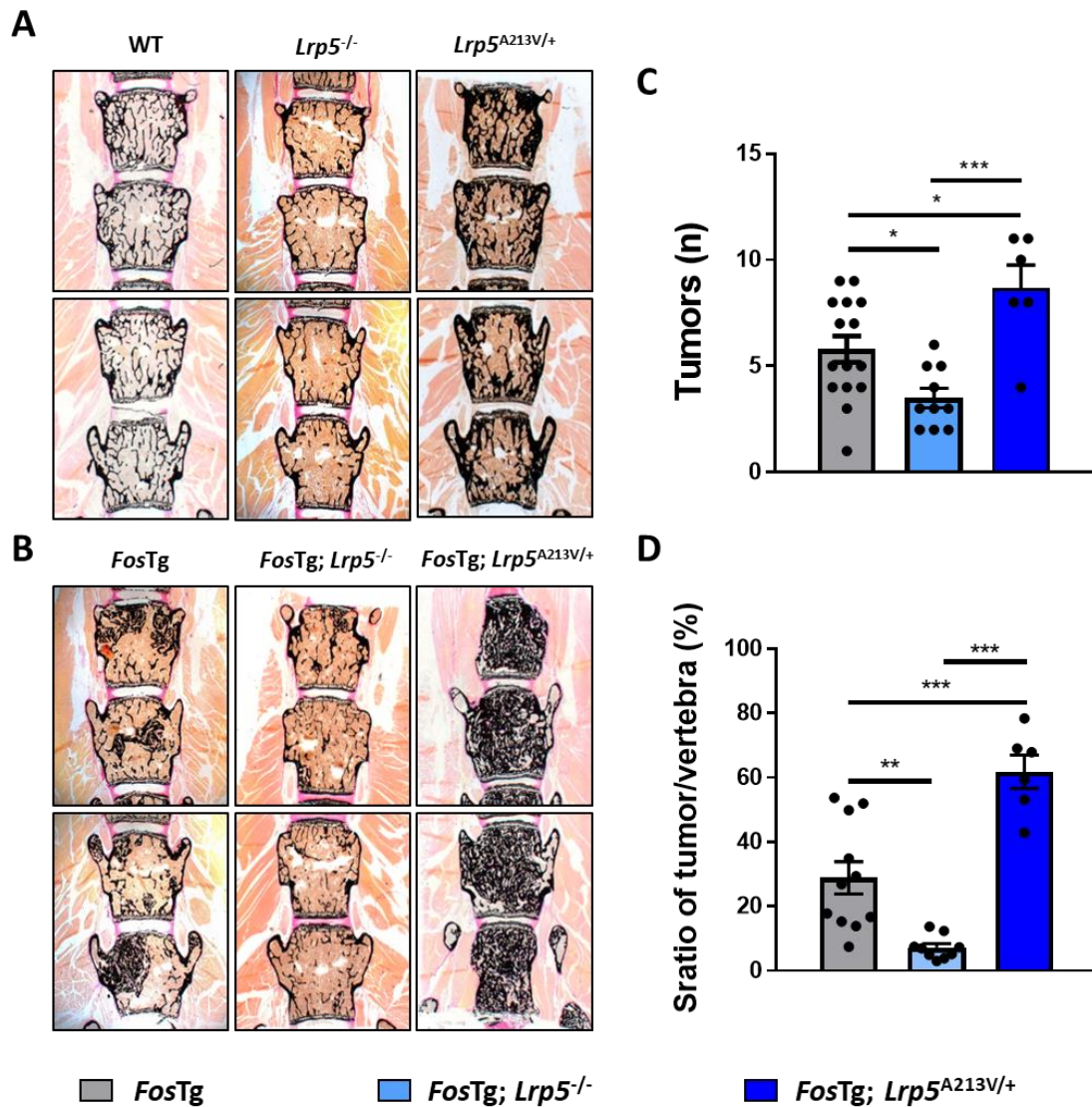


Figure 19: The tumor volume in spine sections of *FosTg* mice is significantly affected by the *Lrp5* genotype.

A-B) Representative images of undecalcified spine sections after Kossa-staining. **C)** Quantification of the number of tumors in spine sections (lumbar vertebral bodies L1-L4) from mice with the indicated genotypes. **D)** Quantification of tumor volume by measuring the surface ratio of tumors on the total vertebral body surface. Data are expressed as mean \pm SEM and analyzed by one-way ANOVA: * $p < 0.05$, ** $p < 0.01$, *** $p < 0.001$ (n=6-9 mice).

To further analyze, how the *Lrp5* genotype affects the composition of the identified osteosarcomas, histomorphometric quantification was performed. Here it was found that the bone volume per tissue volume (BV/TV) inside the tumors was significantly increased in the *FosTg;Lrp5^{A213V/+}* mice, indicative of a higher bone density (Figure 20).

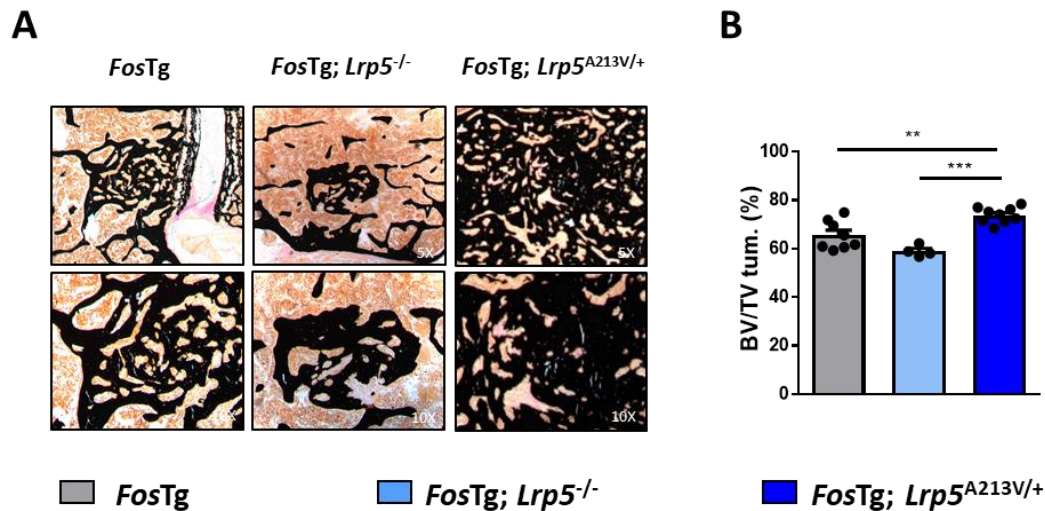


Figure 20: Increased bone volume inside the osteosarcomas of *FosTg;Lrp5^{A213V/+}* mice.

A) Representative images of osteosarcomas in vertebral bodies from mice with the indicated genotypes after Kossa-staining. **B)** Quantification of the bone volume per tissue volume (BV/TV) inside the tumors. Data are expressed as mean \pm SEM and analyzed by one-way ANOVA: ** $p < 0.01$, *** $p < 0.001$ (n=5-9 mice).

It was also evident that some of the osteosarcomas, especially in the *FosTg;Lrp5^{-/-}* mice, were characterized by an accumulation of non-mineralized osteoid (Figure 21A). Although this pathology was quite variable, a quantification of the osteoid volume per bone volume confirmed that *FosTg;Lrp5^{-/-}* tumors had a significant enrichment of osteoid compared to tumors from *FosTg* or *FosTg;Lrp5^{A213V/+}* mice (Figure 21B).

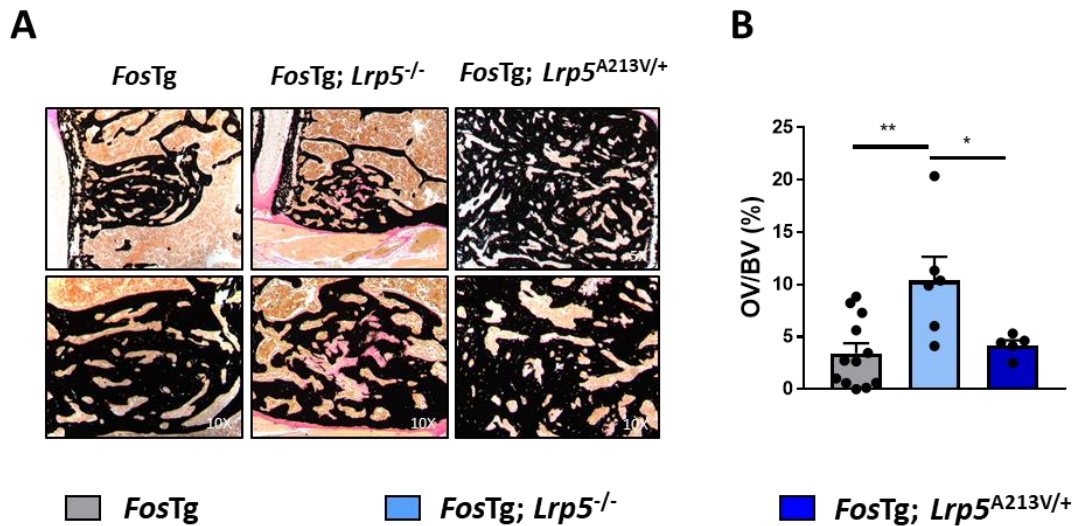


Figure 21: Increased osteoid volume inside osteosarcomas from *FosTg;Lrp5^{-/-}* mice.

A) Representative images of osteosarcomas in vertebral bodies from mice with the indicated genotypes after Kossa-staining. Pink areas represent non-mineralized osteoid. **B)** Quantification of osteoid volume per bone volume (OV/BV). Data are expressed as mean \pm SEM and analyzed by one-way ANOVA: * $p < 0.05$, ** $p < 0.01$.

To define the cellular composition of the osteosarcoma in the different groups of mice, sections stained with Toluidine blue were histomorphometrically analyzed (Figure 22A). Here, a significant decrease in the number of osteoblasts and osteocytes per bone perimeter was observed in the *FosTg;Lrp5^{-/-}* tumors (Figure 22B). No significant differences for these parameters were found between *FosTg* and *FosTg;Lrp5^{A213V/+}* mice. Moreover, osteoclast number per bone parameter was not changed between the different genotypes.

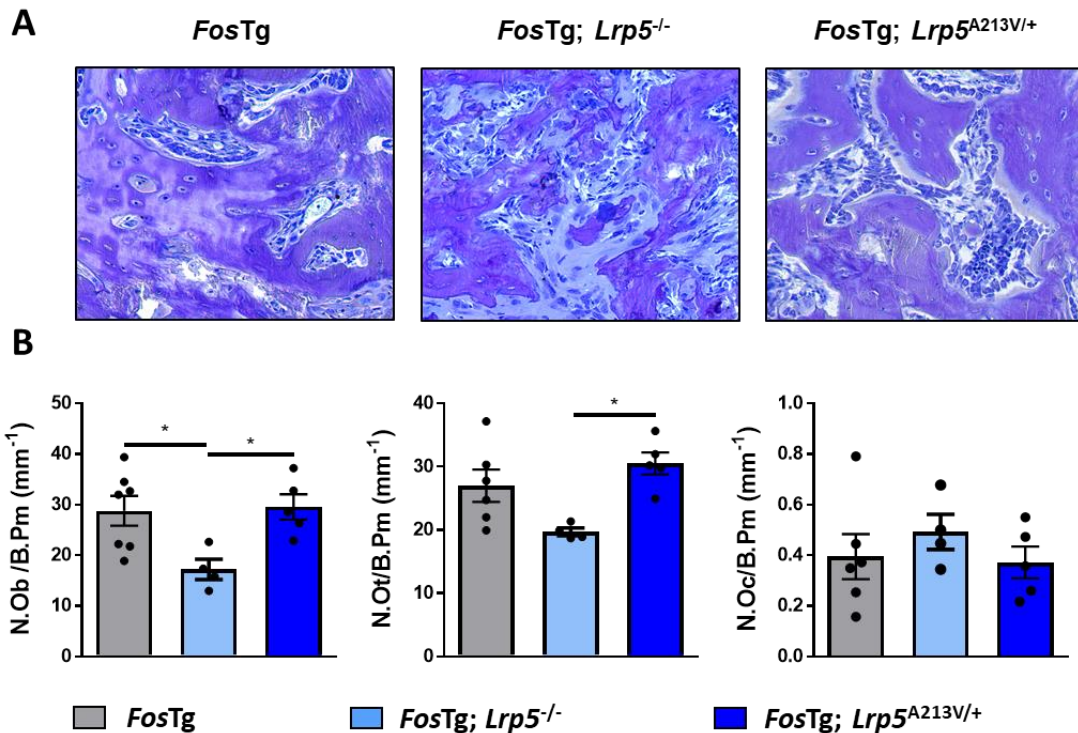


Figure 22: Decreased number of osteoblasts and osteocytes inside *FosTg;Lrp5^{-/-}* osteosarcomas.

A) Representative images of osteosarcomas on undecalcified spine sections from mice with the indicated genotypes after staining with toluidine blue, red arrows indicate osteoblasts. **B)** Quantification of osteoblast number (N.Ob/B.Pm), osteocyte number per bone perimeter (N.Ot/B.Pm) and osteoclast number per bone perimeter (N.Oc/B.Pm). Data are expressed as mean \pm SEM and analyzed by one-way ANOVA: * $p < 0.05$.

Whereas these differences inside the tumor were rather moderate, a more obvious difference between the genotypes was found at the tumor surface (Figure 23A). Here, the number of osteoblasts present in *FosTg;Lrp5^{-/-}* mice was significantly reduced compared to *FosTg* and *FosTg;Lrp5^{A213V/+}* mice (Figure 23B). Interestingly the osteoid surface per tumor surface was even more reduced in *FosTg;Lrp5^{-/-}* mice, suggesting that even so osteoblasts were found at the surface of *FosTg;Lrp5^{-/-}* osteosarcomas, they were less actively producing bone matrix.

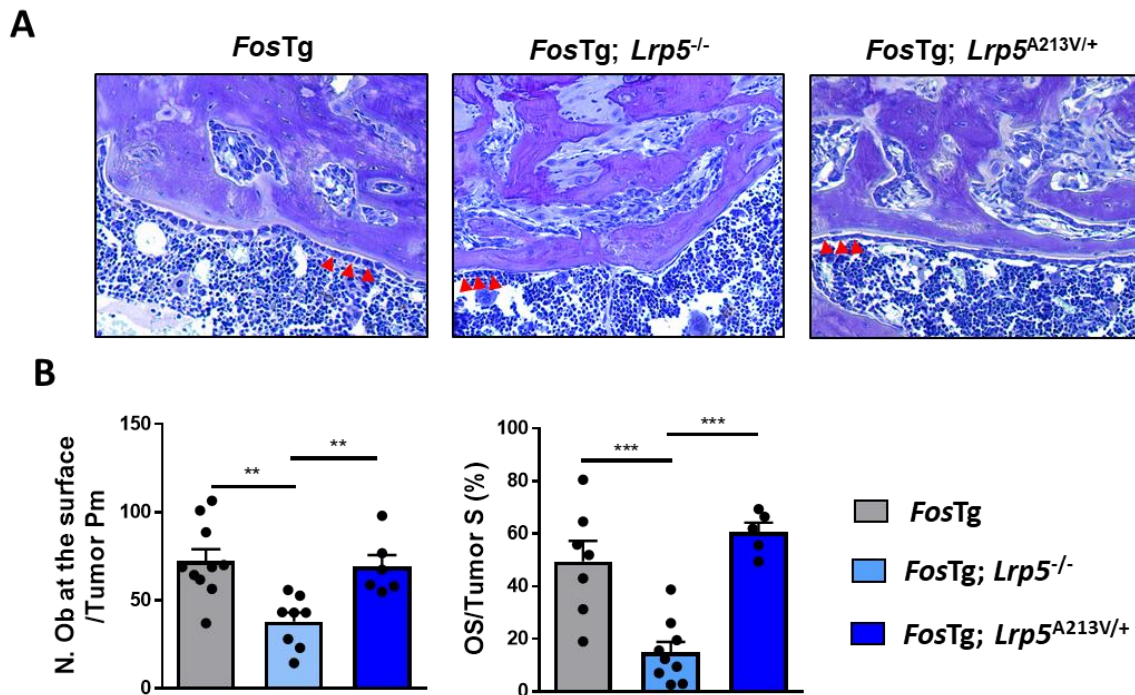


Figure 23: Reduced number of active osteoblasts at the tumor surface of *FosTg;Lrp5^{-/-}* mice.
A) Representative images of osteosarcoma surfaces from mice with the indicated genotypes after staining with toluidine blue, red arrows indicate some osteoblasts. **B)** Quantification of tumor surface osteoblasts (N.Ob at the surface/Tumor Pm) and osteoid production quantified by the ratio of osteoid surface on tumor surface (OS/Tumor S). Data are expressed as mean ± SEM and analyzed by one-way ANOVA: **p<0.01, ***p<0.001 (n=5-9 mice).

Taken together, these results clearly demonstrated that Lrp5 inactivation strongly reduces the growth of osteosarcomas in *FosTg* mice to a similar extent as previously shown for Rsk2 inactivation (David et al., 2005). Based on these findings several other approaches were initiated in an attempt to understand the underlying mechanisms.

5.2.4. Isolation and characterization of osteosarcoma cell lines derived from *FosTg* mice with *Lrp5* activation or inactivation

With the aim to achieve a molecular characterization of the *Lrp5* function in osteosarcoma growth, independent of tumor heterogeneity, cell lines were isolated from osteosarcomas of at least three mice per genotype. Importantly, none of these cell lines displayed an accumulation of polynuclear cells, thereby demonstrating that *Lrp5* deficiency limits osteosarcoma growth by different mechanisms compared to what has been previously described for *Rsk2* deficiency (Figure 24A). This was also supported by analyzing the growth of these cells. Here, *FosTg;Lrp5^{-/-}* cells did not show decreased proliferation, and the growth of the osteosarcoma cells was not impacted either by *Lrp5* deficiency or *Lrp5* activation (Figure 24B).

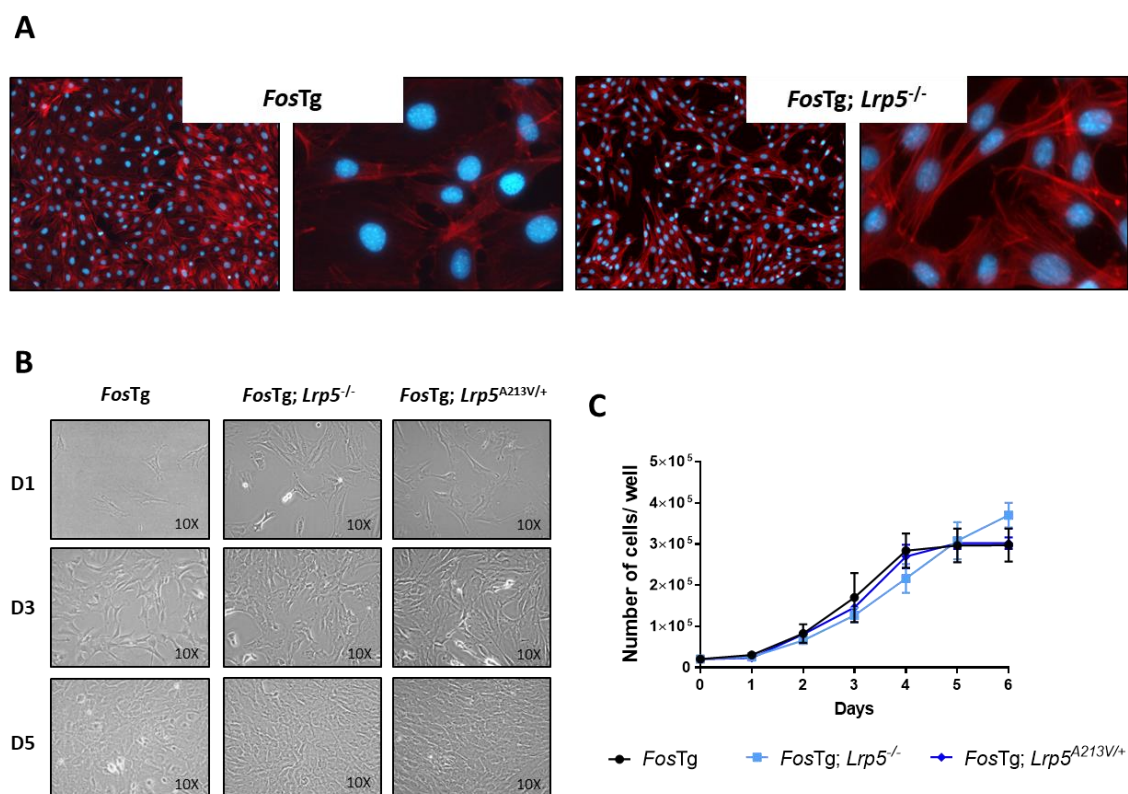


Figure 24: No growth defect observed in *FosTg* cell lines with different *Lrp5* genotypes.

A) Representative images of osteosarcoma cell lines stained with DAPI to visualize nuclei and phalloidin to mark the cytoskeleton (40X). **B)** Representative images of osteosarcoma cell lines derived from *FosTg*, *FosTg;Lrp5^{-/-}* or *FosTg;Lrp5^{A213V/+}* mice at day 1, 3 and 5 after seeding. **C)** Growth curves of the respective cell lines quantified for 6 consecutive days (n=3 independent cell lines per genotype).

To analyze if the differentiation of these cells was impaired, cells were cultured for 15 or 30 days in the presence of ascorbic acid and β -glycerophosphate, which eventually leads to the production of a mineralized matrix. Alizarin red staining was then performed to permit quantification of matrix mineralization, but here no differences between the genotypes were observed (Figure 25A-B).

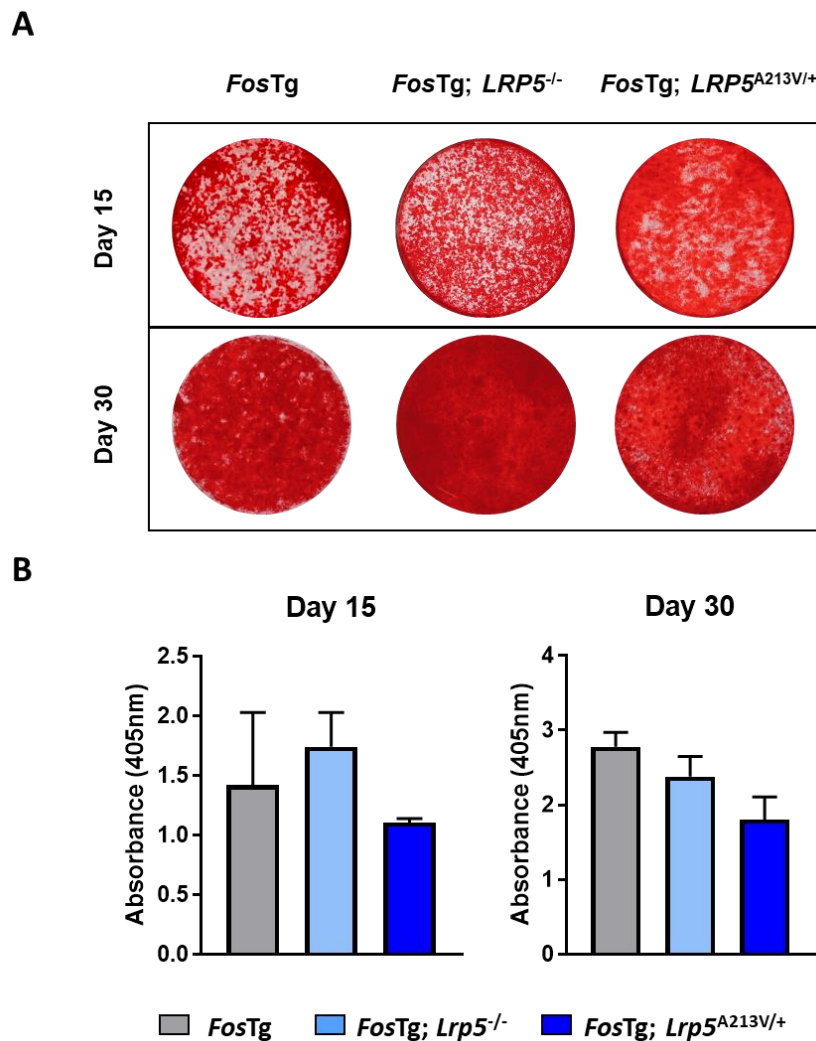


Figure 25: No mineralization impairment of *FosTg* osteosarcoma cells with different *Lrp5* genotypes.

A) Representative images of Alizarin red staining of *FosTg*, *FosTg;Lrp5^{-/-}* and *FosTg;Lrp5^{A213V/+}* osteosarcoma cells at day 15 and day 30 after administration of an osteoblastic differentiation medium. **B)** Quantification of mineralization by absorbance measurement of at 405nm after 15 or 30 days of differentiation induction. Data are expressed as mean \pm SEM.

In conclusion, these *in vitro* analyses did not mimic the processes involved in the osteosarcoma growth impairment observed *in vivo*. One potential explanation for the differences observed *in vitro* and *in vivo* was that Lrp5 acts as a co-receptor of a still unidentified Wnt ligand, which is only present *in vivo*. Since Wnt1 was described as a major bone-anabolic Wnt ligand in mice and humans, a recombinant Wnt1/Sfrp1 protein complex (Vollersen et al., 2021; Esteve et al., 2011), or Sfrp1 alone, was administered to the medium of different *FosTg* cell lines, but no effect on the growth was observed for 6 consecutive days (Figure 26). Similarly, the administration of sclerostin, an anti-osteoblastic molecule acting as a physiological antagonist of Lrp5, did also not impair the growth of *FosTg* osteosarcoma cell lines.

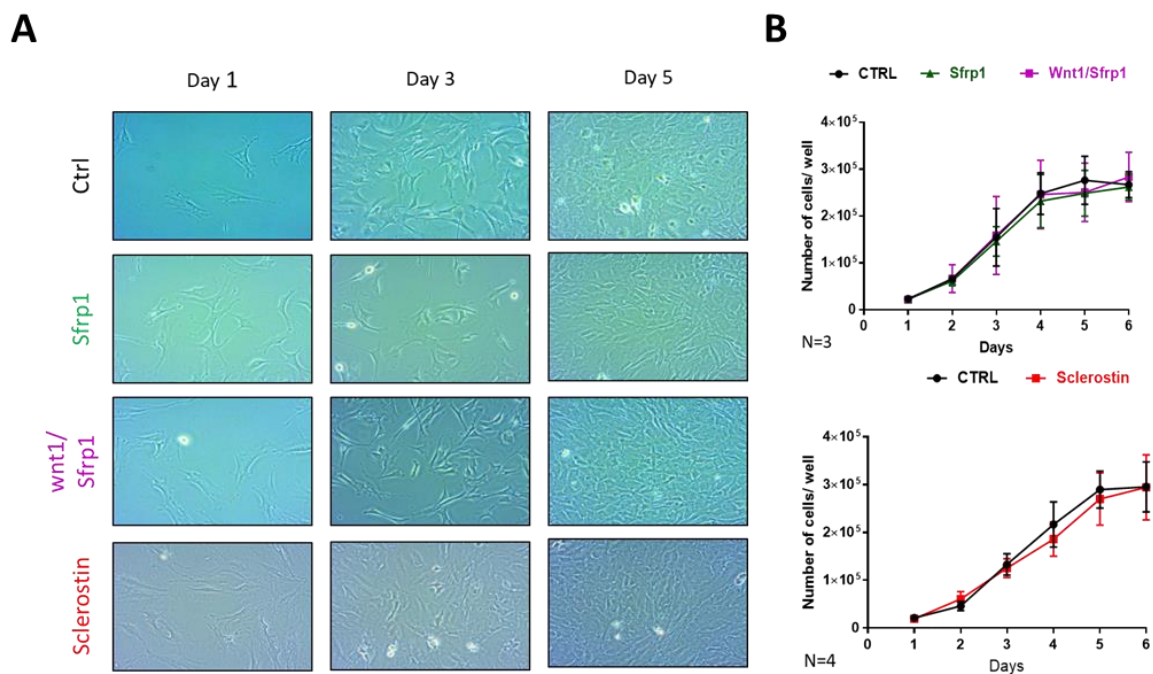


Figure 26: Wnt1 or sclerostin do not affect growth of *FosTg* osteosarcoma cells.

A) Representative images of *FosTg* cell lines cultured with Sfrp1 (50 ng/ml), Wnt1/Sfrp1 (100 ng/ml), sclerostin or DMSO (Ctrl) for 6 consecutive days (10X). **B)** Growth curves of *FosTg* cells quantified for 6 consecutive days stimulated with Sfrp1, Wnt1/Sfrp1, Sclerostin (n= 3-4 independent cell lines).

5.2.5. Transcriptomic comparison of *FosTg* cell lines

Despite no impact of the *Lrp5* genotype on growth and mineralization of *FosTg* osteosarcoma cells *in vitro* was observed, a microarray experiment was performed to screen for potential differences between *FosTg* cell lines with activation or inactivation of *Lrp5*. For this approach, pooled RNA (4 cell lines per genotype) were used to permit the screening of a large panel of genes without a biased choice of specific pathways. Thereby, a list of the most downregulated genes in *FosTg;Lrp5^{-/-}* cells compared to *FosTg* cells was established (Figure 27A). Afterwards qPCR analysis was performed on individual samples (3-5 cell lines per genotype) to confirm the differential gene expression. Here it was found that there were significant differences or tendencies for five genes of potential relevance, i.e. *Prl2c2*, *Prl2c3*, *Efemp1*, *Abca1* and *Ccl2* (Figure 27B). *Prl2c2* and *Prl2c3* encode for proliferins, which belongs to the growth hormone prolactin like gene family and are highly expressed during pregnancy but have also been associated to cancer angiogenesis to favorise tumor development (Toft et al., 2001; Nguyen et al., 2020). Whereas *Ccl2* encodes a chemokine with a potential role in the crosstalk between mesenchymal stromal cells and osteoblasts (Yao et al., 2021), *Abca1* (ATP-binding cassette, sub-family A member 1) encodes a transporter protein acting as a sensor pump of the cellular cholesterol intake with potential involvement in bone metabolism (Tall et al., 2008). Most importantly, *Efemp1* (EGF containing fibulin-like extracellular matrix protein, termed Fbln3) is present in the bone matrix and was found to be overexpressed in osteosarcomas of mice and humans (Wang et al., 2015; Wang et al., 2017).

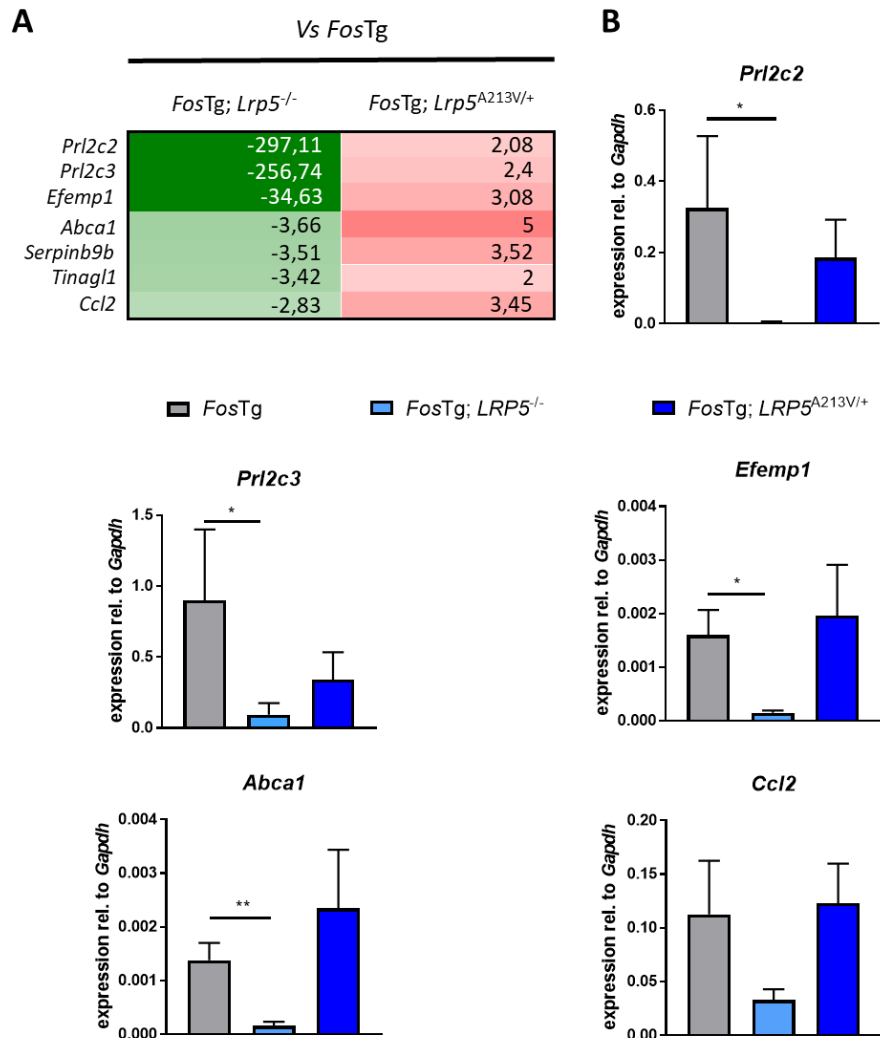


Figure 27: Identification of differentially expressed genes in FosTg osteosarcoma cells with different *Lrp5* genotypes.

A) Microarray analysis was performed with 5 pooled cell lines per genotype. The table represents the 7 most downregulated genes in FosTg;*Lrp5*^{-/-} vs FosTg cells as well as and their relative expression in FosTg;*Lrp5*^{A213V/+} cells. **B)** qPCR analysis monitoring expression of *Prl2c2*, *Prl2c3*, *Efemp1*, *Abca1*, *Ccl2* in the cells with the indicated genotypes. (n=5 individual cell lines per genotype) Data are expressed as mean ± SEM and analyzed by two-tailed Student's t test vs FosTg: *p<0.05, **p< 0.01.

To verify the differential *Efemp1* expression *in vivo*, RNA was extracted from long bone osteosarcomas of wildtype and FosTg mice with different *Lrp5* genotypes. Subsequent qPCR analysis, however, did not confirm the differential *Efemp1* expression observed *in vitro* (Figure 28A). Since a recent article suggested that serum levels of Fln3, the protein encoded by *Efemp1*, can be used as a prognostic tool for aggressiveness and metastasis risk of osteosarcoma (Wang et al., 2020), ELISA measurements of Fln3 were performed. However,

also here no differences between the genotypes were found (Figure 28B). Due to the high tumor heterogeneity observed *in vivo*, immunohistochemistry was applied to analyze if a subset of cells, potentially corresponding to the most aggressive clones, were expressing Fbln3. For this purpose, decalcification of lumbar vertebral bodies followed by sectioning and staining with a Fbln3-specific antibody was performed, with a focus on the most severe osteosarcoma genotype, *FosTg;Lrp5^{A213V/+}*. Although some cells inside the *FosTg;Lrp5^{A213V/+}* tumors appeared strongly stained for Fbln3 compared to other cell types present inside the tumors, the specificity of the immunohistochemical detection appeared limited (Figure 28C). In fact, several other cells outside the tumor were also positive for Fbln3, and unspecific staining was observed in the control incubation (without Fbln3 antibody). Although optimization of this staining may be achievable, the collective findings do not support the hypothesis that Fbln3 is a relevant downstream target of Lrp5 which is involved in the promotion of osteosarcoma growth.

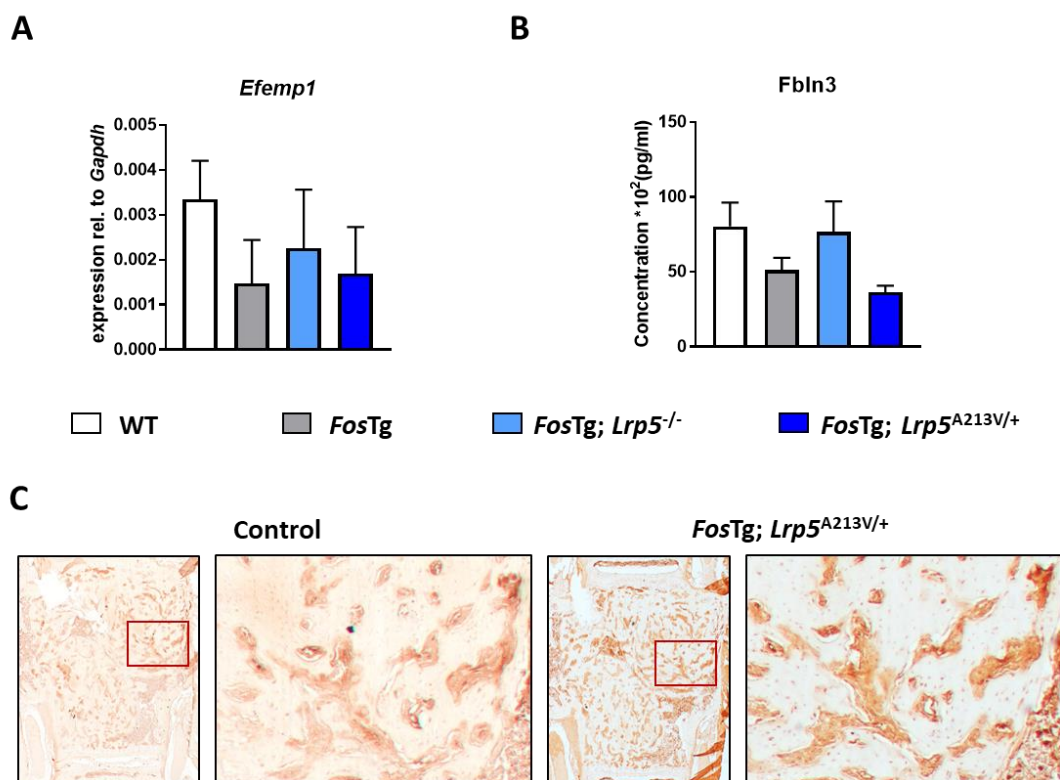


Figure 28: The differential expression of *Efemp1* was not confirmed *in vivo*.

A) qPCR analysis of *Efemp1* expression in RNA extracted from long bones (osteosarcomas for the *FosTg* groups) of mice with the indicated genotypes. Data are expressed as mean \pm SEM. **B)** Serum concentrations of Fbln3 in the same mice. **C)** Representative images of Fbln3 immunohistostaining performed on decalcified spine sections from *FosTg;Lrp5^{A213V/+}* mice, which included osteosarcomas. The control (ctrl) section images represent unspecific staining (without Fbln3 antibody).

5.2.6. Differential gene expression in osteosarcomas *in vivo*

Since Lrp5 deficiency had a clear impact on osteosarcoma formation *in vivo*, transcriptomic analysis was also performed with RNA isolated from tumors of the respective mice, despite the observed heterogeneity. Using pooled RNA samples, extracted from osteosarcomas of long bones (femora and tibiae), specific genes were downregulated in *FosTg;Lrp5^{-/-}* compared to *FosTg* tumors (Figure 29A). Subsequently, qPCR analysis was performed on individual samples per genotype, and RNA from bone of wildtype mice was included as a control. Although this analysis was not consistent for all genes, some of them showed significant overexpression in the tumor samples compared to wildtype samples, namely *Dynap*, *Ptgs2*, *Car12*, *Dmp1* and *Slc13a5* (Figure 29B-C). Moreover, there was a tendency of normalization for some genes (*Dynap*, *Car12* and *Slc13a5*) in *Lrp5*-deficient tumors compared to the other genotypes. Even so the *Lrp5* deficiency did not restore the same level of expression as in the wildtype samples, the differential expression of these genes is potentially interesting, as they are known to have a particular function in bone integrity or in cancer development. Since these genes could be involved in the development of *FosTg* osteosarcomas, their role in tumor development and their regulation by *Lrp5* activation or inactivation will be assessed in future experiments.

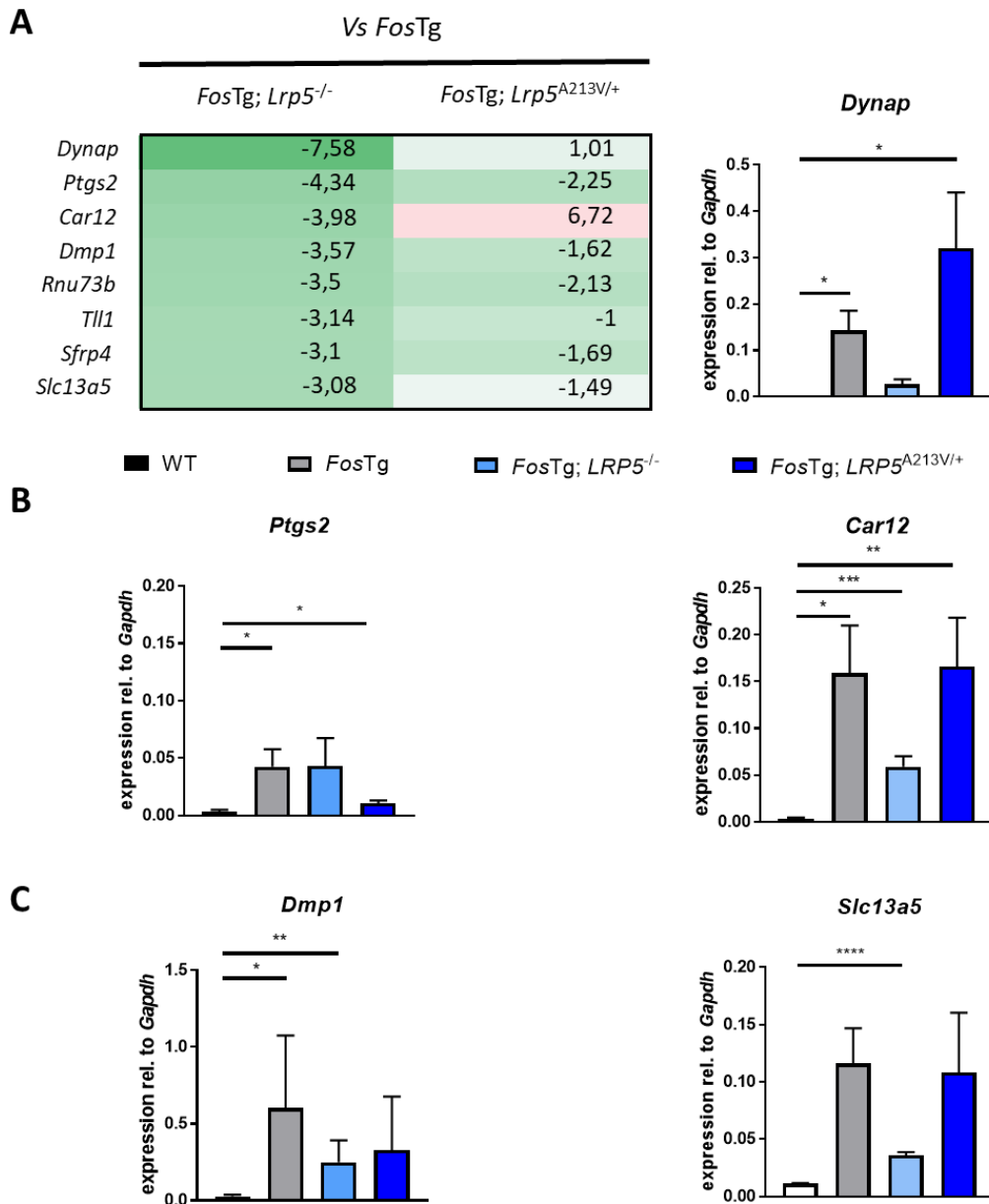


Figure 29: In vivo microarray analysis identified differentially expressed genes in *FosTg* osteosarcomas.

A) Microarray analysis performed with 4 pooled RNA samples from osteosarcomas of *FosTg* mice with different *Lrp5* genotypes. The table represents the 8 most downregulated genes in *FosTg;Lrp5^{-/-}* vs *FosTg* osteosarcoma as well as and their relative expression in *FosTg;Lrp5^{A213V/+}* tumors **B-C)** qPCR analysis monitoring expression of *Dynap*, *Ptgs2*, *Car12*, *Dmp1* and *Slc13a5* in osteosarcomas of mice with the indicated genotypes. Data are expressed as mean \pm SEM and analyzed by two-tailed Student's t test vs control: * $p < 0.05$, ** $p < 0.01$, *** $p < 0.001$, **** $p < 0.0001$ (n=5 individual mice per genotype).

5.2.7. Increased concentration of Fgf21 in sera from *FosTg* mice

In an attempt to identify circulating factors released by osteosarcoma cells that could differ in mice with different *Lrp5* genotype, an antibody assay detecting more than one thousand proteins was performed with serum from mice with the different genotypes (Sciomics GmbH, Heidelberg). The most informative approach for a preliminary analysis regarding the considerable amount of data was to compare the two extremes, i.e. sera from wildtype and *FosTg;Lrp5^{A213V/+}* mice. Based on a scattered dot plot of protein abundance with their values presented as log fold change (Figure 30A) the most differentially regulated proteins were then compiled in a heatmap and compared to the other genotypes corresponding to protein abundance (Figure 30B). Among these proteins, fibroblast growth factor 21 (Fgf21) stood out for its profile, as its serum abundance was low in wildtype mice, higher in *FosTg* mice, normalized by *Lrp5* deficiency and highly present in *FosTg;Lrp5^{A213V/+}* mice. This protein was of particular interest, as *FosTg* mice develop severe lipodystrophy accompanied by overexpression of *Ucp1*, a gene activated by Fgf21 (Fisher et al., 2012). To validate this finding, an ELISA on individual serum samples was performed, which confirmed significant higher serum concentrations of Fgf21 in *FosTg* and *FosTg;Lrp5^{A213V/+}* mice (Figure 30C). Most importantly, serum Fgf21 concentrations in *FosTg* mice were normalized by *Lrp5* deficiency. These data raise the possibility that Fgf21 is causative for the lipodystrophy observed in *FosTg* mice and possibly in patients with osteosarcoma.

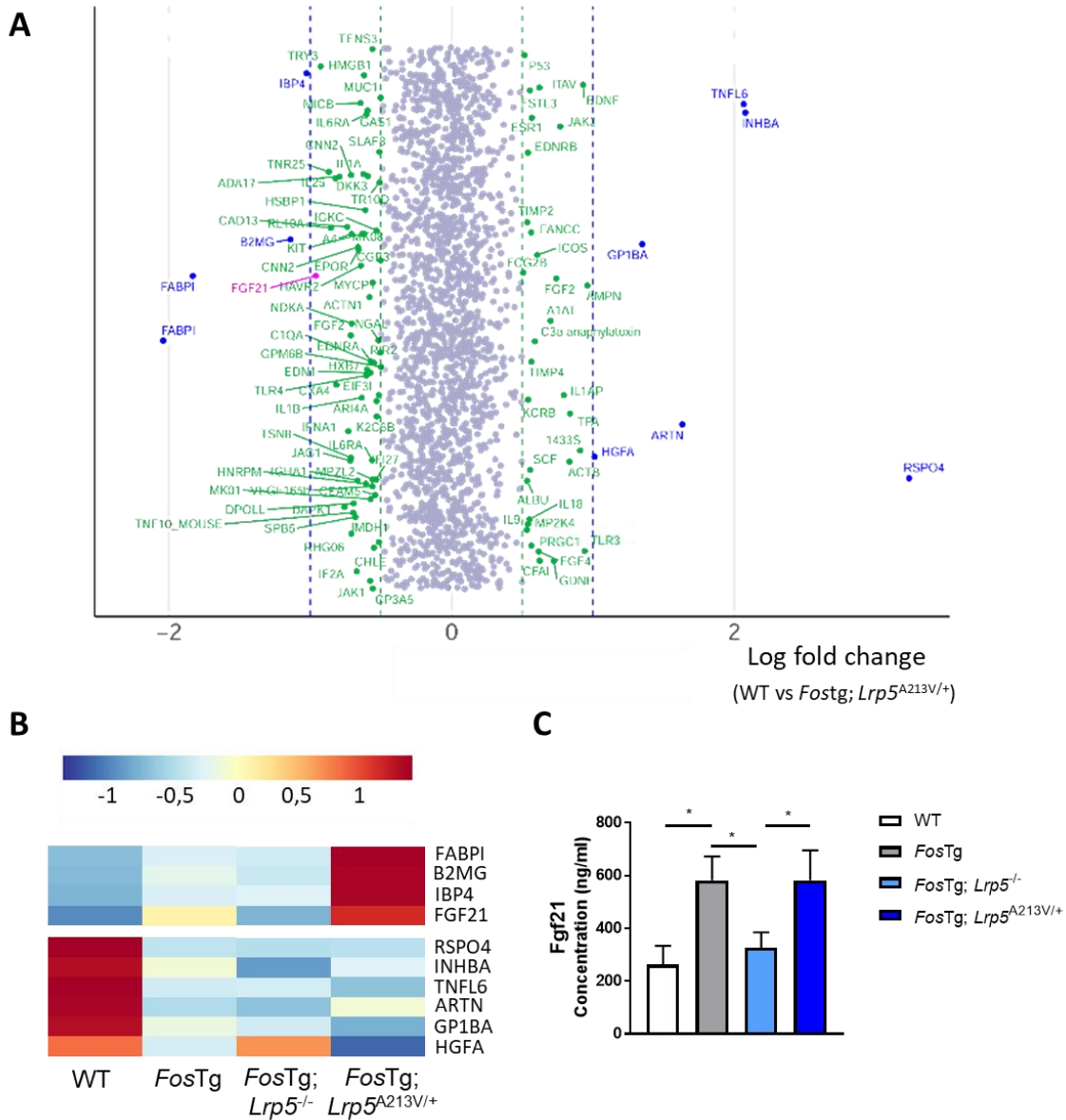


Figure 30: An antibody assay identified increased Fgf21 concentrations in the serum of *FosTg* mice.

A) Antibody array of pooled sera from 16-week-old mice. Results are represented as scattered dot plot of log fold change values between wildtype and *FosTg*;*Lrp5*^{A213V/+} mice. **B)** Heatmap representing the abundance of the most differentially detected proteins present in the sera of mice with the indicated genotypes. **C)** ELISA-based quantification by Fgf21 concentrations in sera of individual mice with the indicated genotypes. Data are expressed as mean ± SEM and analyzed by one-way ANOVA: *p < 0.05.

6. Discussion

Osteosarcoma is a rare bone disease that shows a disease-free survival rate of 60% after 5 years (Meltzer et Helman, 2021). Unfortunately, in the remaining 30% of the cases, metastases are limiting life expectancy. Moreover, therapeutic options did not substantially improve in the last decades and patients are still treated with cytotoxic neoadjuvant drugs. Furthermore, many patients have to undergo surgery, in the most severe cases including amputation, to ensure relapse-free survival. In the era of personalized medicine, cancer research focuses on the identification of tumor-specific mutations and mechanisms in order to develop targeted therapies. Thus, this thesis aimed to define more specific pathways to impact osteosarcoma growth, at least when caused by *Fos* activation. Taken together, the presented results uncover two important modulators of osteosarcoma growth in *FosTg* mice, i.e. *Rsk2* and *Lrp5*, that act through different mechanisms.

6.1. Pharmacological inhibition of the *Rsk2* pathway

The first part of this thesis focused on the role of the *Rsk2* pathway in the context of *Fos*-dependent osteosarcoma development. As observed for osteosarcoma cell lines with genetic inactivation of *Rsk2*, a pharmacological *Rsk* inhibitor (BI-D1870) also led to a diminution of cancer cell proliferation by the accumulation of multiple nuclei and the induction of cancer cells death by mitotic catastrophe. Transcriptomic analysis of *FosTg* cell lines treated with BI-D1870 further revealed a significantly reduced expression of the main cell cycle genes. These results are in full agreement with the data obtained with the genetic inactivation of *Rsk2* in *FosTg* osteosarcoma cell lines.

Cytotoxic drugs targeting highly proliferative cells have been the gold standard in cancer therapy for the last decades, yet they are also associated with deleterious side effects (Schiff et al., 2009). Therefore, specific anti-mitotic drugs have now been developed to permit a more specific treatment. The development of these drugs permitted that above a certain level of genomic instability cells are entering a forced death program also termed mitotic catastrophe. In this context, it is important to state that although chromosome abnormalities

and genetic mutations are cell-transforming events, which permit cancer cells to develop growth and survival abilities in comparison to non-transformed cells, the accumulation of genomic instability is sensitizing them to drugs inducing mitotic catastrophe. Indeed, the inhibition of different cell cycle kinases is inducing polyploidy, followed by mitotic catastrophe induced death in cancer cells, but not in non-cancer cells (Vitale et al., 2011).

Several inhibitors targeting different kinase proteins involved in the regulation of mitosis have been developed and their role has been studied since the 2000s. Rsk2 is one of such kinase, which acts downstream of the MAPK pathway after activation by Erk to promote various cellular processes including proliferation. In the *FosTg* mouse model, a first study showed that Rsk2 deficiency reduced the osteosarcoma volume by the impairment of tumor cell proliferation (David et al., 2005). Furthermore, in another study epidermal growth factor receptor (EGFR) was found mandatory for osteosarcoma growth via the phosphorylation of Rsk2 and Creb (Linder et al., 2018). Finally, Rsk2, in contrast to Rsk1, was found to impact mitotic spindles, and the Rsk2 deficiency was found to impair mitosis progression (David et al., 2005).

Different components of the Rsk pathway were also found overexpressed in various cancer types such as breast, leukemia, osteosarcoma, head and neck (David et al., 2005; Kang et al., 2007; Kang et al., 2010; Stratford et al., 2012). In breast cancer, Rsk2 activation can lead to chemoresistance by the protection from endoplasmic reticulum stress (Li et al., 2020). Controversially to the potential use of Rsk inhibitors in various forms of cancer, it was found, specifically for hepatocarcinoma, that Rsk2 inactivation was increasing migration properties of the cancer cells and correlated with aggressiveness, which was reversed by the induction of Rsk2 in cell lines (Chan et al., 2021). These results suggested a variable role of the expression of Rsk2 in tumorigenesis and a need for further investigations in osteosarcoma.

Current clinical trials using Rsk inhibitors did not lead yet to commercialization but these inhibitors are evaluated as potential next-generation targets for the therapy of melanoma or prostate cancer (Theodosakis et al., 2017; Ushijima et al., 2022). Pharmacological inhibition with BI-D1870 is however not specific for Rsk2, as it inhibits all of the four Rsk proteins, and the same applies to other Rsk inhibitors that have been in clinical trials. The lack of specificity

of these inhibitors is indeed a main limitation, as all Rsk isoforms are essential for different cellular processes. Indeed, some articles were reporting an anti-tumoral role of Rsk3 and Rsk4 in various cancers, which question the application of unspecific Rsk inhibition for osteosarcoma therapy (Bignone et al., 2007). Therefore, this thesis aimed at discovering new downstream effectors potentially targetable in clinical practice.

6.2. Aurora kinase B, another putative target for osteosarcoma therapy

Among the downregulated cell cycle genes by BI-D1870 treatment, *AurkB*, encoding for an aurora kinase having a crucial role in the G2/M transition, was particularly interesting for its therapeutic potential in osteosarcoma. Indeed, like the Rsk family, the members of the aurora family are serine/threonine kinases, which have been functionally studied in numerous cancers where they are overexpressed (Bischoff et al., 1998; Takeshita et al., 2013; Davidson et al., 2014; Honma et al., 2014; Zhang et al., 2015). The first evidence that aurora kinases are key regulators of the cell cycle was described for *Drosophila melanogaster* and *Saccharomyces cerevisiae*, where researchers observed that mutations in these genes were resulting in a failure of centrosome separation (Francisco et al., 1994; Glover et al., 1995). In mammals, the three known aurora kinases (A, B and C) have high homology, but distinct functions. More specifically, whereas aurora kinase A is regulating G2/M phase transition and centrosome maturation, aurora kinase B expression occurs subsequent to aurora kinase A expression after the entrance in mitosis and is responsible for chromosome segregation and cytokinesis (Basant et al., 2015; Krenn & Musacchio, 2015). In cancer biology, aurora kinases were found pro-tumorigenic in leukaemia, and clinical trials are ongoing to test several selective inhibitors of aurora kinase A (MLN8237 also known as Alisertib), aurora kinase B (AZD1152) or both (Dennis et al., 2012; Dees et al., 2012; Manfredi et al., 2011; Goldberg et al., 2014) showing some efficiency in phase II of clinical trial to delay tumor recidiva in patients with advanced solid tumor. In osteosarcoma, aurora kinase A and B were also found overexpressed. Moreover, different drugs inhibiting either aurora kinase A or B were tested on human osteosarcoma cell lines and showed efficiency to induce tumor cell death by apoptosis (Tanaka et al., 2021). Interestingly, mitosis abnormalities have been reported when

cells were treated with these compounds i.e. Hesperadin, MLN8237 or AZD1152 (Hauf et al., 2003; Asteriti et al., 2014; Gully et al., 2010).

In the present thesis, two different inhibitors of aurora kinase B have been studied. Hesperadin is an established inhibitor of aurora kinase B, which is efficient in causing a cell cycle arrest (Hauf et al., 2003). AZD1152, an ATP competitive inhibitor was more recently developed and potentially more selective inhibitor enrolled in clinical trials as Barasertib, where it was administrated to patients with solid tumors (Schwartz et al., 2013). In this thesis it was found that inhibition of aurora kinase B by Hesperadin led to the same polynuclear cells as observed by Rsk deficiency or inhibition. Moreover, Hesperadin treatment for 24 hours led to the downregulation of cell cycle genes, especially those responsible for the G2/M transition. In contrast, AZD1152 did not induce growth impairment of *FosTg* cell lines and failed to induce polynuclear cells. This raises the question if inhibition of aurora kinase B alone is responsible for the induction of mitotic catastrophe and cell death in *FosTg* cell lines. Therefore, it still needs to be analyzed if the effect observed with Hesperadin treatment is attributable to inhibition of aurora kinase B or of other kinases. In fact, although Hesperadin has been described as a specific inhibitor of Aurora kinase B compared to other members of its protein family, some articles reported a diminution of activity of other kinases (AMPk, Lck, Mkk1, Chk1 and Phk) at a higher dose than the one used in this thesis (Hauf et al., 2003). Despite the fact that the selectivity of Hesperadin for aurora kinase B remains to be validated, it seems that this compound can be used as an anti-tumoral drug against *FosTg* cells. Moreover, in a recent article, Hesperadin was found to be efficient in reducing the growth of pancreas tumor cells *in vitro* but also *in vivo*. Furthermore, the administration of Hesperadin to mice seems to be well tolerated, thereby increasing the interest in its use as a new drug candidate in clinic (Zhang et al., 2022).

Other inhibitors targeting kinases from the same pathway have passed clinical trial phases and are now commercialized (Hauschild et al., 2012; Rath et al., 2021). For instance, Braf inhibitors are currently in use as targeted therapies in different cancers like melanoma or brain tumors and permitted, in metastasis cases, a significant increase in life quality and expectancy. The development of Mek inhibitors targeting kinases acting downstream of this pathway have counteracted resistance to Braf inhibitors and recurrence. However, some

patients will not profit from such improvement, not because of a lack of efficiency, but due to multiple organ side effects of these therapies (Theodosakis et al., 2017). Rsk inhibitors or aurora kinase inhibitors are therefore promising drugs, as those kinases are downstream effectors of these cascades involved in Fos- or Braf-driven tumors. To investigate if Rsk2 or aurora kinase B inhibition could not only be beneficial for osteosarcoma patients with overexpression of Fos, but also for osteosarcoma in general, the effect of BI-D1870 or Hesperadin treatment on U2OS cells, i.e. a human osteosarcoma cell line with a different genetic background, was studied in this thesis. Both treatments were inducing a growth impairment associated with a polynucleation of these cells. These results are a preliminary confirmation of the potential utility of these two drugs in osteosarcoma patients.

6.3. The Lrp5 pathway and osteosarcoma progression

The second part of this thesis analyzed if Lrp5 is involved in controlling osteosarcoma development and progression. A pertinent approach to limit secondary effects on other organs is to target bone-specific pathways. The Lrp5 pathway is one of the main bone-anabolic pathways that is implicated in severe human bone pathologies when dysregulated. The highjacking of this pathway by *FosTg* osteosarcoma cells remained to be proven and the characterization of downstream effectors could result in new therapeutic options to treat osteosarcoma patients. In order to study the implication of Lrp5 in osteosarcoma development, *FosTg* mice were bred with mice having either loss-of-function of Lrp5 (*Lrp5*^{-/-}) or gain-of-function mutations of Lrp5 (*Lrp5*^{A213V/+}). μ CT of 16-week-old mice femora was used as a first step for the skeletal characterization of littermate mice. As expected, *Lrp5*^{-/-} mice were developing lower bone mass compared to wildtype controls, whereas *Lrp5*^{A213V/+} mice displayed higher bone mass, either in the absence or in the presence of the *Fos* transgene.

Most importantly, Lrp5 deficiency in *FosTg* mice decreased the number of tumors and strongly reduced the outgrowth of osteosarcomas. In the opposite case, an activating mutation of *Lrp5* resulted in bigger and highly mineralized tumors. Collectively, these findings demonstrated that osteosarcoma cells utilize the Lrp5 pathway for their benefit. A diminution of osteoblasts at the tumor surface and an enlargement of osteoid surfaces were observed

in *Lrp5*-deficient *FosTg* mice, which can explain the impaired expansion of those tumors. These results were not necessarily predictable, since *Lrp5* activation could have resulted in an anti-proliferative influence, as it induces osteoblast differentiation. Indeed, the main downstream effector of the Wnt canonical pathway, i.e. β -catenin, has been associated with controversial functions in tumorigenesis, since both, a tumor suppressor function and an oncogenic effect have been described (Morin et al., 1997; Bukholm et al., 1998; Wong et al., 2002).

An overexpression or inactivation of Wnt pathway regulators (such as *WNT1*, *APC*, *AXIN2*, β -*Catenin*) was also found to be associated with colorectal cancer with *APC* being overexpressed in the majority of them (Morin et al., 1997; Caldwell et al., 2004). Breast cancer was the first cancer to be described, whose growth depends on the Wnt pathway. Indeed, *Wnt1*, the first member of the Wnt gene family, was discovered by the study of the mouse mammary tumor virus (Nusse & Varmus, 1982). Several other studies showed the role of different Wnt ligands like *Wnt1* and Wnt downstream targets in the development of local breast tumors and their dissemination. For example, a study by Wend et al. showed that patients with *WNT10B* overexpression, inducing canonical Wnt signaling, led to the development of the most aggressive form of breast cancer, the triple negative (Wend et al., 2013). Other Wnt ligands were crucial for cancer development and invasion. Among them, *Wnt3a* was found to be overexpressed in aggressive prostate tumor cells (Bonci et al., 2008).

6.4. *Lrp5* and *FosTg*-dependent osteosarcoma growth

In this thesis, it was found that *Lrp5* activation has a pro-tumoral effect and that deficiency of *Lrp5* in *FosTg* mice limited osteosarcoma growth in *FosTg* mice. These findings are in agreement with a previous study which demonstrated that the inhibition of Wnt ligand secretion by the inactivation of *Wls* in *FosTg* mice leads to tumor growth impairment. The authors further showed the involvement of *Wnt7b*, *Wnt9a* and Lysyl oxidase-like 2 (*Loxl2*, a collagen cross-linking enzyme) activation in the development of *FosTg* osteosarcoma (Matsuoka et al., 2020). However, whether *Lrp5* is a key actor of *FosTg* osteosarcoma progression and whether its deficiency would be sufficient to limit tumor growth was not

addressed previously. Another article focused on studying Lrp5 function in osteosarcoma growth with the help of a xenograft model with 143B cells (human osteosarcoma cell line). It was found that transfection of a dominant negative Lrp5 reduced the number of tumors after injection into nude mice (Guo et al., 2008). Importantly, however, unlike this xenograft model, the *FosTg;Lrp5^{-/-}* mouse model permits the study of osteosarcoma in mice with a functional immune system, which is known to play an important role in cancer development.

The 100% penetrance of tumors in all endochondral bones makes the *FosTg* model relevant to study osteosarcoma development and progression. Still, the severity of the phenotype, especially the osteosarcoma paralysis of hips, explains why we chose an early time point for sacrifice (16 weeks) to avoid animal suffering. At that age the increased osteosarcoma formation observed in *FosTg;Lrp5^{A213V/+}* mice did not lead to metastases in the lungs by visual observation. Thus, we can not fully conclude that *FosTg* mice would not develop lung metastases over time. However, the characterization of not yet metastatic osteosarcoma is essential because 30% of osteosarcoma-related death occurs in patients who did not have metastasis at initial diagnosis. The definition of therapeutic targets in the *FosTg* model will permit to counteract osteosarcoma upstream of metastatic events that involve more complex cascades of mutations.

To characterize the role of Lrp5 expression in *FosTg* cancer cells, cell lines derived from *FosTg*, *FosTg;Lrp5^{-/-}* or *FosTg;Lrp5^{A213V/+}* osteosarcomas were established. However, unlike it was previously found for *FosTg;Rsk2^{-/-}* cell lines, growth and mineralization analysis did not show any differences consistent with the *in vivo* phenotypes in mice with different *Lrp5* genotypes. This inconsistency may be explained by the absence of specific ligands in cell culture conditions that are required to activate Lrp5-dependent signaling *in vivo*. Since Wnt1 was one candidate for such a ligand, *FosTg* cells were cultured in the presence of a Wnt1/Sfrp1 complex, yet no difference in cell growth was observed. These data are in principle agreement with the findings reported by Luther et al., which show that Lrp5 is not required for the osteoanabolic influence of Wnt1 in an inducible transgenic mouse model (Luther et al., 2018). Therefore, other potentially relevant Lrp5 activators remain to be tested. Recently, a link between Wnt5a, a protein described in the activation of the Wnt non-canonical pathway, and Lrp5 signaling was investigated. Indeed, it has been reported that endometrial mesenchymal

stem-like cells were overexpressing Fzd5 and that stimulation of these cells with Wnt5a depends on the presence of Fzd5. Furthermore, the blockade of Lrp5 with Dkk1 decreased the binding of Wnt5a to Fzd5. This pathway activated β -catenin, and its target genes, indicating that the arbitrary separation made between the Wnt canonical ligands and the non-canonical ligands is unreliable as, in different situations and times, the identical Wnt ligands are activating both pathways (Li et al., 2022). In future analyses, the relevant Lrp5 ligand needs to be identified and the involvement of β -catenin in this pathway should be further analyzed. In this regard, the created cell lines will be a perfect tool to simplify the research by directly assessing the influence of specific ligands on *FosTg* cells with different *Lrp5* genotypes.

Similarly, several antagonists are known to bind to Lrp5 and an antibody against one of them (Sclerostin) is used for the treatment of osteoporosis. In 2015, it was shown that Sclerostin acts as an Lrp5 antagonist *in vivo*, as the anti-osteoblastic effect of osteoblast-specific Sclerostin overexpression in transgenic mice was abolished by the presence of *Lrp5* high bone mass alleles (Yorgan et al., 2015). In this present thesis, however, no effect of Sclerostin on the growth of *FosTg* cultures was observed when Sclerostin was added to the medium.

6.5. Transcriptomic comparison of *FosTg* osteosarcoma cells

Based on the remarkable influence of Lrp5 deficiency in osteosarcoma growth *in vivo*, the final aim of this thesis was to define downstream effectors of the Lrp5 signaling pathway that could be involved in osteosarcoma development. An *in vitro* transcriptomic analysis was first conducted to compare *FosTg*, *FosTg;Lrp5^{-/-}* and *FosTg;Lrp5^{A213V/+}* osteosarcoma cells. To not select any specific pathway and to permit an unbiased analysis, a microarray was performed on pooled samples (\approx 5 cell lines per genotype), which resulted in a large dataset that remains to be deeply analyzed. Until now, the focus was made on the most downregulated genes in *FosTg;Lrp5^{-/-}* vs. *FosTg* cell lines. The expression of these genes was then confirmed by qPCR on individual samples from *FosTg*, *FosTg;Lrp5^{-/-}* and *FosTg;Lrp5^{A213V/+}* cell lines. These analyses permitted the confirmation of five differentially expressed genes, i.e. *Prl2cl2*, *Prl2c3*, *Efemp1*, *Abca1* and *Ccl2*. Although it has to be taken into consideration that the

immortalization of cells occurs through the natural selection of the most resistant and proliferative clones, this study revealed a significant difference in the expression of specific genes depending on the *Lrp5* genotype.

Prl2c2 (*prolactin family 2, subfamily c, member 2*) encodes for a protein, also known as Proliferin-1, which belongs to a family of growth hormones involved in regulating energy production during pregnancy. In the cancer context and consistent with the *FosTg* mice phenotype, this protein was found to be associated with angiogenic functions (Toft et al., 2001) and to be responsible for the lipolysis occurring during cancer-associated cachexia (Nguyen et al., 2020). Another member of this family, encoded by *Prl2c3*, was also found differentially expressed in this thesis cell lines. However, no article could be found linking this gene to any cancer but a role of *Prl2c3* was described in hematopoietic stem cell proliferation (Choong et al., 2003). *Abca1* (*ATP binding cassette subfamily A member 1*) is a gene coding for a channel transporter protein that regulates cellular cholesterol intake. Interestingly, the Wnt pathway is involved in its regulation, as Wnt5a can inhibit this cholesterol release. More specifically, following Wnt5a binding to its receptor Ror2, *Abca1* is inhibited, thereby leading to an intracellular accumulation of cholesterol. *Ccl2* (*Cc-chemokine ligand 2*) encodes a molecule released in the circulation during inflammation. It was found released by different tumor cell types like glioma or breast cancer (Yoshimura et al., 1989; Kadomoto et al., 2021). *Ccl2* is responsible for the creation of an immunosuppressive tumor microenvironment favorizing cancer cells proliferation, and it was found that its blockage permitted to reestablish treatment efficiency in lung cancer (Wang et al., 2018). Its overexpression in *FosTg* cell lines may be taken in consideration for the development of combined therapy targeting cancer cells and their microenvironment.

Based on literature knowledge, *Efemp1* (*EGF containing fibulin extracellular matrix protein 1*) appeared to be the most interesting gene with differential expression. *Efemp1* encodes an extracellular matrix protein termed fibulin 3 (Fbln3), and its overexpression has been reported in numerous cancers, such as ovarian and pancreatic cancer (Chen et al., 2013; Seeliger et al., 2009). In osteosarcoma, several articles have demonstrated that its expression correlated with aggressiveness and metastasis development (Wang et al., 2020; Zhang et al., 2022). More specifically, Fbln3 expression was found to be low in a human osteoblast cell line

but highly expressed in two human osteosarcoma cell lines, i.e. U2OS and SaOS. While this was also confirmed with immunohistochemistry on osteosarcoma biopsies, a correlation between low Fbln3 expression and survival of osteosarcoma patients was observed. Likewise, *Efemp1* deficiency in nude mice inoculated subcutaneously with a human osteosarcoma cell line (HOS) were reported to display decreased osteosarcoma growth (Wang et al., 2017). Finally, a mechanism involved in metastasis development has been proposed implicating the activation of the Wnt/ β -catenin signaling pathway and epigenetic modification induced by *Efemp1* expression. This epigenetic modification led to the transcription of genes encoding N-cadherin, Snail, Slug and Twist, which are implicated in epithelial-mesenchymal transition (EMT), a phenomenon permitting the proliferation of cancer cells and their spreading into distal organs (Wang et al., 2017).

In the present thesis, the differential expression of *Efemp1* could not be confirmed *in vivo*, possibly explained by the selection of cancer cells with improved proliferation abilities *in vitro*. Therefore, immunohistochemistry of mice vertebral bodies is ongoing to analyze the expression of Fbln3 in specific subsets of osteosarcoma cells. While some preliminary data could already identify some transformed cells with high expression of Fbln3, a more extensive analysis is required in the future. Since it was proposed that Fbln3 serum concentrations should be used as a prognostic tool to evaluate the stage of osteosarcoma development (Wang et al., 2017), Fbln3 serum concentrations were also quantified in *FosTg* mice with different *Lrp5* genotypes. However, since no significant differences were identified, the relevance of *Efemp1* in the context of the present thesis remains questionable.

Based on these conflicting results, a second microarray comparison of *FosTg*, *FosTg;Lrp5^{-/-}* and *FosTg;Lrp5^{A213V/+}* osteosarcomas was performed, where RNA was extracted directly from the tumors. Again, the initial focus was related to the most downregulated genes in *FosTg;Lrp5^{-/-}* tumors compared *FosTg* tumors, which were completely different than the ones found differentially expressed in the *in vitro* analysis. Regardless of this, qPCR confirmation was performed on individual tumor samples for selected genes of interest (*Ptgs2*, *Dynap*, *Dmp1*, *Slc13a5* and *Car12*), as these genes could be of potential relevance in bone biology or osteosarcoma development.

Ptgs2 encodes the prostaglandin-endoperoxide synthase (also known as COX-2) catalyzing the conversion of arachidonic acid into prostaglandin E2 (PGE2), a molecule highly produced during inflammation, bone remodeling and metastatic bone cancer. *Ptgs2* and its product PGE2 were found to be responsible for the growth and invasion properties of ovarian cancer cells (Nagaraja et al., 2016), but also for the progression of other tumors like melanoma (Fang et al., 2022) or colorectal cancer in a study based on human RNA samples (Zahedi et al., 2021). More recently, increased PGE2 production was found associated with chemotherapy resistance, and pharmacological inhibition of COX-2 in cancer cells restored drug efficiency (Bell et al., 2022). Thus, such inhibitors may be used to treat *FosTg* cells and mice to confirm the pro-tumoral role of PGE2 in cancer. In the present thesis *Ptgs2* was found to be upregulated in all mice carrying the *Fos* transgene, but downregulated in *FosTg;Lrp5^{-/-}* mice compared to *FosTg;Lrp5^{A213V/+}* in a microarray study. Surprisingly, however, qPCR analysis did not show such a difference either *in vivo* or *in vitro* on individual samples, thereby suggesting a role of *Ptgs2* in osteosarcoma independent of *Lrp5* expression. Furthermore, the AP-1 transcription factor was found to bind to the promoter of *Ptgs2* (Nakayama et al., 2022), which can be the subject of another study of genes implicated in *FosTg* osteosarcoma.

Dynap (*Dynactin-associated protein*) was the most differentially expressed gene of the microarray, when tumors from *FosTg* and *FosTg;Lrp5^{-/-}* mice were compared. Although the comparative qPCR analysis for this gene did not reach statistical significance, the samples median was reduced by 70% in *FosTg;Lrp5^{-/-}* compared to *FosTg* tumors. Therefore, it is required to increase the number of samples per genotype to counteract tumor heterogeneity. Consistent with this result, some articles have already described the transforming potential of *Dynap* in various cancer types (lung, stomach, breast, liver, etc.). Here, increased *Dynap* mRNA and protein levels were observed in the tumors. In human cancer, the expression of *Dynap* leads to an activation of the proliferation and survival of cancer cells. These advantages are abolished when *Dynap* is pharmacologically inhibited to permit apoptosis of those cells (Kunoh et al., 2010). So far, no role of *Dynap* has been published for osteosarcoma, but its striking downregulation in tumors from *FosTg;Lrp5^{-/-}* mice make it appealing to study.

Next to cancer-associated genes, some osteogenic regulators genes were found differentially expressed. *Dmp1* (Dentin matrix protein gene) is expressed in the bone matrix around osteocyte lacunae. Its expression is specific for bone and dentin, where it has a major role in tissue mineralization (George et al., 1993). It was also found overexpressed in bone-forming tumors (Kashima et al., 2013). *Slc13a5* was another downregulated gene in the *in vivo* microarray of *FosTg;Lrp5^{-/-}* tumors compared to *FosTg* tumor RNA. *Slc13a5* was previously found to be explicitly expressed in long bones and calvaria (Yorgan et al., 2019). Moreover, *Slc13a5* has been described as a major actor of a metabolic pathway regulating bone mineralization which make its impact on tumor growth in the *FosTg* mouse model interesting to define (Dirckx et al., 2022). Unfortunately, however, qPCR performed on individual tumor RNA samples did not show significant differences depending on the presence of *Lrp5*. *Car12* encodes for a protein of the carbonic anhydrase family. This family was described to be relevant for extracellular matrix maintenance, and one member, *Car2*, has an important role in bone resorption, where it participates in the acidification of the matrix to permit calcium dissolution (Lehenkari et al., 1998). Further investigations would be needed to evaluate the role of this specific carbonic anhydrase in osteosarcoma development.

For all these differentially expressed genes a deeper analysis is required to understand their implication in osteosarcoma growth and their potential regulation by *Lrp5*. Moreover, transcriptomic comparisons between cell lines and *in vivo* samples highlighted many differences and the need to optimize cell culture conditions to better reproduce the bone microenvironment. Here it may be useful, for instance, to culture the cell lines in a 3-dimensional environment. Furthermore, the administration of different osteogenic regulators in the culture medium could lead to a more reliable *in vitro* model. Indeed, it is likely that the physiologically relevant *Lrp5* ligand, which still remains to be identified, is missing in the cultured cells. Finally, several extracellular integrins were found to be implicated in the induction of a pro-tumoral and metastatic environment in murine osteosarcoma (Shintani et al., 2008). Recently, a new pathway involving *Wnt7a/ Lrp5* induction of decorin, an integrin implicated in neurogenesis was established (Long et al., 2016). The administration of such molecules in the cell culture medium and the study of their influence on *FosTg* cells with gain- (*Lrp5^{A213V/+}*) or loss-of-function of *Lrp5* (*Lrp5^{-/-}*) should be studied in future experiments.

Although *Lrp5* deficiency reduced tumor sizes, it does not abrogate the appearance of osteosarcomas. Therefore, these tumors are composed of a heterogeneous population of active and inactive osteoblasts increasing the complexity of transcriptomic analysis performed on whole tumor cells. Thus, this project would benefit from a single-cell RNA sequencing approach permitting the identification of cancer cell sub-populations and the definition of their specific gene expression profiles.

6.6. Fgf21, a potential new target to counteract tumor-induced lipodystrophy

A final *in vivo* analysis of this thesis was based on an antibody assay on pooled sera of each genotype. When comparing the data sets of wildtype and *FosTg;Lrp5^{A213V/+}* mice, fibroblast growth factor 21 (*Fgf21*) was identified to be more abundant in the latter. Moreover, *Fgf21* was found highly concentrated in mice carrying the highest tumors burden, i.e. *FosTg* and *FosTg;Lrp5^{A213V/+}* but less abundant in wildtype and *FosTg;Lrp5^{-/-}* mice sera. Similarly, significantly higher levels of *Fgf21* were found in the serum of *FosTg* and *FosTg;Lrp5^{A213V/+}* mice compared to WT mice but normalized in *FosTg;Lrp5^{-/-}* mice sera.

FosTg mice are developing, in parallel to osteosarcomas, a characteristic lipodystrophy close to what is commonly termed “tumor-associated cachexia”, a process that could principally be caused by excessive production of *Fgf21*. Although transcriptomic analysis by qPCR showed that the tumor itself is not responsible for *Fgf21* overexpression (data not shown), some articles define the liver as the primary producer of this growth factor, which is then released into the circulation (Emanuelli et al., 2014). Moreover, *Ucp1* was found to be upregulated in the subcutaneous fat of *FosTg* mice (as outlined in the Introduction), which correlates with this finding. In fact, *Ucp1* is known to be induced by *Fgf21* to cause browning of subcutaneous fat tissue (Fisher et al., 2012). Further studies are now needed to evaluate the potential of *Fgf21* as a new target to counteract tumor-associated cachexia, at least in *FosTg* mice. A recently published article supports this possibility, as it describes the implication of FGF21 in cachexia related to aging in elderly patients (Franz et al., 2019).

7. Materials

7.1. Instruments and softwares

Table 1: List of instruments

Instruments	Model	Manufacturer
Acrylate microtome	Reichert Jung Mod. 1140/Autocut	Cambridge Instruments Co. Ltd. (St. Neots, UK)
Affymetrix Gene Chip®	7G 3000	Thermo Fisher Scientific Inc. (Waltham, US)
Autoclave	5050ELC	Tuttnauer Europe B.V (Breda, NL)
Autotechnicon	2050	Bavimed Laborgeräte GmbH (Birkenau)
BSE detector	Type 202	K.E. Developments Ltd. (Cambridge, UK)
Camera	EOS 200D	Canon K.K (Tokio, JP)
Centrifuge 1	5430R	Eppendorf AG (Hamburg)
Centrifuge 2	5415D	Eppendorf AG (Hamburg)
Centrifuge 3	GS-6	Beckman Coulter, Inc. (Brea, US)
Electrophoresis system	Sub-cell	Bio-Rad Laboratories, Inc. (Hercules, US)
Gene Chip® Fluidics Station	450	Thermo Fisher Scientific Inc. (Waltham, US)
Gene Chip® Hybridization Oven	640	Thermo Fisher Scientific Inc. (Waltham, US)
Grinding machine	Exakt-Apparatebau D-2000	EXAKT Apparatebau GmbH & Co. KG (Norderstedt)
Ice machine	FM-120DE	Hoshizaki Denki K.K. (Toyoake, JP)
Incubator	BBD 6220	Heraeus Holding GmbH (Hanau)
Light table	1634	Hama GmbH & Co KG (Monheim)
Magnetic stirrer	RCT Basic	IKAR-Werke GmbH & CO. KG (Staufen)
Micropipette	Research Plus	Eppendorf AG (Hamburg)
Microplate reader	Versamax	Molecular Devices, LLC (Sunnyvale, US)
Microscope	AxioskopA1	Carl Zeiss AG (Oberkochen)
Microscope		Olympus Medical Systems Corp. (Tokyo, JP)
Microscope camera	Axiocam	Carl Zeiss AG (Oberkochen)
Paraffin microtome	Reichert-Jung Mod. Hn40	Cambridge Instruments Co. Ltd. (St. Neots, UK)
PCR-system	Mastercycler pro S	Eppendorf AG (Hamburg)
PCR-system	Mastercycler egradient S	Eppendorf AG (Hamburg)
pH meter	Hanna Instruments HI 2211	Hanna instruments Deutschland GmbH (Vöhringen)
Pipette controller	Pipetboy acu	INTEGRA Biosciences AG (Zizers, CH)
Real-Time PCR system	StepOnePlus	Applied Biosystems, Inc.(Foster City, US)
Scanner	Scanjet G4050	Hewlett-Packard Inc. (California, US)
Shaker	Innova 4000	New Brunswick Scientific Co., Inc. (Enfield, US)
Spectrophotometer	Nanodrop ND1000	Thermo Fisher Scientific Inc. (Waltham, US)
Tape Station	TapeStation 2200	Agilent Technologies Inc. (Santa Clara, US)
Thermoblock	Thermostat Plus	Eppendorf AG (Hamburg)
Thermoblock	Thermomixer Comfort	Eppendorf AG (Hamburg)
UV Light Table	Universal Hood 75S	Bio-Rad Laboratories, Inc. (Hercules, US)
Vortex mixer	Certomat MV	B.Braun Biotechnologie International GmbH (Hessen)
Water bath	1012	GFL Gesellschaft für Labortechnik GmbH (Burgwedel)
X-ray apparatus	Faxitron Xray Sterile	Faxitron Xray Corp. (Tucson, US)
X-ray Film Processor	Optimax 1170-1-0000	Protec GmbH & Co. KG (Oberstenfeld)
X-ray microtomograph	µCT 40	Scanco Medical AG (Brüttisellen, CH)

Table 2: List of software

Softwares	Version	Manufacturer
Adobe photoshop CC	2018	Adobe Systems Incorporated (San José, US)
Bioquant Osteo	7.00.10	BIOQUANT Image Analysis Corp. (Nashville, US)
GraphPad Prism	7.0	GraphPad Software Inc. (San Diego, US)
ImageJ		National Institutes of Health (University of Wisconsin,US)
MicroCT Software	4.05	Scanco Medical AG (Brüttisellen, CH)
Microsoft Office	2016	Microsoft Corp. (Redmond, US)
Osteomeasure	1.03.0	Osteometrics Inc. (Georgia, US)
Quantity One	4.6.9	Bio-Rad Laboratories, Inc. (Hercules, US)
Softmax Pro	7.1	Molecular Devices, LLC (Sunnyvale, US)
StepOne™ Software	2.3	Applied Biosystems, Inc. (Foster City, US)
Transcriptomics Analysis Console (TAC)	4.0	Thermo Fisher Scientific Inc. (Waltham, US)
Zeiss ZEN Pro	3.4	Zeiss Group (Oberkochen)

7.2. Chemicals, substances and powders

Table 3 : List of chemicals and reagents

Name	Manufacturer
β-Glycerophosphate	Sigma-Aldrich Corp. (St. Louis, US)
1,2-dihydroxyanthraquinon (Alizarin red)	Chroma GmbH & Co. KG (Münster)
1,4-Dimethylbenzene (xylene)	Merck KGaA (Darmstadt)
4-(2-hydroxyethyl)-1- piperazineethanesulfonic acid (HEPES)	Sigma-Aldrich Corp. (St. Louis, US)
Acetic acid	Sigma-Aldrich Corp. (St. Louis, US)
Acid fuchsin	Merck KGaA (Darmstadt)
Agarose (SeaKem® LE)	Lonza Group AG (Basel, CH)
Ammonium hydroxide	Sigma-Aldrich Corp. (St. Louis, US)
Benzoyl peroxide (BPO)	Merck KGaA (Darmstadt)
Bradford solution	Bio-Rad Laboratories, Inc. (Hercules, US)
Bolt™ LDS sample buffer (4X)	Thermo Fisher Scientific Inc. (Waltham, US)
Bolt™ MES SDS running buffer (20X)	Thermo Fisher Scientific Inc. (Waltham, US)
Bolt™ sample reducing agent (10X)	Thermo Fisher Scientific Inc. (Waltham, US)
Bolt™ transfer buffer (20X)	Thermo Fisher Scientific Inc. (Waltham, US)
Bovine serum albumin	Thermo Fisher Scientific Inc. (Waltham, US)
Citroline 2000	Adefo-chemie GmbH (Dietzenbach)
DAB (3,3'-diaminobenzidine) substrate	DakoCytomation (Glostrup, DK)
Diethyl pyrocarbonate (DEPC)	Sigma-Aldrich Corp. (St. Louis, US)
Dimethyl sulfoxide (DMSO)	Carl Roth GmbH & Co. KG (Karlsruhe)
DNA-Ladder 1kb	Thermo Fisher Scientific Inc. (Waltham, US)
Ethanol	Merck KGaA (Darmstadt)
Ethanol 80%	Chemsolute® Th. Geyer GmbH & Co. KG. (Renningen)
Ethylenediaminetetraacetic acid (EDTA)	Merck KGaA (Darmstadt)
Fetal bovine serum	Gibco®, Thermo Fisher Scientific Inc. (Waltham, US)
Formafix 3,5%	Grimm med. Logistic GmbH (Turgelow)
Formaldehyde	Sigma-Aldrich Corp. (St. Louis, US)
Glycerol	Carl Roth GmbH & Co. KG (Karlsruhe)
Glycin	Carl Roth GmbH & Co. KG (Karlsruhe)
Hydrochloric acid	Sigma-Aldrich Corp. (St. Louis, US)
Hydrogen peroxide	Merck KGaA (Darmstadt)
Isopropanol	Carl Roth GmbH & Co. KG (Karlsruhe)
L-Ascorbic acid	Sigma-Aldrich Corp. (St. Louis, US)
Methyl methacrylate	Merck KGaA (Darmstadt)
Methanol	Carl Roth GmbH & Co. KG (Karlsruhe)
Minimum essential medium eagle alpha modification	Sigma-Aldrich Corp. (St. Louis, US)
Monoglycol butylether	Sigma-Aldrich Corp. (St. Louis, US)
Mounting solution DPX	Sigma-Aldrich Corp. (St. Louis, US)
Nitric acid	Sigma-Aldrich Corp. (St. Louis, US)
Nonyl phenoxyethoxyethanol (NP-40)	Sigma-Aldrich Corp. (St. Louis, US)
Nonylphenyl-polyethylenglycol-acetate	Sigma-Aldrich Corp. (St. Louis, US)
Penicillin/Streptomycin (10000 U/ml)	Thermo Fisher Scientific Inc. (Waltham, US)
peqGOLD Trifast (RNA isolation)	Peqlab Biotechnologie GmbH (Erlangen)
Phosphate Buffered Saline	Gibco®, Thermo Fisher Scientific Inc. (Waltham, US)
Phosphatase inhibitor	Roche applied Science AG (Penzberg)
Picric acid	Sigma-Aldrich Corp. (St. Louis, US)
Polyoxyethylene (20) sorbitan monolaurate (Polysorbat 20)	Carl Roth GmbH & Co. KG (Karlsruhe)
Ponceau S solution	Sigma-Aldrich Corp. (St. Louis, US)
Prop-2-enamide	Carl Roth GmbH & Co. KG (Karlsruhe)

Protease inhibitor	Roche applied Science AG (Penzberg)
Protein Ladder	Lonza Group AG (Basel, CH)
Silver nitrate	Merck KGaA (Darmstadt)
Sodium carbonate	Carl Roth GmbH & Co. KG (Karlsruhe)
Sodium chloride	Sigma-Aldrich Corp. (St. Louis, US)
Sodium deoxycholate	Sigma-Aldrich Corp. (St. Louis, US)
Sodium dodecyl sulfate (SDS)	Carl Roth GmbH & Co. KG (Karlsruhe)
Sodium hydrogen carbonate	Sigma-Aldrich Corp. (St. Louis, US)
Sodium hydroxide	Avantor Performance Materials (Center Valley, US)
Sodium phosphate	Sigma-Aldrich Corp. (St. Louis, US)
SYBR™ Green Mastermix	Thermo Fisher Scientific Inc. (Waltham, US)
Taqman® Mastermix	Thermo Fisher Scientific Inc. (Waltham, US)
Tetramethylethylenediamine (TEMED)	Sigma-Aldrich Corp. (St. Louis, US)
Toluidin blue O	Sigma-Aldrich Corp. (St. Louis, US)
Tris(hydroxymethyl)amino-methane base	Sigma-Aldrich Corp. (St. Louis, US)
Tris(hydroxymethyl)amino-methane hydrochloride (Tris/HCl)	Sigma-Aldrich Corp. (St. Louis, US)

7.3. Buffers and solutions

Table 4 : List of prepared solutions

Name	Quantity	Components
Acrylate	0,33 % (w/v) 11 % (v/v)	Benzoyl peroxide Nonylphenyl-polyethylenglycol-acetate ad Methyl methacrylate (destabilized)
Alizarin red staining	40mM	Alizarinred S ad H ₂ O
Blocking buffer (WB)	5 % (w/v)	BSA ad TBST
Collecting buffer (WB)	1,5 M 0,4 % (w/v)	Tris/HCl SDS ad H ₂ O pH 6,8
DEPC-H ₂ O	0,2 % (v/v)	DEPC ad H ₂ O
Infiltration solution 1	0,33 % (w/v)	Benzoyl peroxide ad Methyl methacrylate (destabilized)
Infiltration solution 2	0,33 % (w/v) 11 % (v/v)	Benzoyl peroxide Nonylphenyl-polyethylenglycol-acetate ad Methyl methacrylate (destabilized)
Proteinase K	1 % (w/v)	Proteinase-K ad H ₂ O
RIPA buffer	1 % (v/v) 1 % (w/v) 0,1 % (w/v) 150 mM 2 mM 10 mM	NP-40 Sodium deoxycholate SDS NaCl EDTA Sodium phosphate ad H ₂ O pH 7,4
Running buffer (10X) (WB)	250nM 1,92M 1% (w/v)	Tris/Base Glycin SDS ad H ₂ O
Sectioning solution	0,1% (w/v)	Polysorbat 20 ad H ₂ O
Sodaformol solution	473mM 24,8% (w/v)	Sodium carbonate 37% Formaldehyde ad H ₂ O
Stretching solution	80% (v/v) 1 Drop/L	Isopropyl alcohol Monoglycol butylether ad H ₂ O
TAE buffer (50X)	2 M 50 mM	Tris/HCl EDTA ad H ₂ O pH 7,8
Tail biopsy lysis buffer	100mM 50 mM	EDTA Tris Base pH 8,6
TBS-T	100 ml 1ml 900ml	TBS (10X) Tween 20 H ₂ O
TE-buffer	10mM 1mM	Tris base EDTA add H ₂ O pH 7,5
Tris buffered saline (TBS) (10X)	500mM 1,5 M	Tris/HCl NaCl ad H ₂ O pH 7,4
Toluidinblue staining solution	32,7mM	Toluidin blue O ad H ₂ O pH 4,5
Van Gieson staining solution	4,27mM 10% (v/v) 0,5% (v/v)	Acid fuchsin Glycerol 65 % Nitric acid ad saturated Picric acid
Von Kossa staining solution	194 mM	Silver nitrate ad H ₂ O

7.4. Consumables and commercial kit

Table 5 : List of consumables

Name	Manufacturer
1,5 and 2 ml tubes	Eppendorf AG (Hamburg)
5 ml tubes	Eppendorf AG (Hamburg)
15 and 50 ml tubes	Greiner Bio-One International AG (Kremsmünster, AT)
5ml Polystyrene round-bottom tubes	BD Biosciences (US)
ACCU-Chek® Aviva Glucose control	Roche Diabetes Care Deutschland GmbH (Mannheim)
Adhesive PCR plate foil	Thermo Fisher Scientific Inc. (Waltham, US)
Bottle Top Filter 150mL 0,2 µm	Th. Geyer GmbH & Co.KG (Renningen)
Bottle Top Filter 500mL 0,2 µm	Thermo Fisher Scientific Inc. (Waltham, US)
Cell culture 6 and 12 well plates	Sarstedt AG & Co. (Nümbrecht)
Cell culture round dishes 100x200 mm	Sarstedt AG & Co. (Nümbrecht)
Cell culture flasks 25-175 cm ²	Sarstedt AG & Co. (Nümbrecht)
Cell Scraper	Sarstedt AG & Co. (Nümbrecht)
Cover slips	Carl Roth GmbH & Co. KG (Karlsruhe)
Cryo vials 2ml	Greiner Bio-One International AG (Kremsmünster, AT)
Embedding cassettes	Carl Roth GmbH & Co. KG (Karlsruhe)
Filter Tip 10-1000 µl	Sarstedt AG & Co. (Nümbrecht)
GeneChip™ Mouse Genome 430 2.0 Array	Thermo Fisher Scientific Inc. (Waltham, US)
Nitrile gloves Dermagrip®	WRP Asia Pacific Sdn Bhd (Malaysia)
MicroAmp® Fast 96-well reaction plate	Applied biosystems, Life technologies Corporation (California, US)
MicroAmp® Optical adhesive film	Applied biosystems Life technologies Corporation (California, US)
Microscope slide	Glaswarenfabrik Karl Hecht GmbH & Co. KG (Sondheim)
Microslide 8 well	Ibidi® GmbH (Gräfelfing)
Microtest plates 96-well	Sarstedt AG & Co. (Nümbrecht)
Microtome blade	Leica Biosystems Nussloch GmbH (Nussloch)
Needles 0,6x25 mm	B. Braun Melsungen AG (Hessen)
Nitrocellulose transfer membrane	Schleicher & Schuell GmbH, Whatman, Inc. (Maidstone, UK)
Pasteur pipettes	VWR International, LLC (Radnor, US)
PCR reaction tubes	Biozym Scientific GmbH (Hessisch Oldendorf)
Pipette tips 10, 20, 100, 300, 1000 µl	Sarstedt AG & Co. (Nümbrecht)
Scalpel blade	C. Bruno Bayha GmbH (Tuttlingen)
Syringes 1ml-10ml	B.Braun Medical Inc. (Bethlehem, PA)
Syringe Filter 25mm	Th. geyer GmbH & Co.KG (Renningen)
Serological Pipettes 5, 10, 25 ml	Sarstedt AG & Co. (Nümbrecht)
X-ray films	Agfa-Gevaert N.V. (Mortsel, BE)

Table 6 : RNA/DNA/protein extraction kits

Name	Manufacturer
Phire Animal Tissue Direct PCR kit	Thermo Fisher Scientific Inc. (Waltham, US)
NucleoSpin RNA/Protein kit	Macherey-Nagel GmbH & co. KG, (Düren)
Verso cDNA Synthesis Kit	Thermo Fisher Scientific Inc. (Waltham, US)
GeneChip™WT PLUS Reagent Kit	Thermo Fisher Scientific Inc. (Waltham, US)

8. Methods

8.1. Mouse models

The *FosTg* mouse model was generated by placing the proto-oncogene *c-Fos* under the control of an H-2K^b class I MHC promoter (Grigoriadis et al., 1993; R  ther & Wagner, 1989).

Lrp5^{-/-} mice (B6.129P2-*Lrp5*^{tm1Dgen}/J) were obtained from Jackson Laboratory (#00582) (Maine, US). This targeted mutant was created and characterized by Deltagen, Inc (California, US). *Lrp5*^{A213V/+} mice (B6.129-*Lrp5*^{tm2Mawa}/J) were obtained from Jackson Laboratory (#012672) (Maine, US). These mice carry a targeted mutation (A213V) to reproduce the missense mutation present in humans with a high bone mass phenotype (A214V).

Mice of these separated colonies were then crossbred to create the two additional mouse models relevant for this study, i.e. *FosTg;Lrp5*^{A213V/+} and *FosTg;Lrp5*^{-/-}.

All mice were hosted at the UKE animal facility in a specific pathogen-free environment, in ventilated cages following cycles of rhythm of 12 hours' light/dark. Matings, sacrifices and organs removal were following German regulation with respect to the 3R rules (DRFZ, Berlin, Germany) and approved by the local ethic committee: Org984, N19/053_Metabone and N59/22.

8.2. Genotyping

Tail biopsies were collected by animal caretakers to permit the genotyping of newborn mice. DNA extraction from fresh tail biopsies could be performed using a Phire animal tissue direct PCR kit. If tail biopsies were less freshly collected DNA was extracted with the Phenol/Chloroform method. A mix of 400 µl of tail lysis buffer (TLB) and 50 µl of Proteinase K is added per tube and the samples are then mixed on a warm block at the temperature of 55°C for 2 hours. Then 450 µl of phenol/chloroform was added per tube and shaken vigorously. Tubes were centrifuged for 10 minutes at 13200 rpm and supernatants were put in new tubes. Isopropanol was added with the ratio 1:1, tubes were shaken and centrifuged for 10 minutes at 13200 rpm. Supernatants were then discarded and 400 µl of ethanol 70% was added. A first centrifugation under previous parameters was done and tubes were

emptied fast and put again in the centrifuge for 5 minutes at 13200 rpm. After this last centrifugation, all remaining ethanol was pipetted off and pellets were dried for 5 minutes. Pellets were then dissolved in 50 µl of TE-Buffer. Genotyping was then performed by PCR and migration on 2% Agarose electrophoresis gel at 100 V. Reaction mix for each gene and their appropriate programs are described below.

Table 7: Genotyping programs

Genes:			
Reaction mix (1X)	<i>c-Fos</i> Tg	<i>Lrp5</i> ^{-/-}	<i>Lrp5</i> ^{A213V/+}
10X Buffer	2 µL	2,5 µL	2 µL
DMSO	0,5 µL	0,25 µL	0,5 µL
dNTPs (10mM/dNTP)	0,5 µL	0,5 µL	1 µL
Primer forward (2pM)	3 µL	4 µL	3 µL
Primer reverse (2pM)	3 µL	4 µL	3 µL
Dream Taq polymerase	0,3 µL	0,25 µL	0,3 µL
H2O	9,7 µL	12,5 µL	9,2 µL
DNA	1 µL	1 µL	1 µL
Primers 1 (forward/reverse)	5'-AGT CTG GCC TGC GGG TCT CT-3'	5' GGA TGG ACG GAT GGA CAG AAT G3' (WT)	5'AGT ACT GGC TGG CAC AGA3'
	5'-GTC GGC TGG GGA ATG GTA GTA GG-3'	5'TGG AGC CTT TAT GCT AAC CAC AG 3' (WT)	5'CAG GCT GCC CTT GCA GAT3'
Primers 2 (forward/reverse)		5' CGC TAC CGG TGG ATG TGG AAT GTG T 3' (KO)	
		5'GCT GCC ACT CAT GGA GCC TTT ATG C 3' (KO)	
Program	94°C (4 min) 94°C (40 sec) 52°C (40 sec) 72°C (1 min) 72°C (10 min)	94°C (4 min) 94°C (40 sec) 58°C (40 sec) 72°C (1 min) 72°C (10 min)	94°C (4 min) 94°C (40 sec) 62°C (40 sec) 72°C (1 min) 72°C (10 min)
n Cycles	40	40	48
Size band	600bp	500bp(WT), 400bp(KO)	246bp(WT), 400bp(HBM)

8.2.1. Mice euthanasia and skeleton storage

Mice were euthanized at the age of 16 weeks old, with CO₂ after being anesthetized with a O₂/CO₂ mixture. Mice were weighted and organs were taken out and weighted *post mortem*. Skeletons were then fixed in Formafix 3.5% and after 48 hours stored in ethanol 80%. Xrays were done at 35 KV for 2 seconds and developed on film processor. Tumor count was performed on Xrays images scanned in high resolution. Skeletons were then transferred into 50 ml tubes filled with ethanol 80% and archived.

8.2.2. Serum glucose and serum collection

After euthanasia, blood was collected by cardiac puncture and after 30 minutes of decantation, centrifuged at 6000 rpm for 6 minutes. Supernatants (sera) were then transferred into a new tube and stored at -80°C. Serum glucose was measured from the mouse blood using a glucometer (ACCU-CHECK Aviva, Roche).

8.3. Micro-computed tomography

The right femora of 16-week-old mice were isolated, fixed in formaldehyde 3,5% and stored in 80% ethanol. Soft tissues were then discarded and bones were scanned using Medical Scanco μ CT 40 (Scanco Medical AG, Brüttisellen, Switzerland) with a voxel size of 10 μ m. Measurements were then performed in the trabecular bone area (distal metaphysis) and cortical bone area (middle diaphysis) according to standard guidelines.

8.4. Histology

8.4.1. Undecalcified acrylate histology

8.4.1.1. Preparation of spine samples

Lumbar vertebral bodies (L1-L4) were retrieved from skeletons previously fixed in formaldehyde 3,5% and stored in ethanol. Vertebral bodies were then first dehydrated in ascending ethanol concentrations (80-100%). Samples were then embedded in methylmethacrylate. Samples were cut in the sagittal plane with a microtome to obtain 4 μ m thick sections.

8.4.1.2. Staining

For Von Kossa/van Gieson stainings and Toluidine blue staining vertebral slides were rehydrated in descending ethanol concentrations (100-50%). After rinsing, for Von Kossa/Van Gieson staining, 3 % silver nitrate was added to samples for 5 minutes, washed with water and stained in soda-formol solution. After another washing samples were stained in 5 % sodium thiosulfate 5% and rinsed again in distilled water for 10 minutes. A second staining with van Gieson solution was added for 20 minutes. Finally, the slides were dehydrated in

ascending alcohol concentrations (80-100%) and incubated in xylene 3 times for 5 minutes. Mounting was done in DPX mounting solution and covered with a coverslip. For cellular histomorphometry, samples were stained with a Toluidine blue 1% solution and after 30 minutes of incubation rinsed with water. A dehydration step was then performed using ascending concentrations of ethanol and samples were incubated with xylene. The final step was the montage on glass slides with DPX mounting solution and the addition of coverslides.

8.4.1.3. Tumor area and bone mass calculation on spine

The volume of the tumors was evaluated on images of Von Kossa stained spine sections taken by microscope (Carl Zeiss AG, Oberkochen). The areas of the tumors were measured using ImageJ software and the ratios of tumor areas to the total vertebra areas were calculated for each tumor. Medians of all tumor ratios per mouse were calculated and presented on a graph with one dot representing one mouse. Tumor bone mass measurement was performed on Kossa stained spine sections with the use of Bioquant Osteo software (Bioquant Image Analysis Corp., Nashville, US) and tumor osteoid measurement was performed using OsteoMeasure64 software (Osteometrics Inc., Decatur, GA, US).

8.4.2. Decalcified paraffin sections of spine and immunohistochemistry of Fbln3

Mice vertebral bodies (L1-L4) were decalcified for 10 days on a rolling platform at 4°C using 20% EDTA solution. Then samples were dehydrated using ascending concentrations of ethanol and embedded in paraffin. Sections of 4 µm were cut and the montage of the sections was done on glass slides. To clear out paraffin from vertebral bodies three baths of Xylene (5 minutes) were performed. Descending concentrations of ethanol (100%-70%) were then applied. After that, samples were washed with distilled water. After incubation with a blocking buffer, the primary antibody, rabbit anti-mouse Fbln3 (ab151976 Abcam Inc., Cambridge, US), diluted 1:100 in blocking buffer (TBS-T and 2,5% goat serum) was added to all vertebral slices except the control and incubated at 4°C overnight. The sections were washed and incubated with the secondary antibody associated with labeled polymers for 30

minutes at room temperature (Dako™ EnVision Flex HRP). Images were taken on microscope at the 2,5X objective (Carl Zeiss AG, Oberkochen).

8.4.3. Histomorphometry measurements

Cellular content quantification was performed by histomorphometry analysis on Toluidine blue stained vertebral sections using an OsteoMeasure system (Osteometrics Inc., Decatur, GA, US). Bone cells and bone parameters quantification of tumors were based on the measurement of the number of osteoblasts per bone perimeter (N.Ob/B.Pm), number of osteocytes per bone perimeter (N.Ot/B.Pm), osteoclasts per bone perimeter (N.Oc/B.Pm) inside the tumors, osteoblasts at the surface of the tumor per tumor bone perimeter (N.Ob/B.Pm), osteoid surface per tumor bone surface (OS/BS) at the tumor surface.

8.5. Protein analysis

8.5.1. Antibody assay

A protein profiling assay was used on pooled serum of different genotypes. Therefore, tubes were sent on dry ice to Sciomics GmbH (Heidelberg, Germany). There, after protein extraction, a method involving dual-color detection by the labeling of the samples with fluorescent dyes (SciODye 1 and SciODye 2) was used. Labeled samples were then added to a surface coated with antibodies detecting the abundance of a set of 1300 proteins. This scioDiscover antibody array permits, thanks to the competitive incubation of the samples to have an accurate comparison of protein abundance by the measurement of their respective dye intensity on different spots representing different proteins (following the link to the webpage of the company: <https://www.sciomics.de/services/protein-expression-analysis/protein-profiling>).

8.5.2. Enzyme-linked immunosorbent assay (ELISA)

ELISA kits were used to quantify various proteins in mice sera. They were performed according to the manufacturer's instructions.

Table 8: List of kits

Name	Abbreviation	Reference	Manufacturer
Cross-linked C-telopeptide of type I collagen	CTX	MBS164705	MyBiosource Inc. (San Diego, US)
Fibulin-3	Fbln3	SEF422Mu	Cloud-Clone Corp. (Houston, US)
Fibroblast growth factor 21	Fgf21	MF2100	R&D Systems Inc. (Minnesota, US)
Procollagen type 1 N-propeptide	P1NP	SEA957MU	Cloud-Clone Corp. (Houston, US)

8.5.3. Western Blot

Cells were seeded at a density of 400000 cells per tissue culture dish (100x20 mm). One day after seeding cells were treated either with BI-D1870 (10 μ M) or DMSO (carrier) for 24 and 48 hours. Cells were then scraped in 400 μ l of RIPA buffer supplemented with phosphatase and protease inhibitors and collected in tubes. Tubes were incubated on ice for 15 minutes and centrifuged at 4°C at 14000 rpm. Supernatants containing the proteins were then stored at -80°C. A Bradford assay was performed to determine protein concentration in samples. Aliquots of the samples were diluted in water 1 to 8 with a final volume of 800 μ l and 200 μ l of Bradford reagent was added per sample. A standard curve was made using Bovine serum albumin (BSA) (0 μ g, 5 μ g, 10 μ g, 15 μ g and 20 μ g) diluted in 800 μ l of water. An ELISA reader was then used to determine optical density at 595 nm of the standard curve and samples. Samples concentrations were then calculated based on the standard linear curve.

SDS-PAGE and Western blot to visualize phosphorylated Rsk2 expression in *FosTg* cells treated with BI-D1870 was performed on a 15 wells mini-protein gel (Bolt™ 12 %, Bis-Tris, 1,0 mm from Thermo Fischer Scientific). A reaction mix composed of 15 μ g of protein, 5 μ l of LDS buffer (4X), and 2 μ l of reducing agent (10X) per sample was loaded on the gel that was placed in a western blot chamber previously filled with running buffer (500 ml of distilled water with 5% of 20X Bolt MES SDS running buffer). The protein migration was performed at 200V for 20

minutes. Transfer of proteins was made on 0,45 μm pore nitrocellulose membrane. For this step the membrane was placed in contact with the gel and cover on each side with paper filters and sponges. The montage is then placed in a blot chamber with the anode placed on membrane side and the transfer is performed for 60 minutes at 10V. The membrane was then stained with Ponceau S solution to visualize protein transfer. After washing with TBS-T, the membrane was then blocked for 1 hour in blocking solution. The membrane was then cut in two parts to permit an incubation with two different rabbit anti-mouse primary antibodies, β -actin (#5732 Cell signaling Technology Inc., Danvers, US) and Serine 227 phosphorylated Rsk2 (#3556 Cell signaling Technology Inc., Danvers, US) diluted 1:1000 in blocking solution overnight at 4°C on a moving platform. The following day, the membrane was washed three times with TBS-T and incubated for 1 hour at room temperature with a goat anti-rabbit IgG-HRP-conjugated secondary antibody (#P0448 Dako/Agilent Technologies Inc., Santa Clara, US) diluted 1:2000 in blocking buffer. After washing 1 ml of Pierce™ ECL Western Blotting Substrate solution was added and membrane was kept out of light in the western blot cassette. β -actin revelation was made after 1 minute of exposure and Phosphorylated Rsk2 (ser227) after 3 hours of exposure on Amersham hyperfilm (Ge Healthcare Bio-Sciences AB, Uppsala, SE).

8.6. Cell culture

8.6.1. Cell lines derived from tumors

Tumors from tibiae and femora were collected after mice sacrifice and washed with PBS. Tumors were cut in pieces with a scalpel and pieces were collected in 5 ml of α -MEM medium in a 15 ml falcon. Falcons were centrifuged and pieces of tumors were put in 6 well plates (one per mouse) with 2 ml of medium. The standard cell culture medium used for these cells in this thesis was α -MEM supplemented with 10% of foetal bovine serum (FBS) and 1% penicillin/streptomycin. After 24 hours, fresh medium was added and tumors were left for 5 days without other medium change to permit a good plastic adherence of the cells getting out of the bone pieces. Confluent wells were trypsinized and cells were transferred to a 25 cm^2 , 75 cm^2 and finally 175 cm^2 and passaged every week, with cells growing after passage 10 considered as immortalized and used for experiments but also frozen in vials (in FBS 10%

DMSO) for unlimited future experiments. Cells were incubated at 37°C with 5% CO₂ during the time of the experiments.

8.6.2. Commercial cell line

U2OS is a commercial cell line (ATCC) derived from tibia-osteosarcoma of a 15-year-old woman patient. These cells were cultured in Mc Coy's 5A (Biochrom GmbH, Berlin) medium supplemented with 10% FBS and 1% antibiotics (penicillin/streptomycin). Cells were incubated at 37°C with 5% CO₂ and 100% rH during the experiments time.

8.6.3. Growth and mineralization analysis

Cells were trypsinized at passage >10 and seeded in 12 well plates at a density of 20000 cells per well. During 6 consecutive days, cells were counted in triplicates and growth curves were established of *FosTg*, *FosTg;Lrp5^{-/-}*, *FosTg;Lrp5^{A213V/+}* cell lines (at least 4 cell lines per genotype). Growth curves of *FosTg* cell lines stimulated with a recombinant protein complex: Wnt1/Sfrp1 (100 ng/ml) or an *Lrp5* antagonist, sclerostin (2,5 µg/ml) were also established following the same parameters.

For mineralization analysis cells were seeded in 12 well plates at the density of 50000 cells per well. At 80% of cell confluence an osteoblastic differentiation medium composed of the standard culture medium supplemented with 50 µg/ml of ascorbic acid and 10 mM of β-glycerophosphate was added every two days on the cells for 15 or 30 days. At 15 or 30 days of differentiation, the medium was discarded, and cells were washed with PBS. Cells were fixed in ethanol 90% for 10 minutes at room temperature. After the washing of the wells with distilled water, cells were stained with Alizarin red by incubation at room temperature on a moving platform for 10 minutes. Finally, wells were washed with distilled water until the water was uncolored and pictures of the wells were taken with a Canon EOS 200 camera. For quantification of the staining, cells were incubated with 10% acetic acid (800 µl/well) for 30 minutes at room temperature. Cell layers and supernatants were then collected in 1,5 ml tubes and placed on a heating block at 85°C for 10 minutes. Samples were then centrifuged at 13000 rpm for 10 minutes and 400 µl of supernatant was transferred to a new tube. To

obtain a pH at 4,5, 50 μ l of 10% ammonium hydroxide was added per tube. Finally, 150 μ l of sample were put in a 96-well plate and optical density was measured at 405 nm.

8.6.4. Cell treatments and dose effect curves

Different drugs have been administrated to *FosTg* cells. A Rsk inhibitor, BI-D1870 (Calbiochem[®], Sigma Aldrich, US) was administrated at a dose of 10 μ M. An aurora kinase B inhibitor, AZD1152 (Selleck Chemicals GmbH, US) was administrated to the cells at a dose of 200 nM. Different doses of Hesperadin (Selleck Chemicals GmbH, US), another aurora kinase B inhibitor were administrated to *FosTg* cells (25 nM to 1 μ M) and a dose effect curve was done after counting for six consecutive days cells seeded in triplicates. Polynuclear cells were counted after 24 or 48 hours of treatment and the dose of 100 nM was established for all other experiments.

8.6.5. Fluorescence microscopy

To visualize polynuclearity of *FosTg* cells treated with either BI-D1870 (10 μ M), AZD1152 (200 nM) or Hesperadin (100 nM), seeding was performed at a density of 20000 cells per well in 8 wells microslides (Ibidi[®] GmbH). Fixation was made in PFA 4% during 10 minutes. Cells were then washed three times with ice-cold PBS and stored at 4°C in 250 μ l of PBS per well. For fluorescent staining, PBS was discarded and Phalloidin 546 nm was added diluted 1:40 in antibody dilution buffer (10 ml PBS, 30 μ l Tween20, 10 mg BSA). Incubation was made at room temperature for 90 minutes protected from light. The cells were washed with PBS three times (200 μ l/well). To stain nuclei, 100 μ L of DAPI (2,5 μ g/ml) diluted 1:250 in PBS was added per well. Cells were finally washed in PBS and stored at 4°C until images were taken using a microscope Zeiss Axio Observer (Zeiss Group) with the 10x A-Plan Ph1 objective.

Visualization of the polynucleation of U2OS cells followed identical steps. For *FosTg* and *FosTg; Lrp5^{-/-}* cells, without treatments, cells were seeded at a density of 13000 cells per well.

8.7. Transcriptomic analysis

8.7.1. RNA extraction *in vitro* and *in vivo*

For RNA extraction cells were seeded in tissue culture dishes (100x20 mm), scraped in 1 ml of Trifast solution per dish and collected in 1,5 ml tubes. For direct *in vivo* RNA extraction, wildtype bones or tumors were collected in tubes after mice sacrifice and frozen in liquid nitrogen. Then, with the help of liquid nitrogen, bones were crushed by hand and bone powder was collected in a 2 ml glass tube and kept cold on ice. Then, 1 ml Trifast (peqGold TriFast™, Avantor®) was added. Tubes were put on ultraturax fast to crush the remaining bone pieces and Trifast supernatant part (without bone pieces) was transferred to 1,5 ml tube. To permit separation between DNA, RNA and protein, chloroform was added to both *in vitro* and *in vivo* tubes, samples were shaken to homogenize the two solutions and incubated for 10 minutes on ice. After centrifugation at 14000 rpm and 4 °C for 15 minutes the supernatant was transferred to new tubes, 1:1 ratio of isopropanol was added and after shaking a new centrifugation step was performed with the same parameters. Isopropanol was discarded and 1 ml of ethanol 70% (diluted in DEPC water) was added. A final centrifugation was made, ethanol discarded, and RNA pellets dried for some minutes until no trace of alcohol was visible. Pellets were then dissolved in RNase-free water and RNA concentration was quantified using a spectrophotometer, nanodrop® ND-1000 (peqlab, Biotechnologie GmbH).

8.7.2. Affymetrix gene chip hybridization

For Affymetrix gene chip hybridization new steps of RNA purification were performed on column using a Nucleospin® RNA/Protein kit (Macherey-Nagel GmbH & co. KG, Düren) according to manufacturer instructions. Briefly, column buffer (RP1) was added to previously extracted RNA dissolved in water to a final volume of 450 µl. To adjust RNA binding conditions 350 µl of ethanol 70% was added and mixed by pipetting up and down. The lysate was then loaded on a column, RNA bound to the column and the flow through was discarded after centrifugation. The membrane was then desalted using a specific buffer and then dried by centrifugation. RDNase reaction solution was prepared following kit instructions and 95 µl of the mix was put on the center of the column membrane. An incubation of 15 minutes at room

temperature was mandatory to obtain optimal DNA digestion. Finally, several washing steps of the column were performed and highly pure RNA was eluted in 30 µl of RNase-free H₂O (Sigma-Aldrich Corp., St. Louis, US).

Following the extraction of RNA from *in vivo* and *in vitro* tumor cells, a quality check was performed on a tape station 2200 (Agilent Technologies Inc., Santa Clara, US) permitting the validation of RNA integrity by automated electrophoresis. RNA of 5 mice was pooled per genotype to a final quantity per genotype of 100 ng RNA. The Affymetrix Clariom D gene array was performed according to manufacturer instructions (Thermo Fisher Scientific Inc., Waltham, US). Briefly, the technique implicates a reverse transcription of RNA into cDNA, the fragmentation of cDNA and their labeling before hybridization on Affymetrix Gene Chips (one per genotype). Labeled cDNA on Affymetrix Gene chips were then scanned by Affymetrix Gene Chip® Scanner. Data generated were analyzed using an Affymetrix software (TAC, Thermo Fisher Scientific Inc., Waltham, US) permitting the comparison between the genotypes of 65956 genes transcription.

8.7.3. CDNA synthesis

Reverse transcription of RNA to cDNA was performed using the verso cDNA synthesis kit.

Table 9: CDNA synthesis reaction mix

Reaction mix (1X)		
Probes	<i>In vitro</i>	<i>In vivo</i>
5X Buffer	2 µl	2 µl
dNTP	1 µl	1 µl
OligodT	0,5 µl	0,5 µl
Verso enzyme	0,5 µl	0,5 µl
RT enhancer	0,5 µl	0,5 µl
RNA	500 ng	250 ng
add H ₂ O to 10µl		
Program	42°C=30 min; 92°C=2 min	
Final dilution of cDNA	1:5	1:1,25

8.7.4. QPCR gene expression

Gene expressions were performed by quantitative real-time PCR (qPCR). Two different methods were used, Taqman primers (Table 7) or SYBR® green primers (Table 9) with different master mix and different programs performed on a StepOnePlus real-time PCR system (Applied Biosystems) described as follow (Table 8 and 10). Results were presented as relative expression of genes related to the housekeeping gene *Gapdh* expression.

Table 10: Taqman primers list

Genes	Taqman® Probe	Genes	Taqman® Probe
<i>Abca1</i>	Mm0042646_m1	<i>Chek1</i>	Mm001176757_m1
<i>AurkB</i>	Mm01718146_g1	<i>Chek2</i>	Mm00443844_m1
<i>Car12</i>	Mm00724225_m1	<i>Dmp1</i>	Mm01208363_m1
<i>Ccl2</i>	Mm00441242_m1	<i>Dynap</i>	Mm01268529_m1
<i>Ccnb1</i>	Mm03053893_gH	<i>E2f2</i>	Mm00624964_m1
<i>Ccnd1</i>	Mm00432358_g1	<i>Efemp1</i>	Mm01434321_m1
<i>Ccnd2</i>	Mm00438070_m1	<i>Foxm1</i>	Mm00514924_m1
<i>Ccne1</i>	Mm00432367_m1	<i>Gapdh</i>	4308313
<i>Cdc25b</i>	Mm00499136_m1	<i>Prl2c2</i>	Mm04209415_mH
<i>Cdca5</i>	Mm01233533_m1	<i>Prl2c3</i>	Mm04208101_mH
<i>Cdk1</i>	Mm00772472_m1	<i>Ptgs2</i>	Mm00478374_m1
<i>Cdk2</i>	Mm00443947_m1	<i>Rabgap1</i>	Mm01284516_m1
<i>Cdk4</i>	Mm00726334_s1	<i>Racgap1</i>	Mm00488847_m1
<i>Cdk6</i>	Mm01311342_m1	<i>Slc13a5</i>	Mm01334459_m1
<i>Cdkn1a (P21)</i>	Mm04205640_g1	<i>Trp53</i>	Mm01731287_m1
<i>Cdkn1b (P27)</i>	Mm00438168_m1	<i>Wee1</i>	Mm00494175_m1

Table 11: Taqman qPCR reaction and program.

Reaction mix		Program	
Mastermix Taqman®	10 µL	50°C	2 minutes
H2O	7 µL	95°C	10 minutes
Primer	1 µL	95°C	15 seconds
		60°C	1 minute
+ add of cDNA	2 µL	number of cycles:	40

Table 12: SYBR[®]Green primers.

Genes	Forward primer sequence	Reverse primer sequence
<i>Ccna1</i>	GGAAATTGCAGCTTGTCGGG	GGTGGTTGGAACGGTCAGAT
<i>Cdc25a</i>	CTCAGAAGCTCCTGGGATGTAG	GAGATGCAGGTCGTATTGGCT
<i>Cdc25c</i>	TACCATCCGTTTCAGATTTCCC	TCCTCAAGGTCAGCAGAAGT
<i>cFos</i> endo	TGTGTTCCCTGGCAATAGCGTGT	TGAACATTGACGCTGAAGGAC
<i>cFos</i> Tg	TGTGTTCCCTGGCAATAGCGTGT	GGCAATTCGCCCATAGTGA
<i>Gapdh</i>	GACATCAAGAAGGTGGTGAAGCAG	CTCCTGTTATTATGGGGTCTGG

Table 13: SYBR[®]Green reaction mix and program.

Reaction mix	Volume (1X)	Program
SYBR [®] Green master mix	10 µl	95°C 10 minutes
H ₂ O	7 µl	95°C 15 seconds
Primer Forward	1 µl	60°C 1 minute
Primer Reverse	1 µl	95°C 15 seconds
cDNA	1 µl	60°C 1 minute
number of cycles:	40	

8.7.5. Statistical analysis

Data shown in this thesis are presented as means ± standard error of the mean. Statistical analysis was performed on Graphpad prism software using unpaired or paired two-tailed Student's t-test vs control or one-way, two-way ANOVA. Statistical significance was attributed to p values below 0,05.

9. Bibliography

Aberle H, Bauer A, Stappert J, Kispert A, Kemler R. (1997) beta-catenin is a target for the ubiquitin-proteasome pathway. *EMBO J.* 16(13):3797-804.

ADHR Consortium. (2000) Autosomal dominant hypophosphataemic rickets is associated with mutations in FGF23. *Nat Genet.* 26(3):345-8.

Arnold A, Dennison E, Kovacs CS, Mannstadt M, Rizzoli R, Brandi ML, Clarke B, Thakker RV. (2021) Hormonal regulation of biomineralization. *Nat Rev Endocrinol.* 17(5):261-275.

Asteriti IA, Di Cesare E, De Mattia F, Hilsenstein V, Neumann B, Cundari E, Lavia P, Guarguaglini G. (2014) The Aurora-A inhibitor MLN8237 affects multiple mitotic processes and induces dose-dependent mitotic abnormalities and aneuploidy. *Oncotarget.* 5(15):6229-42.

Anjum R, Blenis J (2008) The RSK family of kinases: emerging roles in cellular signalling. *Nat Rev Mol Cell Biol* 9(10): 747–758

Baldauf C, Jeschke A, Kanbach V, Catala-Lehnen P, Baumhoer D, Gerull H, Buhs S, Amling M, Nollau P, Harroch S, Schinke T. (2015) The Protein Tyrosine Phosphatase Rptp ζ Suppresses Osteosarcoma Development in Trp53-Heterozygous Mice. *PLoS One.*10(9):e0137745.

Baron R, Kneissel M. (2013) WNT signaling in bone homeostasis and disease: from human mutations to treatments. *Nat Med.* 19(2):179-92.

Basant A, Lekomtsev S, Tse YC, Zhang D, Longhini KM, Petronczki M, Glotzer M. (2015) Aurora B kinase promotes cytokinesis by inducing centralspindlin oligomers that associate with the plasma membrane. *Dev Cell.* 33(2):204-15.

Belisario DC, Akman M, Godel M, Campani V, Patrizio MP, Scotti L, Hattinger CM, De Rosa G, Donadelli M, Serra M, Kopecka J, Riganti C. (2020) ABCA1/ABCB1 Ratio Determines Chemo- and Immune-Sensitivity in Human Osteosarcoma. *Cells.* 9(3):647.

Bell CR, Pelly VS, Moeini A, Chiang SC, Flanagan E, Bromley CP, Clark C, Earnshaw CH, Koufaki MA, Bonavita E, Zelenay S. (2022) Chemotherapy-induced COX-2 upregulation by cancer cells defines their inflammatory properties and limits the efficacy of chemoimmunotherapy combinations. *Nat Commun.* 13(1):2063.

Bellido T., Plotkin L., Bruzzaniti A. (2019) Bone Cells. Basic and Applied Bone Biology, Second Edition. Pages 37-55

Berman SD, Calo E, Landman AS, Danielian PS, Miller ES, West JC, Fonhoue BD, Caron A, Bronson R, Boussein ML, Mukherjee S, Lees JA. (2008) Metastatic osteosarcoma induced by inactivation of Rb and p53 in the osteoblast lineage. *Proc Natl Acad Sci U S A*. 105(33):11851-6.

Bignone PA, Lee KY, Liu Y, Emilion G, Finch J, Soosay AE, Charnock FM, Beck S, Dunham I, Mungall AJ, Ganesan TS. (2007) RPS6KA2, a putative tumour suppressor gene at 6q27 in sporadic epithelial ovarian cancer. *Oncogene*. 26(5):683-700.

Bischoff JR, Anderson L, Zhu Y, Mossie K, Ng L, Souza B, Schryver B, Flanagan P, Clairvoyant F, Ginther C, Chan CS, Novotny M, Slamon DJ, Plowman GD. (1998) A homologue of Drosophila aurora kinase is oncogenic and amplified in human colorectal cancers. *EMBO J*. 17(11):3052-65.

Black DM, Rosen CJ. (2016) Clinical Practice. Postmenopausal Osteoporosis. *N Engl J Med*. 374(3):254-62.

Bleyer A, O'Leary M, Barr R, Ries LAG (eds) (2006): *Cancer Epidemiology in Older Adolescents and Young Adults 15 to 29 Years of Age, Including SEER Incidence and Survival: 1975-2000*. National Cancer Institute, NIH Pub. No. 06-5767. Bethesda, MD.

Bonci D, Coppola V, Musumeci M, Addario A, Giuffrida R, Memeo L, D'Urso L, Pagliuca A, Biffoni M, Labbaye C, Bartucci M, Muto G, Peschle C, De Maria R. (2008) The miR-15a-miR-16-1 cluster controls prostate cancer by targeting multiple oncogenic activities. *Nat Med*. 14(11):1271-7.

Bonewald LF. The amazing osteocyte. (2011) *J Bone Miner Res*. 26(2):229-38.

Boss DS, Witteveen PO, van der Sar J, Lolkema MP, Voest EE, Stockman PK, Ataman O, Wilson D, Das S, Schellens JH. (2011) Clinical evaluation of AZD1152, an i.v. inhibitor of Aurora B kinase, in patients with solid malignant tumors. *Ann Oncol*. 22(2):431-7.

Boyce BF, Xing L. Functions of RANKL/RANK/OPG in bone modeling and remodeling. (2008) *Arch Biochem Biophys*. 473(2):139-46.

Boyden LM, Mao J, Belsky J, Mitzner L, Farhi A, Mitnick MA, Wu D, Insogna K, Lifton RP. (2002) High bone density due to a mutation in LDL-receptor-related protein 5. *N Engl J Med*. 346(20):1513-21.

Bozec A, Bakiri L, Jimenez M, Schinke T, Amling M, Wagner EF. (2010) Fra-2/AP-1 controls bone formation by regulating osteoblast differentiation and collagen production. *J Cell Biol.* 190(6):1093-106.

Bryja V, Andersson ER, Schambony A, Esner M, Bryjová L, Biris KK, Hall AC, Kraft B, Cajanek L, Yamaguchi TP, Buckingham M, Arenas E. (2009) The extracellular domain of Lrp5/6 inhibits noncanonical Wnt signaling in vivo. *Mol Biol Cell.*20(3):924-36.

Bukholm IK, Nesland JM, Kåresen R, Jacobsen U, Børresen-Dale AL. (1998) E-cadherin and alpha-, beta-, and gamma-catenin protein expression in relation to metastasis in human breast carcinoma. *J Pathol.* 185(3):262-6.

Caldwell GM, Jones C, Gensberg K, Jan S, Hardy RG, Byrd P, Chughtai S, Wallis Y, Matthews GM, Morton DG. (2004) The Wnt antagonist sFRP1 in colorectal tumorigenesis. *Cancer Res.* 64(3):883-8.

Chae HD, Dutta R, Tiu B, Hoff FW, Accordi B, Serafin V, Youn M, Huang M, Sumarsono N, Davis KL, Lacayo NJ, Pigazzi M, Horton TM, Kornblau SM, Sakamoto KM. (2020) RSK inhibitor BI-D1870 inhibits acute myeloid leukemia cell proliferation by targeting mitotic exit. *Oncotarget.* 11(25):2387-2403.

Chan LK, Ho DW, Kam CS, Chiu EY, Lo IL, Yau DT, Cheung ET, Tang CN, Tang VW, Lee TK, Wong CC, Chok KS, Chan AC, Cheung TT, Wong CM, Ng IO. (2021) RSK2-inactivating mutations potentiate MAPK signaling and support cholesterol metabolism in hepatocellular carcinoma. *J Hepatol.* 74(2):360-371.

Chen RH, Tung R, Abate C, Blenis J. (1993) Cytoplasmic to nuclear signal transduction by mitogen-activated protein kinase and 90 kDa ribosomal S6 kinase. *Biochem Soc Trans.* 21(4):895-900.

Chen RH, Juo PC, Curran T, Blenis J. (1996) Phosphorylation of c-Fos at the C-terminus enhances its transforming activity. *Oncogene.* 12(7):1493-502.

Choong ML, Tan AC, Luo B, Lodish HF. (2003) A novel role for proliferin-2 in the ex vivo expansion of hematopoietic stem cells. *FEBS Lett.* 550(1-3):155-62.

Clément-Lacroix P, Ai M, Morvan F, Roman-Roman S, Vayssière B, Belleville C, Estrera K, Warman ML, Baron R, Rawadi G. (2005) Lrp5-independent activation of Wnt signaling by lithium chloride increases bone formation and bone mass in mice. *Proc Natl Acad Sci U S A.* 29;102(48)

Coffin GS, Siris E, Wegienka LC. (1966) Mental retardation with osteocartilaginous anomalies. *American Journal of Diseases of Children*. 112(3):205-13.

Cong F, Schweizer L, Varmus H. (2004) Wnt signals across the plasma membrane to activate the beta-catenin pathway by forming oligomers containing its receptors, Frizzled and LRP. *Development*.131(20):5103-15.

Cosman F, Crittenden DB, Adachi JD, Binkley N, Czerwinski E, Ferrari S, Hofbauer LC, Lau E, Lewiecki EM, Miyauchi A, Zerbin CA, Milmont CE, Chen L, Maddox J, Meisner PD, Libanati C, Grauer A. (2016) Romosozumab Treatment in Postmenopausal Women with Osteoporosis. *N Engl J Med*. 375(16):1532-1543.

Cui Y, Niziolek PJ, MacDonald BT, Zylstra CR, Alenina N, Robinson DR, Zhong Z, Matthes S, Jacobsen CM, Conlon RA, Brommage R, Liu Q, Mseeh F, Powell DR, Yang QM, Zambrowicz B, Gerrits H, Gossen JA, He X, Bader M, Williams BO, Warman ML, Robling AG. (2011) Lrp5 functions in bone to regulate bone mass. *Nat Med*.17(6):684-91.

Curran T, Peters G, Van Beveren C, Teich NM, Verma IM. (1982) FBJ murine osteosarcoma virus: identification and molecular cloning of biologically active proviral DNA. *J Virol*. 44(2):674-82.

David JP, Mehic D, Bakiri L, Schilling AF, Mandic V, Priemel M, Idarraga MH, Reschke MO, Hoffmann O, Amling M, Wagner EF. (2005) Essential role of RSK2 in c-Fos-dependent osteosarcoma development. *J Clin Invest*. 115(3):664-72.

Davidson B, Nymoen DA, Elgaaen BV, Staff AC, Tropé CG, Kærn J, Reich R, Falkenthal TE. (2014) BUB1 mRNA is significantly co-expressed with AURKA and AURKB mRNA in advanced-stage ovarian serous carcinoma. *Virchows Arch*. 464(6):701-7.

Dees EC, Cohen RB, von Mehren M, Stinchcombe TE, Liu H, Venkatakrisnan K, Manfredi M, Fingert H, Burris HA 3rd, Infante JR. (2012) Phase I study of aurora A kinase inhibitor MLN8237 in advanced solid tumors: safety, pharmacokinetics, pharmacodynamics, and bioavailability of two oral formulations. *Clin Cancer Res*. 18(17):4775-84.

Dennis M, Davies M, Oliver S, D'Souza R, Pike L, Stockman P. (2012) Phase I study of the Aurora B kinase inhibitor barasertib (AZD1152) to assess the pharmacokinetics, metabolism and excretion in patients with acute myeloid leukemia. *Cancer Chemother Pharmacol*. 70(3):461-9.

Dirckx N, Zhang Q, Chu EY, Tower RJ, Li Z, Guo S, Yuan S, Khare PA, Zhang C, Verardo A, Alejandro LO, Park A, Faugere MC, Helfand SL, Somerman MJ, Riddle RC, de Cabo R, Le A,

Schmidt-Rohr K, Clemens TL. (2022) A specialized metabolic pathway partitions citrate in hydroxyapatite to impact mineralization of bones and teeth. *Proc Natl Acad Sci U S A*. 119(45):e2212178119.

Eferl R, Wagner EF. (2003) AP-1: a double-edged sword in tumorigenesis. *Nat Rev Cancer*. 3(11):859-68.

Eferl R, Hoebertz A, Schilling AF, Rath M, Karreth F, Kenner L, Amling M, Wagner EF. (2004) The Fos-related antigen Fra-1 is an activator of bone matrix formation. *EMBO J*. 23(14):2789-99.

Emanuelli B, Vienberg SG, Smyth G, Cheng C, Stanford KI, Arumugam M, Michael MD, Adams AC, Kharitonov A, Kahn CR. (2014) Interplay between FGF21 and insulin action in the liver regulates metabolism. *J Clin Invest*. 124(2):515-27.

Esteve P, Sardonis A, Ibañez C, Shimono A, Guerrero I, Bovolenta P. (2011) Secreted frizzled-related proteins are required for Wnt/ β -catenin signalling activation in the vertebrate optic cup. *Development*. 138(19):4179-84.

Ferron M, McKee MD, Levine RL, Ducy P, Karsenty G. (2012) Intermittent injections of osteocalcin improve glucose metabolism and prevent type 2 diabetes in mice. *Bone*. 50(2):568-75.

Finkel MP, Biskis BO, Jinkins PB. (1966) Virus induction of osteosarcomas in mice. *Science*. 151(3711):698-701.

Fisher FM, Kleiner S, Douris N, Fox EC, Mepani RJ, Verdeguer F, Wu J, Kharitonov A, Flier JS, Maratos-Flier E, Spiegelman BM. (2012) FGF21 regulates PGC-1 α and browning of white adipose tissues in adaptive thermogenesis. *Genes Dev*. 26(3):271-81.

Florencio-Silva R, Sasso GR, Sasso-Cerri E, Simões MJ, Cerri PS. (2015) Biology of Bone Tissue: Structure, Function, and Factors That Influence Bone Cells. *Biomed Res Int*. 2015:421746.

Florenzano P, Gafni RI, Collins MT. Tumor-induced osteomalacia. (2017) *Bone Rep*. 20;7:90-97.

Fukumoto S, Martin TJ. (2009) Bone as an endocrine organ. *Trends Endocrinol Metab*. 20(5):230-6.

Franz K, Ost M, Otten L, Herpich C, Coleman V, Endres AS, Klaus S, Müller-Werdan U, Norman K. (2019) Higher serum levels of fibroblast growth factor 21 in old patients with cachexia. *Nutrition*. 63-64:81-86.

Fuchs N, Winkler K. (1993) Osteosarcoma. *Curr Opin Oncol*. 5(4):667-71.

George A, Sabsay B, Simonian PA, Veis A. (1993) Characterization of a novel dentin matrix acidic phosphoprotein. Implications for induction of biomineralization. *J Biol Chem*. 268(17):12624-30

Glass DA 2nd, Bialek P, Ahn JD, Starbuck M, Patel MS, Clevers H, Taketo MM, Long F, McMahon AP, Lang RA, Karsenty G. (2005) Canonical Wnt signaling in differentiated osteoblasts controls osteoclast differentiation. *Dev Cell*. 8(5):751-64.

Glover DM, Leibowitz MH, McLean DA, Parry H. (1995) Mutations in aurora prevent centrosome separation leading to the formation of monopolar spindles. *Cell*. 81(1):95-105.

Goldberg SL, Fenaux P, Craig MD, Gyan E, Lister J, Kassis J, Pigneux A, Schiller GJ, Jung J, Jane Leonard E, Fingert H, Westervelt P. (2014) An exploratory phase 2 study of investigational Aurora A kinase inhibitor alisertib (MLN8237) in acute myelogenous leukemia and myelodysplastic syndromes. *Leuk Res Rep*. 3(2):58-61.

Gong Y, Slee RB, Fukai N, Rawadi G, Roman-Roman S, Reginato AM, Wang H, Cundy T, Glorieux FH, Lev D, Zacharin M, Oexle K, Marcelino J, Suwairi W, Heeger S, Sabatakos G, Apte S, Adkins WN, Allgrove J, Arslan-Kirchner M, Batch JA, Beighton P, Black GC, Boles RG, Boon LM, Borrone C, Brunner HG, Carle GF, Dallapiccola B, De Paepe A, Floege B, Halfhide ML, Hall B, Hennekam RC, Hirose T, Jans A, Jüppner H, Kim CA, Keppler-Noreuil K, Kohlschuetter A, LaCombe D, Lambert M, Lemyre E, Letteboer T, Peltonen L, Ramesar RS, Romanengo M, Somer H, Steichen-Gersdorf E, Steinmann B, Sullivan B, Superti-Furga A, Swoboda W, van den Boogaard MJ, Van Hul W, Vikkula M, Votruba M, Zabel B, Garcia T, Baron R, Olsen BR, Warman ML (2001) Osteoporosis-Pseudoglioma Syndrome Collaborative Group. LDL receptor-related protein 5 (LRP5) affects bone accrual and eye development. *Cell*. 107(4):513-23.

Grigoriadis AE, Schellander K, Wang ZQ, Wagner EF. (1993) Osteoblasts are target cells for transformation in c-fos transgenic mice. *J Cell Biol*. 122(3):685-701.

Gully CP, Zhang F, Chen J, Yeung JA, Velazquez-Torres G, Wang E, Yeung SC, Lee MH. (2010) Antineoplastic effects of an Aurora B kinase inhibitor in breast cancer. *Mol Cancer*. 9:42.

Hauf S, Cole RW, LaTerra S, Zimmer C, Schnapp G, Walter R, Heckel A, van Meel J, Rieder CL, Peters JM. (2003) The small molecule Hesperadin reveals a role for Aurora B in correcting

kinetochore-microtubule attachment and in maintaining the spindle assembly checkpoint. *J Cell Biol.* 161(2):281-94.

Hauschild A, Grob JJ, Demidov LV, Jouary T, Gutzmer R, Millward M, Rutkowski P, Blank CU, Miller WH Jr, Kaempgen E, Martín-Algarra S, Karaszewska B, Mauch C, Chiarion-Sileni V, Martin AM, Swann S, Haney P, Mirakhur B, Guckert ME, Goodman V, Chapman PB. (2012) Dabrafenib in BRAF-mutated metastatic melanoma: a multicentre, open-label, phase 3 randomised controlled trial. *Lancet.*380(9839):358-65.

Hoang BH, Kubo T, Healey JH, Sowers R, Mazza B, Yang R, Huvos AG, Meyers PA, Gorlick R. (2004) Expression of LDL receptor-related protein 5 (LRP5) as a novel marker for disease progression in high-grade osteosarcoma. *Int J Cancer.* 109(1):106-11.

Hock JM, Gera I. (1992) Effects of continuous and intermittent administration and inhibition of resorption on the anabolic response of bone to parathyroid hormone. *J Bone Miner Res.* 7(1):65-72.

Holm E, Aubin JE, Hunter GK, Beier F, Goldberg HA. (2015) Loss of bone sialoprotein leads to impaired endochondral bone development and mineralization. *Bone.* 71:145-54.

Holmen SL, Zylstra CR, Mukherjee A, Sigler RE, Faugere MC, Bouxsein ML, Deng L, Clemens TL, Williams BO. (2005) Essential role of beta-catenin in postnatal bone acquisition. *J Biol Chem.* 280(22):21162-8.

Honma K, Nakanishi R, Nakanoko T, Ando K, Saeki H, Oki E, Iimori M, Kitao H, Kakeji Y, Maehara Y. (2014) Contribution of Aurora-A and -B expression to DNA aneuploidy in gastric cancers. *Surg Today.* 44(3):454-61.

Jochum W, David JP, Elliott C, Wutz A, Plenk H Jr, Matsuo K, Wagner EF. (2000) Increased bone formation and osteosclerosis in mice overexpressing the transcription factor Fra-1. *Nat Med.* 6(9):980-4.

Kadomoto S, Izumi K, Mizokami A. (2021) Roles of CCL2-CCR2 Axis in the Tumor Microenvironment. *Int J Mol Sci.*22(16):8530.

Kalajzic I, Braut A, Guo D, Jiang X, Kronenberg MS, Mina M, Harris MA, Harris SE, Rowe DW. (2004) Dentin matrix protein 1 expression during osteoblastic differentiation, generation of an osteocyte GFP-transgene. *Bone.* 35(1):74-82.

Kang S, Dong S, Gu TL, Guo A, Cohen MS, Lonial S, Khoury HJ, Fabbro D, Gilliland DG, Bergsagel PL, Taunton J, Polakiewicz RD, Chen J. (2007) FGFR3 activates RSK2 to mediate hematopoietic transformation through tyrosine phosphorylation of RSK2 and activation of the MEK/ERK pathway. *Cancer Cell*12(3):201-14.

Kang S, Elf S, Lythgoe K, Hitosugi T, Taunton J, Zhou W, Xiong L, Wang D, Muller S, Fan S, Sun SY, Marcus AI, Gu TL, Polakiewicz RD, Chen ZG, Khuri FR, Shin DM, Chen J. (2010) p90 ribosomal S6 kinase 2 promotes invasion and metastasis of human head and neck squamous cell carcinoma cells. *J Clin Invest.* 120(4):1165-77.

Kanis JA, Cooper C, Rizzoli R, Reginster JY (2019) Scientific Advisory Board of the European Society for Clinical and Economic Aspects of Osteoporosis (ESCEO) and the Committees of Scientific Advisors and National Societies of the International Osteoporosis Foundation (IOF). European guidance for the diagnosis and management of osteoporosis in postmenopausal women. *Osteoporos Int.* 30(1):3-44.

Kansara M, Teng MW, Smyth MJ, Thomas DM. (2014) Translational biology of osteosarcoma. *Nat Rev Cancer.* 14(11):722-35.

Kashima TG, Dongre A, Oppermann U, Athanasou NA. (2013) Dentine matrix protein 1 (DMP-1) is a marker of bone-forming tumours. *Virchows Arch.* 462(5):583-91.

Kato M, Patel MS, Levasseur R, Lobov I, Chang BH, Glass DA 2nd, Hartmann C, Li L, Hwang TH, Brayton CF, Lang RA, Karsenty G, Chan L. (2002) Cbfa1-independent decrease in osteoblast proliferation, osteopenia, and persistent embryonic eye vascularization in mice deficient in Lrp5, a Wnt coreceptor. *J Cell Biol.* ;157(2):303-14.

Kramer I, Halleux C, Keller H, Pegurri M, Gooi JH, Weber PB, Feng JQ, Bonewald LF, Kneissel M. (2010) Osteocyte Wnt/beta-catenin signaling is required for normal bone homeostasis. *Mol Cell Biol.* 30(12):3071-85.

Krenn V, Musacchio A. (2015)The Aurora B Kinase in Chromosome Bi-Orientation and Spindle Checkpoint Signaling. *Front Oncol.* 5:225.

Kunoh T, Noda T, Koseki K, Sekigawa M, Takagi M, Shin-ya K, Goshima N, Iemura S, Natsume T, Wada S, Mukai Y, Ohta S, Sasaki R, Mizukami T. (2010) A novel human dynactin-associated protein, dynAP, promotes activation of Akt, and ergosterol-related compounds induce dynAP-dependent apoptosis of human cancer cells. *Mol Cancer Ther.* 9(11):2934-42.

Kunoh T, Wang W, Kobayashi H, Matsuzaki D, Togo Y, Tokuyama M, Hosoi M, Koseki K, Wada S, Nagai N, Nakamura T, Nomura S, Hasegawa M, Sasaki R, Mizukami T. (2015) Human

Dynactin-Associated Protein Transforms NIH3T3 Cells to Generate Highly Vascularized Tumors with Weak Cell-Cell Interaction. *PLoS One*. 10(8):e0135836.

Kwong LN, Dove WF. (2009) APC and its modifiers in colon cancer. *Adv Exp Med Biol*. 656:85-106.

Lehenkari P, Hentunen TA, Laitala-Leinonen T, Tuukkanen J, Väänänen HK. (1998) Carbonic anhydrase II plays a major role in osteoclast differentiation and bone resorption by effecting the steady state intracellular pH and Ca²⁺. *Exp Cell Res*. 10;242(1):128-37.

Lens SM, Voest EE, Medema RH. (2010) Shared and separate functions of polo-like kinases and aurora kinases in cancer. *Nat Rev Cancer*. 10(12):825-41.

Li LY, Chen XS, Wang KS, Guan YD, Ren XC, Cao DS, Sun XY, Li AX, Tao YG, Zhang Y, Yin MZ, Wang XL, Wu MH, Yang JM, Cheng Y. (2020) RSK2 protects human breast cancer cells under endoplasmic reticulum stress through activating AMPK α 2-mediated autophagy. *Oncogene*. 39(43):6704-6718.

Li T, Chan RWS, Lee CL, Chiu PCN, Li RHW, Ng EHY, Yeung WSB. (2022) WNT5A Interacts with FZD5 and LRP5 to Regulate Proliferation and Self-Renewal of Endometrial Mesenchymal Stem-Like Cells. *Front Cell Dev Biol*. 10:837827.

Liao N, Koehne T, Tuckermann J, Trivai I, Amling M, David JP, Schinke T, Luther J. (2021) Osteoblast-specific inactivation of p53 results in locally increased bone formation. *PLoS One*. 16(11):e0249894.

Linder M, Glitzner E, Srivatsa S, Bakiri L, Matsuoka K, Shahrouzi P, Dumanic M, Novoszel P, Mohr T, Langer O, Wanek T, Mitterhauser M, Wagner EF, Sibilina M. (2018) EGFR is required for FOS-dependent bone tumor development via RSK2/CREB signaling. *EMBO Mol Med*. 10(11):e9408.

Long K, Moss L, Laursen L, Boulter L, Ffrench-Constant C. (2016) Integrin signalling regulates the expansion of neuroepithelial progenitors and neurogenesis via Wnt7a and Decorin. *Nat Commun*. 7:10354.

Lowry B, Miller JR, Fraser FC. (1971) A new dominant gene mental retardation syndrome: Association with small stature, tapering fingers, characteristic facies, and possible hydrocephalus. *American Journal of Diseases of Children*. 121(6):496-500.

Luther J, Yorgan TA, Rolvien T, Ulsamer L, Koehne T, Liao N, Keller D, Vollersen N, Teufel S, Neven M, Peters S, Schweizer M, Trumpp A, Rosigkeit S, Bockamp E, Mundlos S, Kornak U, Oheim R, Amling M, Schinke T, David JP. (2018) Wnt1 is an Lrp5-independent bone-anabolic Wnt ligand. *Sci Transl Med*. 10(466):eaau7137.

Manfredi MG, Ecsedy JA, Chakravarty A, Silverman L, Zhang M, Hoar KM, Stroud SG, Chen W, Shinde V, Huck JJ, Wysong DR, Janowick DA, Hyer ML, Leroy PJ, Gershman RE, Silva MD, Germanos MS, Bolen JB, Claiborne CF, Sells TB. (2011) Characterization of Alisertib (MLN8237), an investigational small-molecule inhibitor of aurora A kinase using novel in vivo pharmacodynamic assays. *Clin Cancer Res.* 17(24):7614-24.

Matsuoka K, Bakiri L, Wolff LI, Linder M, Mikels-Vigdal A, Patiño-García A, Lecanda F, Hartmann C, Sibia M, Wagner EF. (2020) Wnt signaling and Loxl2 promote aggressive osteosarcoma. *Cell Res.* 30(10):885-901.

Meltzer PS, Helman LJ. (2021) New Horizons in the Treatment of Osteosarcoma. *N Engl J Med.* 385(22):2066-2076

Miller CW, Aslo A, Won A, Tan M, Lampkin B, Koeffler HP. (1996) Alterations of the p53, Rb and MDM2 genes in osteosarcoma. *J Cancer Res Clin Oncol.*122(9):559-65.

Mizutani K, Sud S, McGregor NA, Martinovski G, Rice BT, Craig MJ, Varsos ZS, Roca H, Pienta KJ. (2009) The chemokine CCL2 increases prostate tumor growth and bone metastasis through macrophage and osteoclast recruitment. *Neoplasia.* 11(11):1235-42.

Morin PJ, Sparks AB, Korinek V, Barker N, Clevers H, Vogelstein B, Kinzler KW. (1997) Activation of beta-catenin-Tcf signaling in colon cancer by mutations in beta-catenin or APC. *Science.* 275(5307):1787-90.

Nakayama M, Naito M, Omori K, Ono S, Nakayama K, Ohara N. (2022) *Porphyromonas gingivalis* Gingipains Induce Cyclooxygenase-2 Expression and Prostaglandin E₂ Production via ERK1/2-Activated AP-1 (c-Jun/c-Fos) and IKK/NF-κB p65 Cascades. *J Immunol.* 208(5):1146-1154.

Neer RM, Arnaud CD, Zanchetta JR, Prince R, Gaich GA, Reginster JY, Hodsman AB, Eriksen EF, Ish-Shalom S, Genant HK, Wang O, Mitlak BH. (2001) Effect of parathyroid hormone (1-34) on fractures and bone mineral density in postmenopausal women with osteoporosis. *N Engl J Med.* 10;344(19):1434-41.

Nguyen TD, Miyatake Y, Yoshida T, Kawahara H, Hanayama R. (2021) Tumor-secreted proliferin-1 regulates adipogenesis and lipolysis in cachexia. *Int J Cancer.* 148(8):1982-1992.

Nusse R, Varmus HE. (1982) Many tumors induced by the mouse mammary tumor virus contain a provirus integrated in the same region of the host genome. *Cell.* 31(1):99-109.

Ponzetti M, Rucci N. Osteoblast Differentiation and Signaling : Established Concepts and Emerging Topics. (2021) *Int J Mol Sci.* 22(13):6651.

Prather C, Adams E, Zentgraf W. (2020) Romosozumab: A first-in-class sclerostin inhibitor for osteoporosis. *Am J Health Syst Pharm.* 77(23):1949-1956.

Rath S, Elamarthi P, Parab P, Gulia S, Nandhana R, Mokal S, Kembhavi Y, Perumal P, Bajpai J, Ghosh J, Gupta S. (2021) Efficacy and safety of palbociclib and ribociclib in patients with estrogen and/or progesterone receptor positive, HER2 receptor negative metastatic breast cancer in routine clinical practice. *PLoS One.* 16(7):e0253722.

Rickel K, Fang F, Tao J. (2017) Molecular genetics of osteosarcoma. *Bone.* 102:69-79.

Rivlin N, Brosh R, Oren M, Rotter V.(2011) Mutations in the p53 Tumor Suppressor Gene: Important Milestones at the Various Steps of Tumorigenesis. *Genes Cancer.* 2(4):466-74.

Salmela AL, Kallio MJ. (2013) Mitosis as an anti-cancer drug target. *Chromosoma.* 122(5):431-49.

Roy B, Han SJY, Fontan AN, Jema S, Joglekar AP. (2022) Aurora B phosphorylates Bub1 to promote spindle assembly checkpoint signaling. *Curr Biol.* 32(1):237-247.e6.

Rüther U, Wagner EF. (1989) The specific consequences of c-fos expression in transgenic mice. *Prog Nucleic Acid Res Mol Biol.* 36:235-45.

Sabatakos G, Sims NA, Chen J, Aoki K, Kelz MB, Amling M, Bouali Y, Mukhopadhyay K, Ford K, Nestler EJ, Baron R. (2000) Overexpression of DeltaFosB transcription factor(s) increases bone formation and inhibits adipogenesis. *Nat Med.* 6(9):985-90.

Sapkota GP, Cummings L, Newell FS, Armstrong C, Bain J, Frodin M, Grauert M, Hoffmann M, Schnapp G, Steegmaier M, Cohen P, Alessi DR. (2007) BI-D1870 is a specific inhibitor of the p90 RSK (ribosomal S6 kinase) isoforms in vitro and in vivo. *Biochem J.* 401(1):29-38.

Schiff D, Wen PY, van den Bent MJ. (2009) Neurological adverse effects caused by cytotoxic and targeted therapies. *Nat Rev Clin Oncol.* 6(10):596-603.

Schinke T, Gebauer M, Schilling AF, Lamprianou S, Priemel M, Mueldner C, Neunaber C, Streichert T, Ignatius A, Harroch S, Amling M. (2008) The protein tyrosine phosphatase Rptpzeta is expressed in differentiated osteoblasts and affects bone formation in mice. *Bone.* 42(3):524-34.

Schwartz GK, Carvajal RD, Midgley R, Rodig SJ, Stockman PK, Ataman O, Wilson D, Das S, Shapiro GI. (2013) Phase I study of barasertib (AZD1152), a selective inhibitor of Aurora B kinase, in patients with advanced solid tumors. *Invest New Drugs*. 31(2):370-80.

Seeliger H, Camaj P, Ischenko I, Kleespies A, De Toni EN, Thieme SE, Blum H, Assmann G, Jauch KW, Bruns CJ. (2009) EFEMP1 expression promotes in vivo tumor growth in human pancreatic adenocarcinoma. *Mol Cancer Res*. 7(2):189-98.

Semënov M, Tamai K, He X. (2005) SOST is a ligand for LRP5/LRP6 and a Wnt signaling inhibitor. *J Biol Chem*. 280(29):26770-5

Shimada T, Mizutani S, Muto T, Yoneya T, Hino R, Takeda S, Takeuchi Y, Fujita T, Fukumoto S, Yamashita T. (2001) Cloning and characterization of FGF23 as a causative factor of tumor-induced osteomalacia. *Proc Natl Acad Sci U S A*. 98(11):6500-5. doi: 10.1073/pnas.101545198.

Shintani K, Matsumine A, Kusuzaki K, Morikawa J, Matsubara T, Wakabayashi T, Araki K, Satonaka H, Wakabayashi H, Iino T, Uchida A. (2008) Decorin suppresses lung metastases of murine osteosarcoma. *Oncol Rep*. 19(6):1533-9.

Sobacchi C, Schulz A, Coxon FP, Villa A, Helfrich MH. (2013) Osteopetrosis: genetics, treatment and new insights into osteoclast function. *Nat Rev Endocrinol*. 9(9):522-36.

Sözen T, Özişik L, Başaran NÇ. (2017) An overview and management of osteoporosis. *Eur J Rheumatol*. 4(1):46-56.

Takeshita M, Koga T, Takayama K, Ijichi K, Yano T, Maehara Y, Nakanishi Y, Sueishi K. (2013) Aurora-B overexpression is correlated with aneuploidy and poor prognosis in non-small cell lung cancer. *Lung Cancer*. 80(1):85-90.

Tall AR, Yvan-Charvet L, Terasaka N, Pagler T, Wang N. (2008) HDL, ABC transporters, and cholesterol efflux: implications for the treatment of atherosclerosis. *Cell Metab*. 7(5):365-75.

Tanaka K, Yu HA, Yang S, Han S, Selcuklu SD, Kim K, Ramani S, Ganesan YT, Moyer A, Sinha S, Xie Y, Ishizawa K, Osmanbeyoglu HU, Lyu Y, Roper N, Guha U, Rudin CM, Kris MG, Hsieh JJ, Cheng EH. (2021) Targeting Aurora B kinase prevents and overcomes resistance to EGFR inhibitors in lung cancer by enhancing BIM- and PUMA-mediated apoptosis. *Cancer Cell*. 39(9):1245-1261.e6.

Teitelbaum, S. L. (2000). Bone resorption by osteoclasts. *Science* 289, 1504-8.

Terada Y, Tatsuka M, Suzuki F, Yasuda Y, Fujita S, Otsu M. (1998) AIM-1: a mammalian midbody-associated protein required for cytokinesis. *EMBO J.* 17(3):667-76

Theodosakis N, Micevic G, Langdon CG, Ventura A, Means R, Stern DF, Bosenberg MW. (2017) p90RSK Blockade Inhibits Dual BRAF and MEK Inhibitor-Resistant Melanoma by Targeting Protein Synthesis. *J Invest Dermatol.* 137(10):2187-2196.

Toft DJ, Rosenberg SB, Bergers G, Volpert O, Linzer DI. (2001) Reactivation of proliferin gene expression is associated with increased angiogenesis in a cell culture model of fibrosarcoma tumor progression. *Proc Natl Acad Sci U S A.* 98(23):13055-9.

Ushijima M, Shiota M, Matsumoto T, Kashiwagi E, Inokuchi J, Eto M. (2022) An oral first-in-class small molecule RSK inhibitor suppresses AR variants and tumor growth in prostate cancer. *Cancer Sci.* 113(5):1731-1738.

Vigneron S, Brioudes E, Burgess A, Labbé JC, Lorca T, Castro A. (2010) RSK2 is a kinetochore-associated protein that participates in the spindle assembly checkpoint. *Oncogene.* 29(24):3566-74

Vitale I, Galluzzi L, Castedo M, Kroemer G. (2011) Mitotic catastrophe: a mechanism for avoiding genomic instability. *Nat Rev Mol Cell Biol.* 12(6):385-92.

Vollersen N, Zhao W, Rolvien T, Lange F, Schmidt FN, Sonntag S, Shmerling D, von Kroge S, Stockhausen KE, Sharaf A, Schweizer M, Karsak M, Busse B, Bockamp E, Semler O, Amling M, Oheim R, Schinke T, Yorgan TA. (2021) The WNT1^{G177C} mutation specifically affects skeletal integrity in a mouse model of osteogenesis imperfecta type XV. *Bone Res.* 9(1):48.

Wang S, Zhang D, Han S, Gao P, Liu C, Li J, Pan X. (2017) Fibulin-3 promotes osteosarcoma invasion and metastasis by inducing epithelial to mesenchymal transition and activating the Wnt/ β -catenin signaling pathway. *Sci Rep.* 7(1):6215.

Wang Z, Kang J, Lian J, Huang L, Xie W, Zhao D, Ma H, Lin Z. (2020) EFEMP1 as a Potential Biomarker for Diagnosis and Prognosis of Osteosarcoma. *Biomed Res Int.* 2020:5264265.

Wang ZQ, Liang J, Schellander K, Wagner EF, Grigoriadis AE. (1995) c-fos-induced osteosarcoma formation in transgenic mice: cooperativity with c-jun and the role of endogenous c-fos. *Cancer Res.* 55(24):6244-51.

Weinberg RA. (1991) Tumor suppressor genes. *Science.* 254(5035):1138-46.

Wend P, Runke S, Wend K, Anchondo B, Yesayan M, Jardon M, Hardie N, Loddenkemper C, Ulasov I, Lesniak MS, Wolsky R, Bentolila LA, Grant SG, Elashoff D, Lehr S, Latimer JJ, Bose S, Sattar H, Krum SA, Miranda-Carboni GA. (2013) WNT10B/ β -catenin signalling induces HMGA2 and proliferation in metastatic triple-negative breast cancer. *EMBO Mol Med.* (2):264-79.

Yao Z, Chen P, Fan L, Chen P, Zhang X, Yu B. (2021) CCL2 is a critical mechano-responsive mediator in crosstalk between osteoblasts and bone mesenchymal stromal cells. *FASEB J.* 35(10):e21851.

Yorgan TA, Peters S, Jeschke A, Benisch P, Jakob F, Amling M, Schinke T. (2015) The Anti-Osteoanabolic Function of Sclerostin Is Blunted in Mice Carrying a High Bone Mass Mutation of *Lrp5*. *J Bone Miner Res.* 30(7):1175-83.

Yorgan TA, Peters S, Amling M, Schinke T. (2019) Osteoblast-specific expression of *Panx3* is dispensable for postnatal bone remodeling. *Bone.* 127:155-163.

Yoshimura T, Yuhki N, Moore SK, Appella E, Lerman MI, Leonard EJ. (1989) Human monocyte chemoattractant protein-1 (MCP-1). Full-length cDNA cloning, expression in mitogen-stimulated blood mononuclear leukocytes, and sequence similarity to mouse competence gene *JE*. *FEBS Lett.* 244(2):487-93.

Zahedi T, Hosseinzadeh Colagar A, Mahmoodzadeh H. (2021) *PTGS2* Over-Expression: A Colorectal Carcinoma Initiator not an Invasive Factor. *Rep Biochem Mol Biol.* 9(4):442-451.

Zhang D, Han S, Pan X, Li H, Zhao H, Gao X, Wang S. (2022) EFEMP1 binds to STEAP1 to promote osteosarcoma proliferation and invasion via the Wnt/ β -catenin and TGF- β /Smad2/3 signal pathways. *J Bone Oncol.* 37:100458.

Zhang Y, Wu J, Fu Y, Yu R, Su H, Zheng Q, Wu H, Zhou S, Wang K, Zhao J, Shen S, Xu G, Wang L, Yan C, Zou X, Lv Y, Zhang S. (2022) Hesperadin suppresses pancreatic cancer through ATF4/GADD45A axis at nanomolar concentrations. *Oncogene.* 41(25):3394-3408.

Zhao Z, Jin G, Yao K, Liu K, Liu F, Chen H, Wang K, Gorja DR, Reddy K, Bode AM, Guo Z, Dong Z. (2019) Aurora B kinase as a novel molecular target for inhibition the growth of osteosarcoma. *Mol Carcinog.* 58(6):1056-1067.

10. Appendix

All chemicals were used according to safety data sheets.

10.1. List of hazardous substances used in the study according to GHS.

Table 15: Hazard (H)- and precautionary (P) phrases.

Chemicals	CAS#	H-Phrases	P-Phrases
1 α ,25-Dihydroxyvitamin-D3	67-97-0	330-311-301-372	280-304+340-302+352-309+310
Acetic acid	64-19-7	226-290-314	210-280-301+330+331- 305+351+338-308-310
Agarose (SeaKem® LE)	9012-36-6		
Ammonium hydroxide	1336-21-6	290-314-335-400	260-273-280-301+330+331-303+361+353-305+351+338
Carbon dioxide	124-38-9	280	403
Ethanol	64-17-5	225-319	210-240-305+351+338-403+233
Ethylenediaminetetraacetic acid	60-00-4	319	305+351+338
Formaldehyde	50-00-0	301+311+331-314-317-335-341-350-370	201-260-280-301+310-330-303+361+353-304+340-310-305+351+338-308+310-403+233
Isopropyl alcohol	67-63-0	225-319-336	210-233-240-305+351+338-403+235
N,N-Dimethyl formamide	68-12-2	226-312-332-319-360D	201-210-302+352-304+340-305+351+338-308+313
N,N-Dimethyl-p-toluidine	99-97-8	301-311-373-412	261-273-280-301+310-311
Nitric acid	7697-37-2	272-290-331-314	280-301+330+331-305+351+338-308+310
Nitrogen	7727-37-9	280	403
Penicillin	118-53-6	315-317-320-334-335-361	264-304+340-305+351+338-312-337+313-332+313
Potassium chloride	7447-40-7		
Potassium phosphate	7778-53-2	318-335	280-304+340+312-305+351+338
Silver nitrate	7761-88-8	272-290-314-410	210-220-260-280-305+351+338-370+378-308+310
Sodium acetate	6131-90-4		
Sodium carbonate	5968-11-6-	319	260-305+351+338
Sodium hydrogen carbonate	144-55-8		
Sodium hydroxide	23340-32- 1	290-314	280-301+330+331-305+351+338-308+310
Sodium phosphate	7601-54-9	315-319-335	261-305+351+338
Streptomycin	57-92-1	302-361	281
Toluidin blue O	92-31-9		
Tris(hydroxymethyl)amino \oplus methane base	77-86-1	315-319-335	261-305+351+338
Tris(hydroxymethyl)amino \oplus methane hydrochlorid	1185-53-1	315-319-335	261-305+351+338

10.2. List of hazard statements

Number	Hazard statement
201	Explosive; mass explosion hazard
225	Highly flammable liquid and vapour
226	Flammable liquid and vapour
228	Flammable solid
241	Heating may cause a fire or explosion
271	May cause fire or explosion; strong oxidizer
272	May intensify fire; oxidizer
280	Contains gas under pressure; may explode if heated
290	May be corrosive to metals
301	Toxic if swallowed
302	Harmful if swallowed
304	May be fatal if swallowed and enters airways
311	Toxic in contact with skin
312	Harmful in contact with skin
314	Causes severe skin burns and eye damage
315	Causes skin irritation
317	May cause an allergic skin reaction
318	Causes serious eye damage
319	Causes serious eye irritation
320	Causes eye irritation
330	Fatal if inhaled
331	Toxic if inhaled
332	Harmful if inhaled
334	May cause allergy or asthma symptoms or breathing difficulties if inhaled
335	May cause respiratory irritation
336	May cause drowsiness or dizziness
340	May cause genetic defects
341	Suspected of causing genetic defects
350	May cause cancer
351	Suspected of causing cancer
360	May damage fertility or the unborn child
361	Suspected of damaging fertility or the unborn child
370	Causes damage to organs
372	Causes damage to organs through prolonged or repeated exposure
373	May cause damage to organs through prolonged or repeated exposure
400	Very toxic to aquatic life
410	Very toxic to aquatic life with long lasting effects
411	Toxic to aquatic life with long lasting effects
412	Harmful to aquatic life with long lasting effects

10.3. List of precautionary statements

Number	Precautionary statement
201	Obtain special instructions before use
210	Keep away from heat/sparks/open flames/hot surfaces – No smoking
220	Keep/Store away from clothing/.../combustible materials
233	Keep container tightly closed
235	Keep cool
240	Ground/bond container and receiving equipment
260	Do not breathe dust/fume/gas/mist/vapours/spray
261	Avoid breathing dust/fume/gas/mist/vapours/spray
262	Do not get in eyes, on skin, or on clothing
264	Wash ... thoroughly after handling
270	Do not eat, drink or smoke when using this product
273	Avoid release to the environment
280	Wear protective gloves/protective clothing/eye protection/face protection
281	Use personal protective equipment as required
301	IF SWALLOWED:
302	IF ON SKIN:
303	IF ON SKIN (or hair):
304	IF INHALED:
305	IF IN EYES:
308	IF exposed or concerned:
309	IF exposed or you feel unwell:
310	Immediately call a POISON CENTER or doctor/physician
311	Call a POISON CENTER or doctor/physician
312	Call a POISON CENTER or doctor/physician if you feel unwell
313	Get medical advice/attention
330	Rinse mouth
331	Do NOT induce vomiting
332	If skin irritation occurs:
333	If skin irritation or a rash occurs:
337	If eye irritation persists:
338	Remove contact lenses if present and easy to do. continue rinsing
340	Remove victim to fresh air and keep at rest in a position comfortable for breathing
342	If experiencing respiratory symptoms:
351	Rinse continuously with water for several minutes
352	Wash with soap and water
353	Rinse skin with water/shower
361	Remove/Take off immediately all contaminated clothing
370	In case of fire:
378	Use ... for extinction
403	Store in a well ventilated place
420	Store away from other materials
501	Dispose of contents/container to ...

11. Acknowledgements

In the first place I would like to thank **Prof. Dr. rer. nat. Thorsten Schinke** to have taken over my PhD supervision, for his unbreakable support during all phases of this thesis, the stimulating discussion to permit the development of this project and its great help in writing in a synthetic way. I would also address him my sincere greatfullness for his understanding regarding unfortunate events that happened during these 4 years. I am conscious of the chance I have to be able to continue working in his team and benefit from his research expertise.

I would like to thank **Prof. Dr. med. Michael Amling** to have given me the great opportunity to perform this thesis in the Institute of Osteology and Biomechanics where I was offered great work conditions and knowledge expertise.

I would like to express my sincere gratitude to **Prof. Dr. med. Elke Oetjen** and **Prof. Dr. Sandra Pohl** for their support and availability at every stages of this thesis.

I would like to extend my sincere thanks to **Prof. Dr. Peter Heisig** and **Prof. Dr. rer. nat. Hartmut Schlüter** to have accepted to be part of my defense committee.

I would like to also thank all colleagues from the institute and especially: **Dr. rer. nat. Julia Luther**, **Dr. rer. nat. Laura Brylka**, **PDr. rer. nat. Timur Yorgan**, **Dr. Anke Baranowsky**, **Dr. med. Wenbo Zhao**, **Mona Neven**, **Lana Rosenthal**, **Olga Winter**, **Andrea Thiecke**, **Claudia Reymers** and **Nannan Liao** for their contributions to the completion of my project by their teaching of so many techniques, friendly advices and any kind of help I was in need of.

Thanks should also go to the workers of the UKE animal facility and especially to **Gudrun Arndt**, **Maria Kuschel** and **Philipp Missberger** for taking so great care of my mice.

Words cannot express my gratitude for **Dr. Jean-Pierre David** who gave me the envy to come to work with him in Germany on this thesis and without whom I would not have been able to present this work today. Research field and Bretagne are missing one of their more passionate doctor who gave until the end his support to this project. I am glad to have been able to make my first steps in this thesis by his side trying to learn how to have a more translational

approach of the human research world where everything can be connected and where you should try to think outside of conventional boxes.

I am also grateful to have such a supportive family who helped me to come to Germany and gave me the opportunity to proceed that far on my studies. Special thanks to all the friends I have made here which I consider as my Hamburg family and who always cheered me up along this journey. Finally, thank you to **Sascha Böckmann** that often had to bear my absence but who never complained and always supported me.

Hiermit versichere ich an Eides statt, die vorliegende Dissertation selbst verfasst und keine anderen als die angegebenen Hilfsmittel benutzt zu haben. Die eingereichte schriftliche Fassung entspricht der auf dem elektronischen Speichermedium. Ich versichere, dass diese Dissertation nicht in einem früheren Promotionsverfahren eingereicht wurde.

I hereby declare on oath, that I have written the present dissertation by my own and have not used other than the acknowledged resources and aids. The submitted written version corresponds to the version on the electronic storage medium. I hereby declare that I have not previously applied or pursued for a doctorate (Ph.D. studies).

02.05.2023

Date

A handwritten signature in black ink, appearing to be 'A. B. C.', written over a horizontal line.

Signature